DISSERTATION

TOOLS FOR CHARACTERIZING AND MONITORING NATURAL SOURCE ZONE DEPLETION

Submitted by

Maria Irianni Renno

Department of Civil and Environmental Engineering

In partial fulfillment of the requirements

For the Degree of Doctor of Philosophy

Colorado State University

Fort Collins, Colorado

Spring 2024

Doctoral Committee:

Advisor: Susan K. De Long
Co-advisor: Thomas C. Sale

Trent A. Key
Joseph Scalia
Mary Stromberger

ABSTRACT

TOOLS FOR CHARACTERIZING AND MONITORING NATURAL SOURCE ZONE DEPLETION

Although natural source zone depletion (NSZD) has gained acceptance by practitioners as a remediation technology for mid- to late-stage sites containing light non-aqueous phase liquids (LNAPL), challenges remain for broader regulatory adoption of NSZD as the sole remedy. Adoption of NSZD as a remedy requires verifying that it is occurring. NSZD can be an efficient and cost-effective solution for LNAPL zones, but acceptance of this bioremediation technology relies on a multiple-lines-of-evidence approach that requires a solid understanding of baseline conditions and effective monitoring. Emerging use of *in situ* oxidation-reduction potential (ORP) sensors shows promise to resolve spatial and temporal redox dynamics during NSZD processes. Further, next generation sequencing (NGS) of present and active microbial communities can provide insights regarding subsurface biogeochemistry, associated elemental cycling utilized in electron transport (e.g., N, Mn, Fe, S), and the potential for biodegradation.

Microbially-mediated hydrocarbon degradation is well documented. However, how these microbial processes occur in complex subsurface petroleum impacted systems remains unclear, and this knowledge is needed to guide technologies to enhance biodegradation effectively. Analysis of RNA derived from soils impacted by petroleum liquids allows for analysis of active microbial communities, and a deeper understanding of the dynamic biochemistry occurring during site remediation. However, RNA analysis in soils impacted with petroleum liquids is challenging due to: 1) RNA being inherently unstable, and 2) petroleum impacted soils containing problematic levels of polymerase chain reaction (PCR) inhibitors (e.g., aqueous phase

metals and humic acids) that must be removed to yield high-purity RNA for downstream analysis.

Herein, a new RNA purification method that allows for extracting RNA from petroleum-impacted soils was developed and successfully implemented to discriminate between active (RNA) and present (DNA) microbes in soils containing LNAPL. A key modification involved reformulation of the sample pretreatment solution by replacing water as the diluent with a commercially available RNA preservation solution consisting of LifeGuard™ (Qiagen) Methods were developed and demonstrated using cryogenically preserved soils from three former petroleum refineries. Results showed the new soil washing approach had no adverse effects on RNA recovery but did improve RNA quality by removing PCR inhibitors, which in turn allows for characterization of active microbial communities present in petroleum impacted soils.

To optimally employ NSZD and enhanced NSZD (ENSZD) at sites impacted by LNAPL, monitoring strategies are required. Emerging use of subsurface Soil redox sensors shows promise for tracking redox evolution, which reflects ongoing biogeochemical processes. However, further understanding of how soil redox dynamics relate to subsurface microbial activity and LNAPL biodegradation pathways is needed.

In this work, soil redox sensors and DNA and RNA sequencing-based microbiome analysis were combined to elucidate NSZD and ENSZD (biostimulation via periodic sulfate addition and air sparging) processes in columns containing LNAPL impacted soils from a former petroleum refinery. Herein, microbial activity was directly correlated to continuous soil-ORP readings. Results show expected relationships between continuous soil redox and active microbial communities. Continuous data revealed spatial and temporal detail that informed interpretation of the hydrocarbon biodegradation data. Redox increases were transient for sulfate

addition, and DNA and RNA sequencing revealed how hydrocarbon concentration and composition impacted microbiome structure and naphthalene biodegradation. When alkanes were present, naphthalene degradation was not observed, likely because naphthalene degraders were outcompeted. Further, the results of the sulfate addition experiment indicated a direct correlation of *Desulfovibrio* spp. with naphthalene biodegradation and showed that *Smithella* spp. were enriched in sulfate enhanced soils containing alkanes. Periodic air sparging did not result in fully aerobic conditions suggesting observed increased rates of biodegradation could be explained by stimulating alternative anaerobic metabolisms that were more energetically favorable compared to baseline/control conditions (e.g., iron reduction due to air oxidizing reduced iron).

Methods developed and emerging continuous monitoring tools that were tested in lab soil columns were also applied to a mid- and late-stage LNAPL site. Herein, a case study is presented that advances integration of multiple nascent technologies for characterizing mid- and late-stage LNAPL sites including: 1) cryogenic coring, 2) multiple level internet of things (IoT) soil redox and temperature sensors in soil, and 3) application of RNA- and DNA-based molecular biological tools (MBTs) for site characterization. The integration of the data sets produced by these tools allowed for progress of NSZD to be evaluated in parallel under LNAPL site-relevant biogeochemical conditions. Collectively, the research presented in this dissertation support combining cryogenic coring sampling, continuous redox and temperature sensing and microbiome analysis to provide insights beyond those possible with each monitoring tool alone.

The synergy achieved between microbiome characterization and soil continuous sensing illustrates how the integration of new characterization tools can provide insight into complex biogeochemical systems. Further understanding of these technologies will lead to improved

predictions on remediation outcomes. The modern tools tested for middle- and late-stage LNAPL sites offer opportunities to more effectively and efficiently manage legacy LNAPL sites.

ACKNOWLEDGMENTS

This Dissertation is dedicated to Dion Renno who will always journey with me in my heart and to my son Lucas Sky Renno who is an example of what it means to “shine your light onto the world”. I love you both forever!

I would like to thank everyone who made this path possible for me and God for putting them in front of me.

I thank my dearest professor Dr. Susan De Long for being my mentor, for her academic leadership and all the opportunities she provided me with (including unrestricted access to her awesome lab), for showing up when I needed her most, whether it was to pick me up or make me cry. I thank her for her patience and empathy and for leading by example with what it means to be a person of excellence.

I thank Dr. Trent Key, for his mentorship and for sharing with me his technical perspective and insights on bioremediation and for showing me how applied research works. I thank him for his teachings on anchoring my heart in the right place. Most of all I thank Dr. Key for the unexpected spiritual guidance that was provided to me so I could “punch through”.

I thank Dr. Tom Sale for the opportunity to work with him in the CCH and for training me in field work and for providing unique hands-on experiences that molded my career. I thank Dr. Sale for the times he shared with me his work vision and creativity.

I thank Dean Stromberger; I look up to her and her career and it is an honor and a privilege to be able to gain her insights into to my work. I also thank her for her open-door policy

and for her providing a safe space for me to express my concerns when I had any and for her guidance on how to address them.

I thank Dr. Scalia for his insights and guidance during the earlier writing stages of the dissertation and his help with the column experimental set-up. I am looking forward to his insights on the newer parts of this work, as well.

I also thank Dr. Blotevogel, who often shared with me mechanistic insights regarding differences between kinetics and thermodynamics and who taught me how thermo-kinetics can make the impossible possible.

I thank Cat Powers, Cali Campbell, Kayvan Karimi Askarani, Jorge Rico, Zach Ferrie, Sam Gallo, Mitch Olson, Saeed Kiaalhosseini, Helen Dungan, Paige Griffin, Natalie Zeman and Jaqueline Chaparro for being my lab buddies, editors, computational gurus, etc. Their contributions to the work presented herein are very valuable.

I thank Nin for new adventures, for the love and support and for all the laughter shared with me that keep me going forward. I thank Mama, Papa, Tom, and Jean for being the best parents in the world and even better grandparents. I also want to thank my sister, brother, and friends (Baby, Paul, Sole, Loli, Tata, Ceci, Barbie Jose, Agus, Deanna, Peter and Ana) for being there for me and picking up my slack when things got tough.

I thank ExxonMobil, Chevron and BP for the technical support, field opportunities and funding that supported my Ph.D. path.I thank Tom Haren and AGPROfessionals for taking a chance on me and bringing me on to the team. I thank them for their support in completing my Ph.D. and for helping me create a new vision on how I can contribute to advancing agriculture.

TABLE OF CONTENTS

LIST OF TABLES

LIST OF FIGURES

CHAPTER 1. INTRODUCTION AND BACKGROUND

1.1. Petroleum in Soils and Groundwater

The world relies on petroleum for ground, air, and sea transportation, manufactured goods, such as plastics, and for powering and heating industrial and domestic sectors of society. While petroleum has facilitated, and continues to facilitate, human progress, its exploitation, processing, and distribution can result in environmental spills. Inadvertent petroleum hydrocarbon (PHC) releases to soil-groundwater systems can result in zones containing light non-aqueous phase liquids (LNAPL). The focus of this research is advancing remediation approaches that rely on biodegradation of LNAPLs in the subsurface.

1.2. Petroleum Subsurface Fate

PHCs in soils and shallow groundwater are a ubiquitous problem and can pose a threat to human health and the environment (Sale et al., 2018). Upon being released to the subsurface, LNAPL migrates downward through the pore space into the vadose zone and to the top of the capillary fringe due to gravity (Chapple et al., 1998). Typically, LNAPL will laterally expand as it sheens on the groundwater surface (Bruce & Biagi, 1997), and water table fluctuations will cause smearing allowing for LNAPL expansion in the vertical direction, as well. These vertical fluctuations can cause LNAPL entrapment in vadose zone pore spaces (Newell et al., 1995).

Lighter hydrocarbons also can partition from the free phase liquids to the vapor phase and migrate through the vadose zone, where they can be biodegraded or escape to the surface depending on the existing vadose zone biogeochemical conditions. Further, dissolution of LNAPL in the pore water leads to the formation of dissolved-phase PHC plumes that can be attenuated via natural processes. The monitoring of these attenuation processes are referred to as

monitored natural attenuation (MNA) (Wiedemeier et al., 1999). MNA is a well-established remedial technology for PHC plumes. Similarly, LNAPL source depletion processes are referred to as NSZD (ITRC, 2018). Although dissolution, sorption and volatilization contribute to NSZD, LNAPL biodegradation is the key depletion process (Garg et al., 2017; Sihota et al., 2011).

Figure 1.1. Schematic representation of a shallow LNAPL impacted subsurface (ITRC, 2018).

1.3. LNAPL Biodegradation

NSZD biodegradation pathways are, in large part, dictated by electron acceptor availability. NSZD can occur via aerobic and anaerobic biodegradation. Anaerobic LNAPL biodegradation is commonly mediated by nitrate, manganese, iron, sulfur, thiosulfate, and sulfate (Garg et al., 2017; Meckenstock et al., 2015; Taggart et al., 2021). Absent these electron acceptors, biodegradation of LNAPLs occurs mainly through syntrophic interactions that involve fermentation and methanogenesis (Morris et al., 2013; Rotaru et al., 2016). Syntropy has been defined as a "tightly coupled mutualistic interaction" between at least two organisms to overcome thermodynamic and kinetic constraints (Sieber et al., 2012). Depending on the pathway, biodegradation of LNAPL can result in the production of hydrogen, carbon dioxide, methane, volatile fatty acids (e.g., acetate and formate), sulfide, and reduced and oxidized species of elements (e.g., manganese and iron) cycled during biologically mediated electron transport processes (Riser-Roberts, 2020). Understanding key biological processes underpinning

NSZD can lead to insights regarding LNAPL depletion in subsurface environments and can potentially be applied to remediation enhancements.

1.4. Molecular Biology Tools (MBTs)

MBTs can be applied to site characterization to provide evidence of microbially-mediated LNAPL depletion pathways (Löffler & Edwards, 2006; Taggart et al., 2021; Taggart & Key, 2023). Modern environmental MBTs rely on the detection of genes (DNA) or the detection of expressed genes (RNA and proteins) to evaluate biodegradation. Next generation sequencing (NGS) of present (DNA) and active (RNA) microbial communities can provide insights regarding subsurface biogeochemistry, associated cycling of elements utilized in electron transport (e.g., N, Mn, Fe, S), and help elucidate biodegradation pathways and ways to optimize these pathways. Quantitative polymerase chain reaction (qPCR) and reverse transcription qPCR (RT-qPCR) can quantify genes and transcripts, respectively. The detection of genes and transcripts associated with a given function can provide more direct evidence of the occurrence of a known biodegradation process. For example, the detection of *alkB* transcripts indicates active aerobic biodegradation of alkanes. Microbial ecology data are usually integrated with geochemical data to deduce biodegradation pathways in the subsurface and can inform on how to best measure degradation in the environment. For example, identifying sulfate reducers in the environment can lead to measuring sulfate concentration changes over time or space to establish a sulfate-dependent hydrocarbon degradation rate (Wiedemeier et al., 1999). Similarly, measurements of carbon dioxide and methane efflux are used to measure biodegradation rates.

1.5. Measuring Biodegradation

NSZD loss rates can be on the order of 10,000 to 100,000 of liters per hectare per year at middle and late-stage sites (McCoy et al., 2015). NSZD rates commonly exceed depletion rates

that can be achieved with active remedies (McCoy et al., 2015). However released LNAPL volumes are commonly large enough that LNAPL can persist for extended periods of time (Huntley & Beckett, 2002).

The importance of methanogenesis in the long-term evolution of hydrocarbon source zones has been acknowledged by researchers, field practitioners, and regulators alike (Garg et al., 2017; Irianni Renno et al., 2016; Sihota et al., 2011). However, characterizing NSZD and documenting evidence of degradation under field conditions remains challenging given uncertainties associated with subsurface heterogeneities. Under methanogenic conditions degradation rates are slow and the complexity and diversity of syntrophic methanogenic pathways further complicates characterization (Cavaliere et al., 2017). Further, as hydrocarbon sites evolve, key depletion processes might shift. An evolving conceptual site model (CSM) can thus help to adequately monitor NZSD progress (Lari et al., 2019). Being able to monitor *in situ* progress of hydrocarbon biodegradation is central to developing evolving CSMs that will aid in the modern management of PHCs in soil and groundwater.

Methods for monitoring NSZD rates include measuring gas fluxes associated with NSZD processes (e.g., via the gradient method (Johnson et al., 2006), the chamber method (Sihota et al., 2012), or the trap method (McCoy et al.,2015). More recently, multiple level temperature sensors were applied to measuring heat generated through NSZD (Karimi Askarani et al., 2018). The exothermic reaction of aerobic methane oxidation (i.e., methanotrophy) generates quantifiable levels of heat that can be used to calculate NSZD rates (Karimi Askarani et al., 2018; Karimi Askarani et al., 2024).

Complimentary to continuous temperature sensing and rate determination based on oxidation of methane produced by anaerobic PHC degradation is a newly developed technology

that allows for collecting continuous biogeochemical ORP (Burge et al., 2018; Sale et al., 2021). Sale et al., (2021) present in their work a comprehensive and synergistic dataset that shows how continuous ORP data can serve as an indication of a subsurface geochemical environment. Further, they show how, when coupled with other subsurface biogeochemical data, ORP data can potentially lead to the elucidation of governing LNAPL biodegradation processes.

1.6. Research Objectives

There is a critical need to develop bioremediation technologies including NSZD to address LNAPL source zones. Although NSZD has been accepted by field practitioners as an efficient remediation technology, regulatory approval has been lagging mainly because of challenges associated with consistently demonstrating its occurrence (Davis et al., 2023). The research presented herein focuses on expanding available tools (e.g., development of an RNA purification protocol from LNAPL impacted soils) and on demonstration of the merits of synergistic implementation of recently developed continuous monitoring tools (e.g., soil redox sensors, cryogenic sample preservation, and microbiome analysis) under laboratory and field conditions.

The objectives of the work presented herein are to:

1. Develop an RNA purification method suitable for samples containing petroleum liquids. Demonstrate the new RNA purification method's utility to better resolve processes governing the longevity of LNAPL source zones.

2. Couple our understanding of microbial community structure and redox, measured by ORP sensors in soil, to further our ability to predict hydrocarbon remediation outcomes based on these parameters.

3. Explore the application of recently developed assessment technologies to an LNAPL site to demonstrate how the integration of these technologies can facilitate the construction of a CSM that supports NSZD.

4. Show how better characterization and NSZD progress monitoring at mid- and late-stage LNAPL sites can, via "a multiple line of evidence approach", support NSZD as a primary remedy.

Benefits of achieving these objectives include:

1. Better protection of human health and the environment.

2. Reduced societal costs for managing subsurface releases of petroleum hydrocarbons.

3. Increased understanding regarding LNAPL biodegradation.

4. A better understanding of validity and utility of continuous soil redox sensors.

1.7. Guide to Content

New microbial tools and sensor technologies for NSZD and ENSZD would be effective and widely adopted if there were a sound interpretation of the monitored parameters. The latter in turn requires a clear understanding of biogeochemical processes and how process shifts may affect the monitored parameters. First, the work presented herein addresses the potential of microbial tools focusing on biodegradation process resolution via the development of a new

RNA extraction method for LNAPL impacted soils. Our new method relies on a soil washing approach that has no adverse effects on RNA recovery and improves RNA quality by removing PCR inhibitors (e.g., XYZ), which in turn allows for characterization of active microbial communities present in petroleum impacted soils. Measuring active microorganisms in LNAPL impacted soils in combination with collection and interpretation of other geochemical data provides valuable insights regarding key biodegradation processes. In addition, this dissertation presents laboratory soil column experiments that explored relationships between characterized microbial ecology and continuous sensor-based soil ORP measurements. In addition to examining these relationships under baseline methanogenic conditions, the experiment was used to study the effects of two different hydrocarbon biodegradation enhancements (pulsed sulfate addition and pulsed air sparging) under representative environmental conditions. Lastly, this research implements emerging NSZD monitoring technologies (cryogenic coring and continuous sensing of soil redox and temperature) to the characterization and monitoring of NSZD at a hydrocarbon-impacted field site. Central to adopting NSZD as a remedy is verifying that NSZD is occurring. As with MNA of dissolved phase hydrocarbons in plumes, multiple lines of evidence can be used to demonstrate and document occurrence and rates of NSZD. Thus, dynamic, high-resolution characterization of LNAPL zones provides a basis for more sustainable remedies for LNAPLs. This case study shows how continuous monitoring at appropriate spatial and temporal scales coupled with a robust biogeochemical characterization can help advance remedies for management of LNAPL impacted sites.

1.8. Publication Status

Chapter 2. ***Advanced methods for RNA recovery from petroleum impacted soils*** was published in MethodsX in 2021 (an Elsevier peer-reviewed Journal) (Irianni-Renno et al., 2021).

Coauthors are Thomas C. Sale and Susan K. De Long**. Chapter 3.** ***Evaluating Natural Source Zone Depletion (NSZD) and enhanced NSZD in Laboratory Columns Via Soil Redox Continuous Sensing and Microbiome Characterization*** was submitted for publication to the Journal of Hazardous Materials and is currently undergoing the peer review process. Coauthors are Jorge L. Rico, Trent A. Key and Susan K. De Long. **Chapter 4.** ***Implementing an Expanded Toolbox for Characterization and Monitoring of NSZD at a mid-to-late-stage LNAPL Release Site*** is undergoing an internal review process with ExxonMobil and is intended to be submitted for publication to Science of the Total Environment (STOTEN), after completion of my Ph.D. Likely co-authors include Jorge Rico, Calista Campbell, Kayvan Karimi Askarani, Trent A. Key, Tom C. Sale and Susan K. De Long.

CHAPTER 2. ADVANCED METHODS FOR RNA RECOVERY FROM PETROLEUM IMPACTED SOILS

2.1. Chapter Synopsis

Microbially-mediated hydrocarbon degradation is well documented. However, how these microbial processes occur in complex subsurface petroleum impacted systems remains unclear, and this knowledge is needed to guide technologies to enhance microbial degradation effectively. Analysis of RNA derived from soils impacted by petroleum liquids would allow for analysis of active microbial communities, and a deeper understanding of the dynamic biochemistry occurring during site remediation. However, RNA analysis in soils impacted with petroleum liquids is challenging due to: A) RNA being inherently unstable, and B) petroleum impacted soils containing problematic levels of polymerase chain reaction (PCR) inhibitors that must be removed to yield high-purity RNA for downstream analysis. A previously published soil wash pretreatment step and a commercially available DNA extraction kit protocol were combined and modified to be able to purify RNA from soils containing petroleum liquids.

- A key modification involved reformulation of the pretreatment solution by replacing water as the diluent with a commercially available RNA preservation solution.
- Methods were developed and demonstrated using cryogenically preserved soils from three former petroleum refineries. Results showed the new soil washing approach had no adverse effects on RNA recovery and did improve RNA quality by PCR inhibitor removal, which in turn allows for characterization of active microbial communities present in petroleum impacted soils.

- In summary, our method for extracting RNA from petroleum-impacted soils provides a promising new tool for resolving metabolic processes at sites as they progress toward restoration via natural and/or engineered remediation.

2.2. Introduction

Broad realization has come to the fact that soils, comingled at a pore-scale with nonwetting petroleum liquids, are populated by microbes that can transform petroleum into CO_2. Surprisingly, rates of depletion of petroleum liquids via microbially-mediated processes commonly rival and/or exceed depletion rates achieved with engineering remedies (Garg et al., 2017; Sale et al., 2018) These processes of converting petroleum liquids in soil-groundwater systems are referred to as natural source zone depletion (NSZD) per ITRC (2009).

NSZD has been well-demonstrated through various lines of evidence, including quantification of CO_2 efflux through the vadose zone using a gas gradient method (Lundegard et al., 2006), the dynamic chamber method (Sihota et al., 2013), and CO_2 traps (McCoy et al., 2015). Also, and perhaps more definitively, NSZD has been demonstrated by quantification of the heat generated from biotic oxidation of petroleum hydrocarbons in soil groundwater (Karimi Askarani et al., 2018; Karimi Askarani et al., 2020). Biotic oxidation of petroleum hydrocarbons, like oxidation of organic composts, produces CO2 and heat.

While the fact that NSZD happens is clear, the microbially-mediated biochemistry of NSZD, and how it might be enhanced, is not clear. A promising approach to better resolving the biochemistry of NSZD is characterization of microbial communities in soils impacted with petroleum liquids (Irianni-Renno et al., 2016; Lovely et al., 1993; Zeman et al., 2014). However, most hydrocarbon source zone research has characterized systems at the DNA level (Garg et al., 2017; Irianni-Renno 2016), only providing information on microbe presence. Since presence or

absence of a genetic sequence does not reflect active (biodegrading) or even viable microbes, DNA-based analysis might paint an incomplete picture of processes driving hydrocarbon biodegradation at the time of sampling. In contrast, assessing a microbial community at the RNA level provides more direct information regarding active organisms at impacted sites. Herein, methods are advanced for RNA purification, quantification of gene expression, and sequencing in support of resolving the active (RNA-based) vs. the historical (DNA-based), metabolic processes driving NSZD. The challenge for RNA-based characterization of microbial ecology is the molecular instability of RNA, and petroleum-impacted sites present a unique challenge in this regard. Given instability, preservation during purification of RNA is critical. With respect to RNA preservation at contaminant-impacted field sites, cryogenic collection of soil samples is promising (Kiaalhosseini et al., 2016; Olson et al., 2017). The primary challenge with resolving active microbial ecologies in soils impacted by petroleum liquids is extraction and purification of high-quality RNA. Herein, a novel sample pretreatment procedure is advanced ("Step 2", Methods section) for removing polymerase chain reaction (PCR) inhibitors from soils containing petroleum liquids, while preserving the integrity.

Techniques are demonstrated using soil cores collected from three former petroleum refineries (Sites). The benefits of the new pretreatment wash method are demonstrated with samples from Site 1, spiked with *E. coli* as a source of RNA. Improved RNA quality and lack of inhibitors is further demonstrated with samples from Site 2. Lastly, samples from Site 3 are used to illuminate that subsurface microbial communities are dynamic, as evidenced by differences between the microbial phylotypes that were active at the time of sampling (RNA) and the microbial phylotypes that were present (DNA). Microbial data combined with other Site 3 characterization (unpublished data) provided evidence for a transition from historical

anaerobically-mediated NSZD to an emerging, more aerobic, NSZD at the leading edge of a subsurface petroleum pool. Overall, documented RNA methods combined with DNA data provide a promising new tool for resolving the dynamic biochemistry of sites as they progress toward restoration via natural and engineered remedies.

2.3. Research Objectives

The objectives of this chapter are to 1) develop an RNA purification method suitable for samples containing petroleum liquids and 2) demonstrate its utility to better resolve processes governing the longevity of LNAPL source zones.

2.4. Methods

The following describes our RNA extraction methods and demonstrative applications of our methods using soil core from three former refineries. In order to continue with downstream PCR based analysis, recovered RNA is transcribed to stable cDNA (a DNA copy of the recovered RNA), and cDNA is used to resolve RNA-based microbial communities.

2.4.1. RNA Extraction Procedures

Figure 2.1 provides an overview of our extraction workflow and subsequent analyses. The following outlines key steps in RNA isolation from soil matrices impacted by petroleum hydrocarbons.

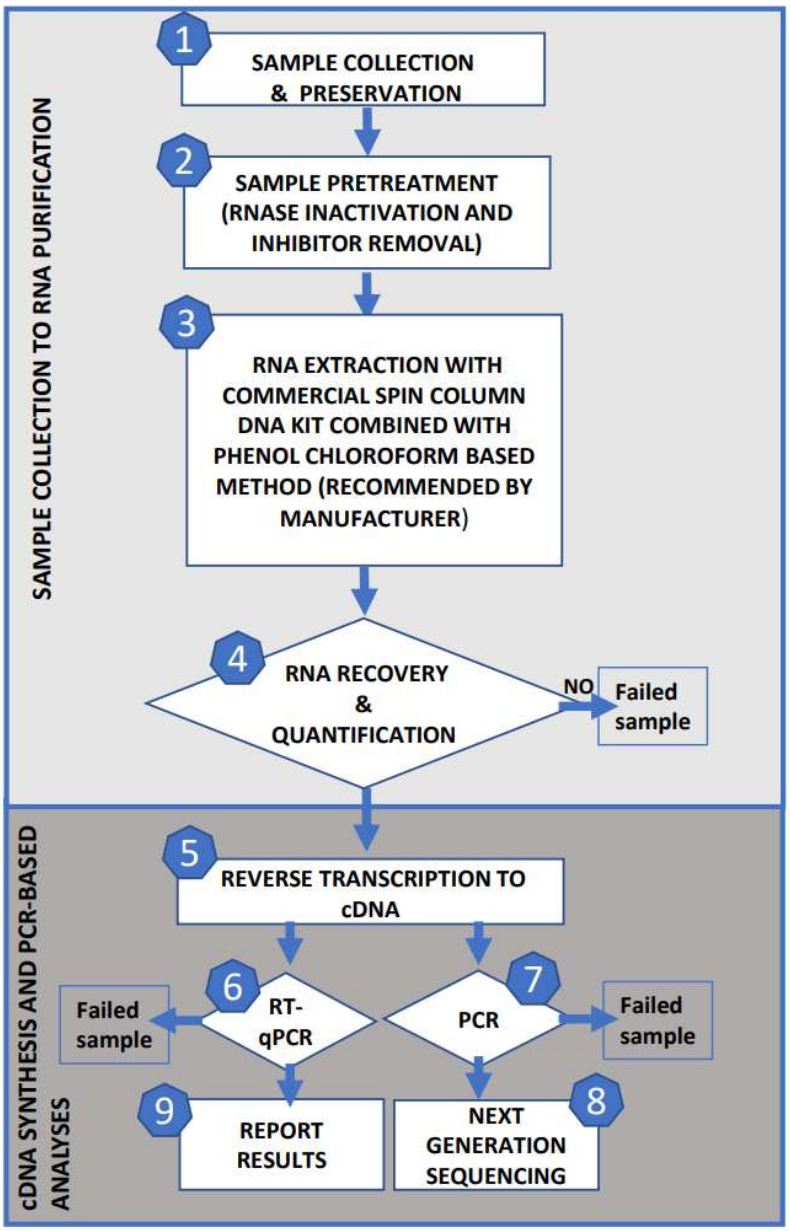

Figure 2.1. Flow chart summary of RNA processes. Sample processes are summarized, from sample collection to RNA purification, followed by cDNA synthesis and PCR based analyses.

The novel aspect of our method (Step 2) involves a modification of a previously published sample pretreatment wash (Kraan et al., 2010) used to purify DNA from petroleum liquid impacted soils. Our methods include washing samples with sodium chloride, disodium-EDTA, TritonX-100, dehydrated skimmed milk and polydeoxinocinic-deoxycytidilic-acid

(pdIdc) to remove PCR inhibitors (e.g., XYZ). Disodium-EDTA chelates metals, such as iron, so metals do not precipitate out of solution (Zaitoun et al., 1997). Iron is found at sites impacted by petroleum liquids and interferes with PCR-based reactions. Low concentrations of a mild detergent, such as TritonX-100, will not lyse cells but promotes petroleum desorption, allowing petroleum liquids to float at the top of the wash solution (Sui et al., 2010). Dehydrated skimmed milk, in high salinity environments, binds biological macromolecules such as lipids and sugars (Livney, 2010). Organic molecules and chelated metals in solution are removed from the soil mix via discarding the supernatant in each washing step, after centrifugation. Polydeoxinocinic-deoxycytidilic-acid (pdIdc) is a nucleic acid surrogate and may interact with RNAses. Further, our modification consists of replacing deionized (DI) water as the wash solution diluent with LifeGuard™ solution (Qiagen, Germantown, MD), to protect RNA from degradation during inhibitor removal wash steps. In addition to preserving nucleic acid integrity, by inactivating RNASes, LifeGuard™ solution prevents new microbial growth (Qiagen, Germantown, MD). Referenced solutions C1-C6 are proprietary components of the PowerSoil Powerlyzer™ DNA isolation kit (Qiagen, Germantown, MD).

2.4.1.1. Sample Collection and Preservation

Attributes of soil sample collection sites and soil sample collection methods are presented in Table 2.1. All samples were shipped for analysis to Colorado State University (CSU).

Table 2.1. Site attributes and sampling method

	Site 1	Site 2	Site 3
Site History	Crude oil refinery 1923 to 1982	Crude oil refinery 1904 to 1982	Crude oil refinery 1931 to 1986
Depositional Environment / Sediment	Braided stream channel deposit/Poorly sorted sands and gravel	Overbank flood plain deposit/ fine grained sand and silt	Glacial valley train deposit/ Poorly sorted sands and gravel
Primary Petroleum Liquids	Weathered gasoline and diesel	Weathered gasoline, diesel, and jet fuels	Weather gasoline, jet fuel, and diesel
Sampling Method	Direct push sampling of a single hole	Cryogenic coring (Kiaalhosseini et al., 2016)	Cryogenic coring per (Kiaalhosseini et al., 2016)
Samples and sample depth(s) below ground surface (bgs)	S1A – 2.4 m S1B – 0.2 m	S2 – 2.6 m	S3A, S3B, S3C – Samples collected from co-located triplicate boring from 9.3 m
Sample Preservation	Non-cryogenic direct push core collection. Sample immediately placed in a cooler with ice and shipped overnight to CSU. Stored at -20 °C until analyzed.	Liquid nitrogen-based cryogenic hollow stem auger core collection. Sample immediately placed in a cooler on dry ice in the field and shipped overnight to CSU. Stored at -80C° until analyzed.	
Total Petroleum Hydrocarbon Carbons in Soil (TPH)	S1A – 8500 mg/kg, 90% diesel range, 10% gasoline range S1B – <10 mg/kg	S2– 11,270 mg/kg 70% diesel range, 30% gasoline range	S3A – 12,917 mg/kg, 59% diesel range, 41% gasoline range S3B– 11,776' mg/kg, 51% diesel range, 49% gasoline range S3C – 8658mg/kg, 40% diesel range, 60% gasoline range

2.4.1.2. Sample Pre-treatment

A) Five-gram frozen soil samples were removed from the freezer and placed in 50ml centrifuge tubes. B) 80 ng of dehydrated skimmed milk (VWR, Radnor PA.), 10 µg of pdIdc (Sigma-Aldrich, St. Louis, MO), and 1 ml of LifeGuard™ Soil Preservation Solution (Qiagen, Germantown, MD) were added to each sample. PdIdc and milk casein, present in the added dehydrated skimmed milk, act as adsorption competitors for nucleic acids. C) The soil mixtures were vortexed with a Gennie-II vortex (Qiagen, German, MD) for one minute and were incubated on ice for an additional minute. D) Next, pretreated soil samples were washed three times with three different solutions (described below). E) Between washes the samples were vortexed for 2 min, centrifuged at 13,000 rpm for 3 min in a Sorvall Legend XTR™ centrifuge

(Thermoscientific, Ashville, NC), and the supernatant discarded. F) During the first wash step, the reagents added to the mixture were: 8 ml of Lifeguard™ preservation solution, 500 µl of 50 mM trisHCl (pH=8.3) (Sigma-Aldrich), 400 µl of 200 mM NaCl (VWR), 100 µl of 5 mM Na2EDTA (Sigma-Aldrich), and 5 µl of Triton X-100 (5% V/V) (Sigma-Aldrich). G) During the second wash step the following was added to the mixture: 9 ml of LifeGuard™ Soil Preservation Solution followed by the addition of 500 µl of 50 mM tris-HCl (pH=8.3), 400 µl of 200 mM NaCl, and 100 µl of 5 mM Na2 EDTA. H) The third washing solution contained 9.4 ml of LifeGuard™ Soil Preservation Solution, 500 µl of 50 mM tris-HCl (pH=8.3), and 100 µl of 5 mM Na2 EDTA. After centrifugation and supernatant discard, the remaining soil solutions were ready for RNA extraction.

2.4.1.3. RNA Extraction

RNA was extracted using the PowerSoil Powerlyzer™ DNA isolation kit (Qiagen, Germantown, MD), via an alternative protocol with modifications adapted to isolate and purify RNA. In detail, A) approximately 0.5 g of pretreated sample (or untreated for controls) were added to a dry bead tube from the commercial kit (compared to the manufacturer recommended 0.25 g.) B) Next the following were added to each sample: 500 µl of the kit Bead Solution including 200 µl phenol:chloroform:isoamyl alcohol (pH 7-8) (Amresco, Solon, OH), and 60 µl of Solution C1. The addition of 200 µl phenol: chloroform: isoamyl alcohol (pH 7- 8) was a modification recommendation by the manufacturer (MoBio) and is not included as part of the protocol provided with the commercial kit. C) The tubes were then vigorously shaken in a PowerlyzerTM (Qiagen, Germantown, MD.), according to the kit's provided protocol. D) After 1 minute of full-speed (13,000 rpm) centrifugation, solution C2 (200 µl) and solution C3 (100 µl) were added to the supernatant. E) Each mixture was incubated for 5 minutes at 4 °C and then

centrifuged again for 1 minute. F) The supernatant (approximately 650 µl) was removed to a new centrifuge tube and combined with 650 ul of solution C4. G) The resulting lysate preparation was vortexed vigorously for 5 seconds. H) Next, 650 µl of the vortexed solution were added to the kit's purification columns in new centrifuge tubes. I) After sample binding to the columns, the columns were washed with 650 µl of 100% ethanol followed by a wash with 500 µl of Solution C5. J) The columns were then dried by centrifugation (2 minutes at 13,000 rpm), prior to being transferred to a clean centrifuge tube.

2.4.1.4. RNA Recovery and DNA Removal

A) RNA elution was performed with 50 µl of Solution C6. B) The purified RNA was treated (according to protocol provided by manufacturer) with AMBION DNA-Free™ DNase (Life Technologies, Grand Island, NY) to remove co-extracted DNA prior to C) RNA quantification via optical density at 260 nm with a NanoDrop (Thermoscientific, USA).

2.4.1.5. RNA Transcription to cDNA

RNA was reverse transcribed to cDNA utilizing the SuperScript™ IV First-Strand Synthesis System (Invitrogen, Carlsbad, CA).

2.4.1.6. Reverse Transcription Quantitative Polymerase Chain Reaction (RT-qPCR)

Assays were prepared as 25 µl reactions in a 96-well plate as follows. (A) A master mix was prepared by adding 12.5 µl of Power SYBR Green™ qPCR reaction mix (2X) (Life Technologies, Grand Island, NY), 1.5 µl forward and reverse primers (2.5 µM), and 7.5 µl PCR grade water. (B) Then, 23 µl of the master mix was added to each reaction well, followed by (C) the addition of 2 µl 0f 0.5 ng of cDNA template (based on OD260) to each well. Commercially available genomic DNA (America Type Culture Collection) was used as calibration standards. (D) Once the well plate was prepared, it was run using an ABI 7300 real-time PCR system

(Applied Biosystems, Foster City, CA) programmed with the following thermocycling conditions: 95 °C for 10 min, followed by 40 cycles of 95 °C for 45 s, 56 °C for 30 s, and 60 °C for 30 s. (E) Dissociation curve (i.e., melt curve) analysis was conducted to confirm amplicon specificity. (F) For each target assay, primer sets and genomic DNA controls were chosen per current published methods including: (i) bacterial 16S rRNA transcripts (Suzuki et al., 2000), (ii) archaeal 16S rRNA transcripts (Suzuki et al., 2000), (iii) methanogens via *mcrA* (Juottonen et al., 2006) and R15 (McGenity et al., 2016), (iv) anaerobic benzene degraders via *abcA* (Waals et al., 2017), (v) anaerobic alkane degraders via *assA*, primer set *assA2F/ass A2R*, (Aitken et al., 2013), and (vi) alkane oxidizers via *alkB* (Guo et al., 2017).

2.4.1.7. PCR Amplification

A) 15 to 20 µl of cDNA and DNA from samples 3-A, B and C obtained from environmental triplicates were placed in centrifuge tubes and shipped on blue ice to Research and Testing Laboratory, LLC (Lubbock, TX) for analysis of active and total present microbial communities. B) As a first step, and prior to sequencing the samples, Research and Testing Laboratory, LLC (Lubbock, TX) generated barcoded 16S rRNA amplicons via PCR amplification from the provided cDNA and DNA

2.4.1.8. Next Generation Sequencing PCR Amplification

A) If generated, 16S rRNA amplicons (see step 7) were sequenced via Illumina MiSeq following methods described in (Irianni-Renno et al., 2016). B) Sequence data analysis was performed by Research and Testing Laboratory, LLC using the RDP classifier in conjunction with the Silva database for taxonomic identification of the 16S rRNA sequences (https://www.arb-silva.de/). C) Relative abundance (%) data generated by sequencing were used to construct histograms that represent active and total microbial community composition for each sample,

based on their phylogeny. Analyses were done at the genus level. In cases where genera were unclassified, higher level taxonomic identifications are reported, but grouped taxa shared >97% sequence identity.

2.4.2. Methods Demonstration

Demonstration variables and details regarding core samples are presented in Table 2.2. Demonstration variables include 1) sample preservation, 2) *E. coli* spikes 3) absence/presence of petroleum liquids, and 4) inclusion/exclusion of pretreatment Step 2. Non-cryogenically preserved Site 1 samples, spiked with *E. coli*, provided a basis for resolving RNA recovery given a known amount of RNA. Due to the non-cryogenic preservation of Site 1 samples, little, if any, RNA was likely present in the sample prior to *E. coli* spiking. Cryogenically preserved petroleum impacted samples from Site 2, analyzed with and without Step 2, provided a basis for demonstrating the merits of our methods with respect to the quality of the recovered RNA. Site 3 data document an NSZD-driven shift in microbial ecology by comparing communities observed at the RNA and DNA levels at the leading edge of a petroleum body; the plume leading edge was identified by additional, unpublished results from site investigations. The following describes methods associated with samples from each of the study sites.

Table 2.2. Summary of demonstration variables and study samples

	Cryogenic Preservation	Petroleum Liquids	*E. coli* Spike	Step 2 – Sample Pretreatment
S1A-1 to S1A-3 - Triplicate	No	Yes	Yes	Yes
S1A-4 to S1A-6 -Triplicate	No	Yes	Yes	No
S1B-1 to S1B-3 - Triplicate	No	No	Yes	Yes
S1B-4 to S1B-6 - Triplicate	No	No	Yes	No
S2-1 to S2-3 - Triplicate	Yes	Yes	No	Yes
S2-4 to S2-6 - Triplicate	Yes	Yes	No	No
S2-7 to S2-9 - Triplicate	Yes	Yes	No	Yes
S3A, S3B, S3C - Field triplicate*	Yes	Yes	No	Yes

* (each split for RNA and DNA characterization).

Site 1 - A) *E. coli* was grown overnight in LB medium at 37 °C. B) When the *E. coli* culture contained approximately 8 x10^8 cells per ml, 3 ml (in two 1.5 ml aliquots) of culture were pelleted by centrifugation at 3000 rpm for 5 minutes. The supernatant was removed, and the pellet was re-suspended in 200 µl of lysis buffer from the Powerlyzer™ DNA extraction kit (Qiagen, Germantown MD). S1A and S1B samples (30g) were each homogenized with a mortar and pestle. C) After homogenization, the S1A and S1B samples were subdivided into six subsamples (5g each), and each subsample was spiked with approximately 2.4 x109 *E. coli* cells suspended in 200 µl lysis buffer. D) Lastly, the spiked soil samples were flash frozen using liquid nitrogen to simulate cryogenic sample preservation and stored at -80°C until RNA extraction. Samples were extracted following described methods including and excluding "Step 2", and after DNase treatment, RNA yielded by all samples was quantified as described in Step 4 and reported as µg of RNA / g of soil.

Site 2 - A) RNA was extracted from triplicate subsamples of S2 (S2-1 to S2-3) and analyzed using the steps in our procedure. Similarly, triplicate subsamples of S2 (S2-4 to S2-6) were extracted excluding Step 2 (sample pre-treatment). B) Four different masses of RNA (0.5, 1, 2.5 and 5 ng) were analyzed via RT-qPCR for each extraction to determine quantities of 16S rRNA transcripts present, as a function of ng of RNA. The objective of this experiment was to

determine the suitability of the RNA obtained with or without the pretreatment (Step 2), for quantification of 16S rRNA via RT-qPCR. At a later time, other S2 samples were extracted in triplicate (S2-7 to S2-9) and analyzed via RT-qPCR, targeting common hydrocarbon degradation biomarker genes to verify that the RNA yielded by extraction with the newly developed method also was suitable for performing analyses relevant to degradation of petroleum liquids.

Site 3 - A) RNA extracted from S3 field triplicates was analyzed via next generation sequencing (NGS) as detailed in Step 8. B) In addition, DNA was also extracted from samples S3 A, B and C following methods described in (Irianni-Renno et al., 2016) and sequenced following methods outlined in Step 8. C) DNA and cDNA sequence data were used to identify microbial communities present, and active, in the surveyed soils. Objectives for sequencing DNA and cDNA obtained from field triplicate S3 samples include: 1) to evaluate the feasibility of performing sequencing analyses with cDNA obtained from RNA purified with our described method, and 2) to document additional information gained from preforming sequencing analysis targeting microbes that are both present and active, instead of just microbes present.

NGS for S3 samples provided phylogenetic identities and % abundance for the active and present microorganisms. Sequence data were analyzed as described previously (Irianni-Renno et al., 2016). Briefly, The RDP classifier was used in conjunction with the Silva database for taxonomic placement of the 16S rRNA sequences analyzed (https://www.arb-silva.de/). Relative abundance (%) data were used to construct bar charts that show microbial community composition for each sample, based on their phylogeny.

2.5. Results

Figure 2.2 shows RNA recovery from the *E. coli* spiked Site 1 soils with and without petroleum liquids and with and without Step 2. With Step 2, mean RNA recovery from

petroleum impacted samples is 35% greater than without Step 2. By contrast, mean RNA recovery from samples without petroleum is 20% less with Step 2 than without it. However, results from Tukey adjusted p-value analysis performed on RNA yield after ANOVA showed that there were no significant differences in RNA recovery between samples extracted with or without Step 2, for both samples with and without petroleum liquids. A limitation of the Figure 2.2 data is that the form and distribution of RNA in the *E. coli* spiked samples may not be representative of RNA in field soils. Microbes, and their RNA, in field vadose zone soils occur primarily as thin biofilms in water bound to soil surfaces (Or et al., 2007).

Step 2's main function is removing PCR inhibitors that compromise RNA utility for downstream analyses, including characterization of microbial ecology via transcript quantification with RT-qPCR or sequencing (Toni et al., 2018). For example, the presences of metallic ions such as iron in solution (Sidsted et al., 2020) and organic acids are known to inhibit PCR reactions (Albers et al., 2013). Both ferrous iron and organic acids are common byproducts of petroleum biodegradation (Coates et al., 1995), and thus potentially be present in petroleum impacted samples. Molecular assay disruption can include inaccurate quantification of transcripts or even non-detection of molecular targets. RNA was extracted from Site 2 soils with and without Step 2 and copied to cDNA yield. Results are reported as μg RNA/g of soil.

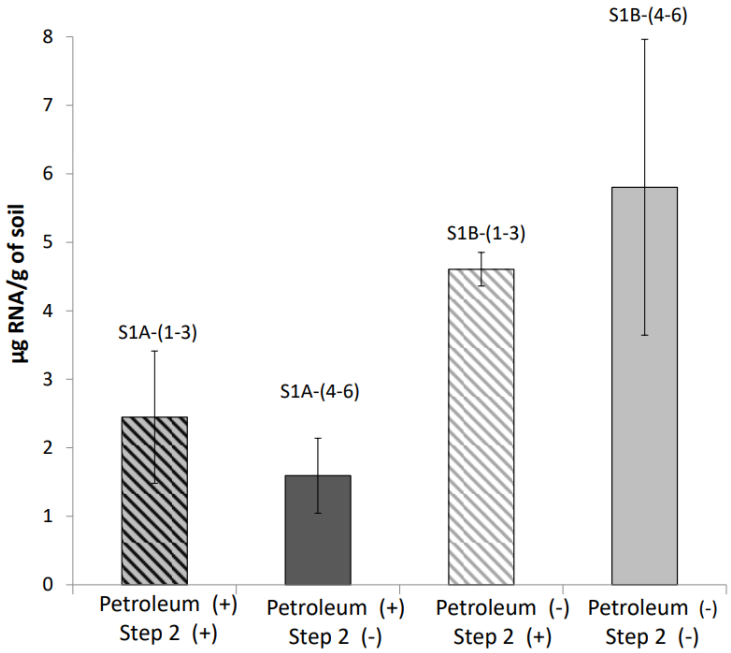

Figure 2.2. Site 1 RNA yield per g of soil. Error bars show 95% confidence intervals for an n=3.

Figure 2.3 shows bacterial 16S rRNA transcripts as a function of the RNA mass used for samples from S2-1 to S2-6. Results of RT-qPCR analyses using Step 2 show a linear relationship between 16S rRNA transcripts quantified and RNA mass used for analysis, which demonstrates inhibitors were well removed by Step 2. In contrast, results of RT-qPCR excluding Step 2 do not show an appropriate linear relationship between 16S rRNA transcripts quantified and RNA mass. The lack of an appropriate linear relationship between transcript or gene quantities and template mass is attributable to inhibitors (Kontanis et al., 2006).

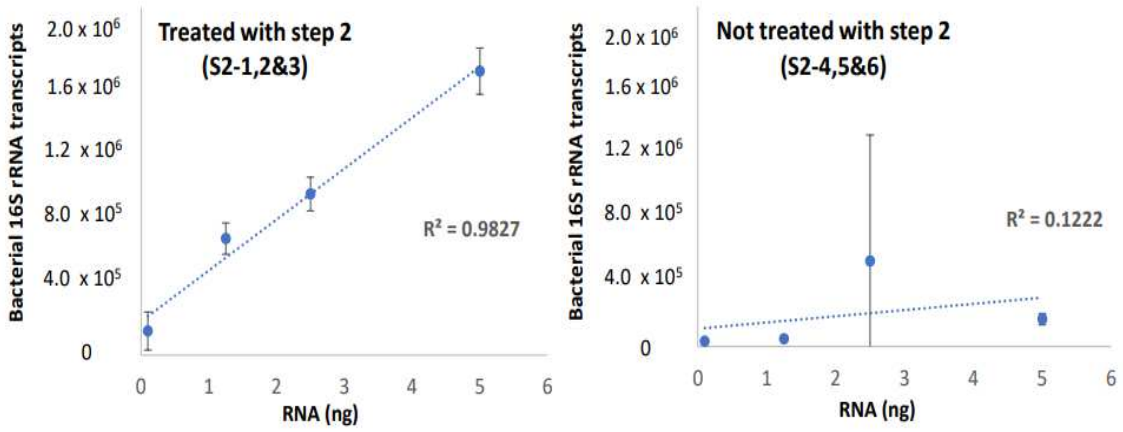

Figure 2.3. Bacterial 16S rRNA transcripts versus RNA mass.

Continuing with Site 2, Figure 2.4 plots *alkB*, *R15* and *mcrA* transcripts as a function of the mass of RNA analyzed for samples S2-7 through S2-9. RNA from samples S2-7 through S2-9 was extracted including pretreatment Step 2. RT-qPCR data shown on Figure 2.4, targeting petroleum degradation processes, show a linear relationship between detected transcripts and template mass. Detected hydrocarbon degradation biomarkers in S2-7 through S2-9 include expressed *alkB* genes, which encode part of an alkane hydrolase. *alkB* is an enzyme involved in alkane degradation under aerobic conditions (Shao et al., 2013). Detected methanogenic markers included *R15* (phylogenetic marker for aero-tolerant methanogens) and *mcrA* (functional marker for methane reductase). Additional petroleum degradation targets were assayed and not detected, including transcripts for *assA* (which encodes the α subunit of the first enzyme in the anaerobic alkane degradation pathway) and *abcA* (a functional marker for anaerobic benzene degradation). Figure 2.4 results illustrate that RNA obtained with our method is suitable for analysis of a variety of transcripts encoding hydrocarbon degradation enzymes.

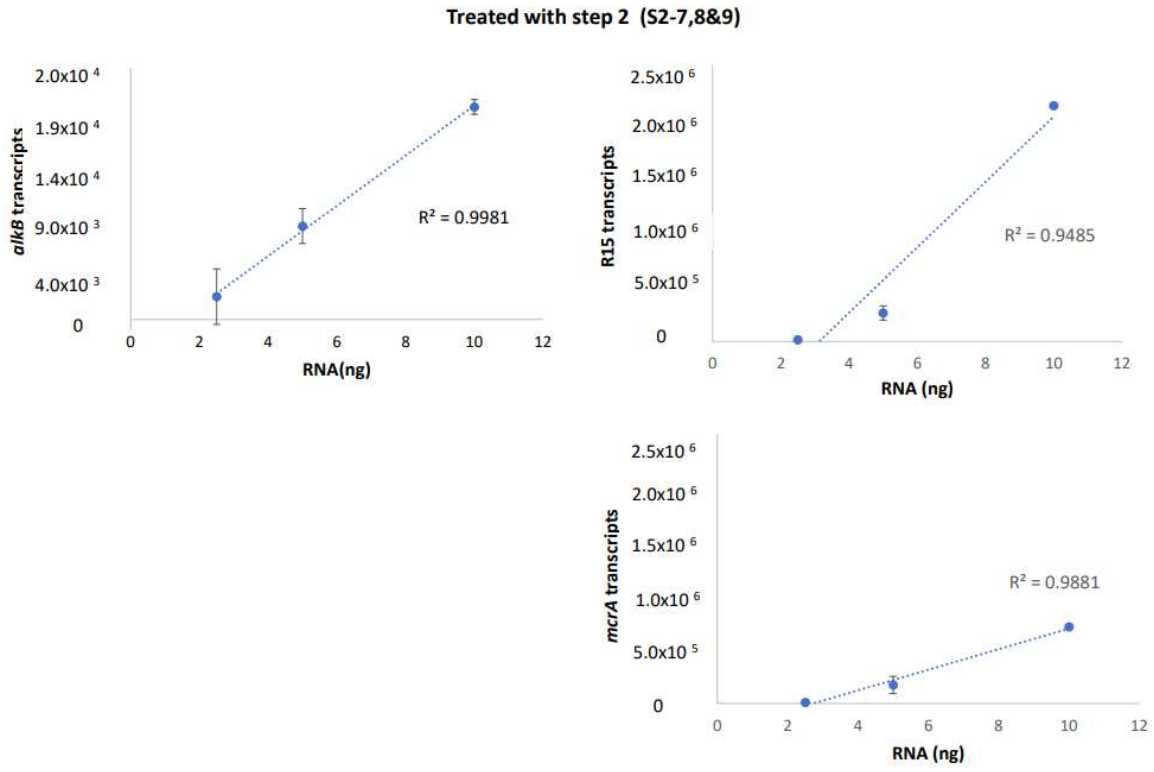

Figure 2.4. *alkB*, *R15* and *mcrA* transcripts versus RNA mass. Analysis was done for sample triplicates S2 -7,8, and 9 extracted including treatment Step 2.

Lastly, Site 3 soils were used to compare microbial communities based on RNA and DNA analyses. Figure 2.5 shows the relative abundance of microorganisms at the identified grouped taxa level (grouped sequences shared >97% identity). Bacterial community analyses were generated by sequencing A) 16S rRNA bacterial genes (DNA) or B) 16S rRNA bacterial transcripts (RNA). Step 2 modifications were only employed for RNA. Microbial communities illuminated by RNA and DNA were distinct. At the DNA level, the community characterization shows taxa previously associated with anaerobic hydrocarbon degradation including putative fermenters such as: *Pelotomaculum* (Scher et al., 2012), unclassified *Clostridia* (Jimenez et al., 2016), *Deltaproteobacteria* (Moreira et al., 2006), *Firmicutes* (An et al., 2013), unclassified *Anaerolineaceae* (An et al., 2013), and *Smithella* (Liang et al., 2015). At the RNA level, Step 2

was employed to obtain RNA in support of resolving microorganisms that were active at the time of sampling. Interestingly, the active bacterial community was predominantly aerobic. Specifically, identified aerobic microorganisms previously associated with hydrocarbon degradation include *Citrobacter* (Liang et al., 2015), *Corynebacterium* (Linda et al., 2012), *Kluyvera* (Shekar et al., 2015), and *Staphylococcus* (Bhuvaneswar et al., 2012).

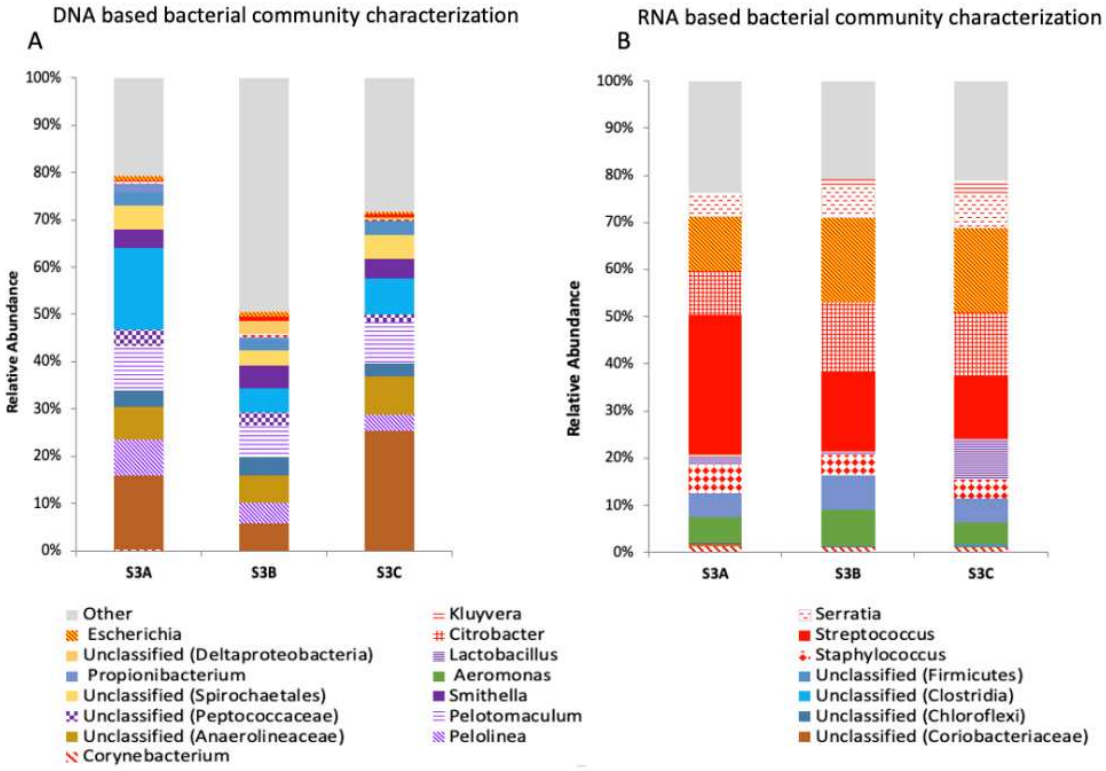

Figure 2.5. Relative abundance of microorganisms. Analyses based on DNA A) and RNA B) acquired from splits of cryogenic samples obtained from 9.3 m bgs. from three adjacent borings. Analyses were done at the genus level. In cases where genera were unclassified, higher level taxonomic identifications are reported but grouped taxa shared >97% sequence identity.

Identifying an active aerobic microbial community in the analyzed soil is consistent with on-going historical disappearance of petroleum liquids and degradation products in groundwater wells for the study area. Based on other site characterization efforts, the study area is known to lie at the leading edge of a large historical subsurface body of petroleum liquids. Also

noteworthy in Figure 2.5 are the similarities of identified communities in the three closely located collected cryogenic cores for both the DNA and RNA-based methods, suggesting methods are generally reproducible.

2.6. Conclusions

The pretreatment wash (Step 2) did not improve RNA yield and had no adverse effects on RNA yield. Importantly, clear improvements in purity of the extracted RNA were achieved with Step 2. Benefits of improved RNA purity include a reduced potential for failed or inhibited amplification of molecular targets, which would lead to inaccurate quantification of targeted genes or transcripts and potentially inaccurate relative abundance data from sequencing. Overall cleanup of nucleic acids prior to analyses, such as RT-qPCR and sequencing, can improve the quality of RNA-based characterizations of microbial communities. Lastly, results illustrate that RNA obtained with our method is suitable for the identification and quantification of a variety of transcripts associated with hydrocarbon degradation. An intriguing aspect of this work is the potential to use differences between RNA- and DNA-based characterization of microbial communities to illuminate microbial community activity and dynamics, which play critical roles in progress to site restoration. Herein, the difference between the overall microbial communities present, observed via DNA-based tools, and the active microbial communities, observed via RNA-based tools, is striking. Hydrocarbon degradation kinetics are generally known to be up to an order of magnitude faster under more oxidizing conditions (aerobic and nitrate reducing) versus more reduced conditions (sulfate reducing and methanogenic conditions) (Bojan et al., 2021). Thus, our observation that the active microbial communities at the time of sampling were aerobic is consistent with on-going historical disappearance of petroleum liquids and related compounds in groundwater in wells in the study area, as described in unpublished site

investigation reports. Critically, this insight into the putative role of aerobic microbial metabolism in remediation at study Site 3 would have been overlooked based on DNA analysis alone given that the DNA-based microbial characterization identified a predominantly anaerobic fermenting community. Less than 2% of the microbial community identified based on the DNA analysis was characterized as aerobic. Overall, our methods for extracting RNA from petroleum impacted soils, in combination with DNA data, provide a promising new tool for resolving evolving metabolic processes and biochemistry at sites progressing toward restoration via natural and/or imposed remedies. Ongoing work is focused on further explorations of concurrent RNA/DNA based characterization of microbially mediated processes contributing to restoration of sites impacted by petroleum hydrocarbons and other contaminants of concern.

CHAPTER 3. EVALUATING NATRUAL SOURCE DEPLETION (NSZD) AND ENHANCED (NSZD) IN LABORATORY COLUMNS VIA SOIL REDOX CONTINOUS SENSING NAD MICROBIOME CHARACTERIZATION

3.1. Chapter Synopsis

Implementation of natural source zone depletion (NSZD) and enhanced NSZD (ENSZD) as remedies for light non-aqueous phase liquids (LNAPL) rely on a multiple-lines-of-evidence based approach that requires effective monitoring. Redox evolution of an LNAPL-impacted subsurface can reflect ongoing biogeochemical LNAPL degradation pathways and provide information regarding NSZD and ENSZD progress. Emerging uses of ORP sensors show promise to continuously resolve soil redox conditions. However, further understanding of soil redox dynamics and how these conditions relate to subsurface microbial activities and LNAPL degradation is needed. In this work, using columns containing LNAPL-impacted soils from a former petroleum refinery, we evaluate the merits of soil redox sensors to monitor performance of two known NSZD enhancements, biostimulation with periodic sulfate addition or periodic air sparging. After enhancements were tested, the columns were cryogenically preserved and their microbiomes were analyzed via DNA and RNA sequencing, along with geochemical parameters. Results show expected relationships between continuous soil redox measurements and active microbial communities. Additionally, continuous data revealed spatial and temporal detail that informs interpretation of the hydrocarbon biodegradation data. Periodic sulfate doses of 1.3+/-0.6g to 0.7L of the soil column system resulted in transient redox increases in both sulfate enhanced columns. However, subtle differences were observed in the redox patterns between sulfate reducing columns that were likely associated with methanogenesis. Periodic pulses of 25L of air to 0.7L of the soil column system did not result in fully aerobic conditions suggesting

that improvements in biodegradation may be explained by alternative anaerobic metabolisms (e.g., iron reduction due to air oxidizing reduced iron). Additionally, microbiome analysis revealed insights into how hydrocarbon concentration and composition impacted microbiome structure and activity within investigated redox ranges. These collective data suggest that combining continuous redox sensing with microbiome analysis can provide insights beyond those possible with either monitoring tool alone.

3.2. Introduction

At sites impacted by light non-aqueous phase liquids (LNAPL), natural source zone depletion (NSZD) processes can be sufficient to achieve site restoration (Garg et al., 2017; Kulkarni et al., 2020; Sihota et al., 2011). LNAPL mass removal through NSZD mass have been found to be comparable to those achieved by engineered systems (Sihota et al., 2018) and even surpass mass removal rates achieved via engineered systems (Mccoy et al., 2015). It has been shown that natural attenuation of hydrocarbon plumes can be enhanced via subsurface biogeochemical manipulation such as air sparging, sulfate and nitrate addition (Chen et al., 2010; Jørgensen, 2011). Additionally, recent work has shown that LNAPL source zone depletion by naturally occurring processes can be further enhanced by sulfate addition to the subsurface via induced infiltration by land surface application (Sra et al., 2023). NSZD and enhanced NSZD (ENSZD) are attractive remedial strategies for hydrocarbon sites given that they can be efficient, cost-effective, lower energy or resource consumption alternatives compared to active remedies (Pishgar et al., 2022; Statham et al., 2023). However, appropriate tools are needed to elucidate ongoing biodegradation processes at field sites, for monitoring, and to demonstrate and quantify the effectiveness of NSZD and ENSZD as compared to other hydrocarbon remediation technologies (Bouchard et al., 2018).

Herein, we explore the use of continuous multiple-level oxidation-reduction potential (ORP) sensors in soil (Sale et al., 2021) combined with microbiome analysis, as a monitoring strategy for NSZD and ENSZD of LNAPL impacted soil in laboratory columns. Soil redox, an indicator of electron acceptor availability, constrains the potential hydrocarbon biodegradation processes (e.g., aerobic biodegradation processes can only occur under aerobic redox). Further, microbial community structure and activity is dynamically influenced by and influences evolving redox conditions, and active biodegradation processes are dependent on the microorganisms present. As redox dictates energetic gain from reducing an organic contaminant (Levar et al., 2017), when multiple electron-accepting processes are feasible, the redox regime will determine the process that occurs. Compared to redox measurement, molecular microbial analyses cannot be deployed currently to provide continuous field data. Combining temporally discrete molecular analysis of subsurface microbiomes with continuous redox sensor application can be used to provide insight regarding the dynamic microbiological activities that underly remediation outcomes. Thus, a key component of this work was to establish relationships between measured redox in soils and microbiomes. While advancing knowledge regarding this novel continuous monitoring strategy, this work also explores the effect of two ENSZD technologies, periodic sulfate addition and pulsed air sparging (including biosparging), for soils derived from a late stage LNAPL impacted site (characterized by nearly-complete depletion of LNAPL) (Sale et al., 2018). The work includes efforts to better understand microbial processes governing NSZD and characterize the merits of continuous soil redox sensors to monitor enhancements.

While NSZD can outperform *in situ* or *ex situ* engineered remedies, process enhancements (i.e., ENSZD) may be required to achieve clean-up goals (Bouchard et al., 2018). Two commonly practiced enhancements are sulfate addition (Kolhatkar & Schnobrich, 2017)

and pulsed air-sparging (Azubuike et al., 2016). Periodic sulfate addition (Kümmel et al., 2015; Wei et al., 2018; Zhang et al., 2021) and pulsed air-sparging (Clarke et al., 2018; Johnson et al., 2001) are both field scalable technologies and have been demonstrated to enhance degradation of petroleum hydrocarbon constituents (e.g., benzene, naphthalene, etc.). While research has been published regarding the implementation of these hydrocarbon attenuation enhancement technologies (Adams & Reddy, 2003; Davis et al., 2022; Mancini et al., 2003; Wartell et al., 2021;), enhancement mechanisms are not fully understood, hindering accurate prediction of treatment outcomes (Boll et al., 2020). LNAPL sites are biogeochemically complex and evolving, in great part, due to the occurrence of NSZD (Bruckberger et al., 2021; Irianni-Renno et al., 2016), and introduction of external sources of electron acceptors adds further complexities.

Sulfate is a viable electron acceptor, but there are several pathways that can lead to sulfate utilization during LNAPL degradation, and controlling parameters that drive the activation of individual hydrocarbon constituent biodegradation pathways in mixtures are not well understood (Meckenstock et al., 2015; Michas et al., 2020; Wartell et al., 2021). The different biodegradation pathways observed under sulfate-reducing conditions in hydrocarbon rich environments have been linked to hydrocarbon-composition (Shafieiyoun et al., 2020). The addition of sulfate to environments with only polycyclic aromatic hydrocarbons (PAHs) as the carbon source have resulted in sulfate serving as the electron acceptor for the oxidation of hydrocarbons, including naphthalene (Shafieiyoun et al., 2020) and phenanthrene (Shin et al., 2019). In other studies, where alkanes such as hexane were present, the addition or presence of sulfate was associated with bolstering methanogenesis via the production of hydrogen from the fermentation of hydrocarbons (Embree et al., 2015; Ma et al., 2017; Shin et al., 2019). Further

knowledge regarding the system response to sulfate addition is needed to optimize hydrocarbon enhancements and to be able to predict long-term contaminant fate.

Air sparging adds oxygen, typically by bubbling atmospheric air (78% N_2, 21% O_2, balance other gases), into the formation. Pulsing replenishes oxygen and renews mixing (Johnson et al., 2001). Additionally, sparged air delivered to into the aquifer can stimulate aerobic hydrocarbon degradation (i.e., biosparging) (Johnson et al., 2001). Unfortunately, with air, remedy efficacy can be limited by low oxygen content relative to stoichiometric demand and by mass transfer from sparse entrapped air bubbles. Additionally, reactive minerals in the subsurface, such as iron sulfides, can exert an oxygen demand. Kinetics likely favors the reoxidation of these minerals (Dong et al., 2022; Hunter et al., 1998) so the addition of air to methanogenic environments can result in activation of alternative anaerobic hydrocarbon degradation pathways, such as those depending on iron and manganese oxides or sulfur-based compounds as electron acceptors.

Varying subsurface geochemistry, whether by naturally occurring processes or via enhancement addition, affects the subsurface redox environment, microbiology, and consequentially biodegradation processes (Patel et al., 2022; Snousy et al., 2017; Yin et al., 2021). How specific enhancements and their delivery affect the subsurface biogeochemistry remains poorly understood. Given the complexity and heterogeneity of subsurface environments, outcomes could be predicted most accurately with measurement data at high spatial and temporal resolution, elucidating processes at relevant scales and in sufficient detail. Advances in internet of things (IOT) technologies have brought continuous sensing to the forefront of industrial monitoring and present an opportunity for the remediation industry. Currently, there are limited practical tools to monitor redox evolution at LNAPL impacted sites. Emerging uses of ORP

sensors show promise to continuously resolve ORP conditions in soil, and correspondingly, provide insight regarding governing NSZD processes (Burge et al., 2018 - Patent No. 15/237,230; Sale et al., 2021). ORP sensors are currently being used at multiple field sites; S3NSE Technologies reports deployment of their ORP sensors at 18 sites with a data collection rate of 56,600 measurements per day (Sale et al., 2021). Additionally, further research is warranted to improve understanding of how ORP can be interpreted to predict microbial processes governing NSZD and ENSZD.

3.3. Research Objective

The objective of this study is to couple our understanding of microbial community structure and redox, measured by ORP sensors in soil, to further our ability to predict hydrocarbon remediation outcomes based on these parameters.

3.4. Methods

3.4.1. Overview of Approach

Our approach involved ENSZD laboratory column studies with impacted soils from a former petroleum refinery decommissioned in the1980s. Columns were operated under baseline methanogenic conditions with no enhancements, and with periodic sulfate addition and pulsed air sparging. Results advance novel insights regarding NSZD biodegradation processes, merits and limitations of sulfate and air sparging ENSZD, and utility of multilevel ORP sensors in soil systems.

In this study, soils from a former petroleum refinery were employed. Given the age of the spill this soil-LNAPL system can be considered to represent a mature LNAPL site, where LNAPL mobility is reduced, and most of the remaining hydrocarbons have been weathered. Columns were originally set up as described previously (Emerson, 2016). At the beginning of

this study, the columns were equipped with continuous soil redox sensors and gas and water sampling systems. Soil samples were collected from the columns, during sensor installation and at the end of the experiment. At the end of the experiment, soil columns were flash frozen on dry ice and cryogenically preserved for endpoint analyses. Collected soil samples were used to characterize the system biogeochemistry. Aqueous and gas chemistry data were collected periodically for the duration of the experiment. Continuous redox readings were recorded and analyzed, every 30 minutes, for the duration of the experiment. In total each sensor collected at least 20,000 readings. Two soil columns served as baseline controls and were methanogenic; two columns were enhanced by periodic sulfate addition; and two columns were enhanced by pulse air sparging

3.4.2. Description of Soils

An in-depth biogeochemical characterization of the site where the soil used in the columns was originally collected is detailed in Irianni Renno et al., (2016). Soil was collected from the LNAPL-impacted zone, and TPH concentration was approximately 9,000 mg/kg soil. LNAPL was also collected from a well at the field site (Emerson, 2016). This field LNAPL was spiked with commercially available hexacosane, tetradecane, dodecane, naphthalene and benzene at 1.5X the original LNAPL concentrations, such that these spiked compounds were measurable over other TPH. Then different masses of this spiked LNAPL were added to soils, resulting in TPH (C3-C28) concentrations ranging from 9,000 to 37,000 mg/kg. n-hexacosane (CAS 630-01-3, Sigma-Aldrich, St. Louis, MO), n-tetradecane (≥99% CAS 629-59-4, Aldrich St. Louis, MO), n-dodecane (≥99% CAS 112-40-3, Sigma-Aldrich, St. Louis, MO), naphthalene (99.6% CAS 91-20-3 Alfa Aesar Ward Hill, MA), and benzene (ACS grade, CAS 71-43-2, EMD Chemicals China) were used for spiking.

3.4.3. Column Setup

Soil columns from Emerson (2016) were sampled in an anaerobic chamber for baseline conditions. Sensors were installed during baseline sampling. First, the contents (soil, LNAPL and water) of each column were poured into a sterile stainless-steel bowl. Soil materials for each column were homogenized, and one sample was collected from each column for the various time zero, biogeochemical characterization analyses. Next, the columns were equipped with sensors. Lastly, the equipped columns were repacked with the remaining homogenized column materials. Time zero analyses included hydrocarbon analyses (see section 3.4.8) and microbiome analyses (16S rRNA gene sequencing for DNA and RNA, see section 3.4.9) sequencing analyses. Due to the number of analyses performed and limited available soil material, samples for technical replicates could not be collected for each column.

Figure 3.1 shows a schematic of the column setup. The columns were 61 cm long glass columns, with an internal diameter of 4.1 cm. Each column was equipped with a gas sampling port and gas collection system, a water sampling port and six soil-redox sensors. To facilitate equipping and re-filling the columns with soil, the monitoring system was mounted on a glass rod. Figure SA.1 shows a picture of the skeleton of the sampling system and the ProtonTM chip board (Particle IO., San Francisco, CA) used for continuous soil redox monitoring. The gas and water sampling ports were built as specified in Irianni Renno et al., (2016). The gas sampling port was located at the top of each column and connected via a glass tube to a 1-L TedlarTM bag (Restek, Bellafonte, PA). The water sampling port was placed close to the column center, 40 cm from the top (Figure 3.1). The 6 soil redox sensors were mounted on the glass rod every ten centimeters (at 10 to 60 cm from each column top), and a Ag-AgCl reference electrode was located at the bottom.

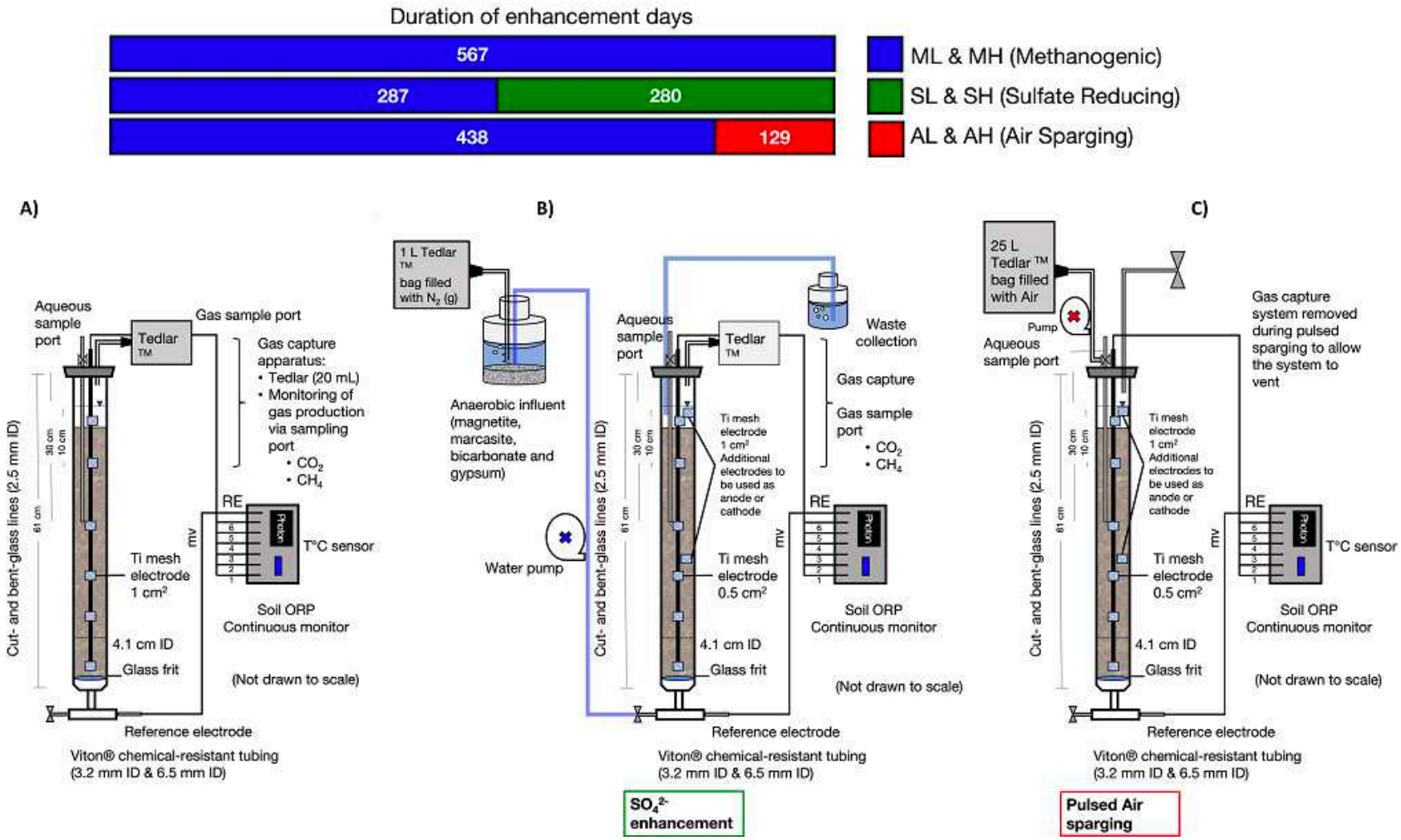

Figure 3.1. Columns under different treatments. A) Methanogenic, B) periodic sulfate addition and C) pulsed air sparging.

3.4.4. Description of Soil Redox Sensors

Soil redox sensors were constructed similar to sensors used for field applications (Sale et al., 2021) (S3NSE^{TM}, Fort Collins, CO) and the MiProbe microbial ORP sensor (Burge et al., 2017). The soil-redox sensors were composed of 0.5-cm^2 Ti mesh sensing electrodes and a Ag-AgCl reference electrode (World Precision Instruments, DriRef 5). Sensing and reference electrodes were connected via copper wires to a Proton^{TM} chip board (Particle, San Francisco, CA) that collected data every 30 minutes; data were stored in a cloud-based dashboard hosted by UBIDOTS^{TM} (UBIDOTS, Doral, FL). Prior to use, the sensors were validated using a YSI commercial ORP standard solution (YSI, Yellow Springs, OH).

3.4.5. NSZD Enhancements

Prior to the beginning of this work, the soil columns had been incubated under strict anaerobic conditions for a six-year period, during and post a prior study (Emerson, 2016). Hydrocarbon analysis at the beginning of this study showed variable initial concentrations, representative of different zones in an LNAPL-impacted site. The columns were separated into two groups of three columns each according to their initial TPH concentrations. The three columns with lower TPH concentrations, ranging from 10,142 mg/kg to 11,610 mg/kg, were designated as L, and the three columns with higher TPH concentrations, ranging from 17,433 mg/kg to 23,026 mg/kg, were designated as H. Columns were randomly selected from each group and assigned to either methanogenic (Figure 3.1A), periodic sulfate addition (Figure 3.1B) or pulsed air sparging (Figure 3.1C). The column experiment was run for 567 days, and enhancements were commenced after a baseline operation phase (Figure 3.1). For the periodic sulfate addition columns (SL and SH), the enhancement was applied for 280 days. For the pulsed air sparging columns (AL and AH), the enhancement was applied for 129 days. No enhancement

was applied to the baseline methanogenic control columns (ML and MH) over the 567-day experiment.

Sulfate generally was added to the systems once per week (on three occasions treatment lagged 10, 14 and 21 days), via replacement of the column pore fluids with a sulfate saturated solution (Figure 3.1 B). Sulfate concentrations were measured in the column influent, in the column pore fluids prior to replacement, and at the end of the volume addition to verify final sulfate concentration in the pore volume before turning the pump off. The sulfate saturated solution contained above solubility levels of $CaSO_4.2H_2O$ (i.e., gypsum) (Merk, Darmstad, Germany) and was amended with marcasite (FeS_2) (125 mg/L) (CAS 1309-36-0, Alfa Aesar, Ward Hill, MA) and magnetite (Fe_3O_4) (125 mg/L) (CAS 1309-38-2, Alfa Aesar, Ward Hill, MA) to scavenge oxygen and prevent it from entering the anaerobic column. The buffering capacity of the influent was increased by adding ACS grade sodium bicarbonate (CAS 144-55-8, EMD Chemicals Incorporated Gibbstown, NJ), to maintain a pH of 7.5. The sulfate saturated solution was pumped with a peristaltic pump (Cole-Parmer, Chicago IL) at an approximate rate of 500 ml/h. One column pore volume was replaced during each sulfate addition or approximately 500 ml of liquid volume was replaced each time, based on measurement of effluent volume during replacement.

Air was sparged once per week at the center of each column (Figure 3.1C). 25 L of air were loaded into a Tedlar™ bag and connected to a peristaltic pump (Cole-Parmer, Chicago IL) with Master Flex™ tubing (Cole-Parmer, Chicago, IL.). The air was pumped from the Tedlar™ bag utilizing the water sampling port at a rate of 12.5 L/ hr. During air sparging the columns were disconnected from the gas collection apparatus, and gas collection tubing was used to purge the system, to prevent pressure build up.

3.4.6. Gas and Water Monitoring Over Time

Gases were collected from the Tedlar™ bags on a weekly basis (Figure 3.1). Gas volume was measured, and CO_2 and CH_4 content were quantified via gas chromatography with a thermal conductivity detector (GC-TCD), following methods described previously (Emerson, 2016; Zeman et al., 2014;).

Water samples (2-ml) were collected from the sulfate enhanced columns once per week. Additionally, 2-ml water samples were collected from the remaining four columns at the beginning, during, and at the end of each enhancement application. Samples were filtered following methods described in Irianni-Renno et al., (2016) and submitted to the Collett Laboratory in the department of Atmospheric Sciences, Colorado State University (Fort Collins, CO) for sulfate analysis. Sulfate was measured using a Dionex ICS-3000 ion chromatograph 1500 (Thermofisher Scientific, CO) and a Dionex IonPac AS14A analytical column (4 x 250 mm) employing an eluent of 1 mM sodium bicarbonate and 8 mM sodium carbonate at a flowrate of 1 mL/min. The sample injection volume was 50 µL, and the run time was 17 min. Additionally, pH was measured for sample aliquots utilizing Whatman Panpeha Nr.112 strips (Sigma-Aldrich, US) with 0.5 pH unit sensitivity.

3.4.7. Endpoint Sampling for Microbial and Hydrocarbon Analyses

Prior to ending the experiment, a final enhancement application was conducted for each treated column to ensure microbial communities relevant to each enhancement were active at the time of sampling. The columns were sampled destructively in a manner that mimics cryogenic coring (Kialahosseinni et al., 2016). The columns were wrapped in electrical tape and freeze-preserved, using dry ice instead of N_2 (l) for safety reasons, to achieve a temperature at or below -40 ^{0}C. The annular space between an outer PVC pipe and each glass column was filled with

pelleted dry ice, and the top of the column was also covered with pelleted dry ice. The time required for the center of a water-soil-LNAPL column to reach a temperature of -40 ^{0}C was experimentally determined to be 20 minutes. Once the freezing time was determined, all 6 soil columns were preserved via this freezing method as shown in Figure SA.2. After freezing, the columns were stored at -80^{0}C for 48hrs prior to subsampling.

Subsamples were collected around each sensor in contact with soil. Sample depths with respect to the column tops were as follows: 20, 30, 40, 50 and 60 cm. The steps for obtaining the subsamples were as follows: 1) The glass from the column was removed by making a longitudinal cut through the electrical tape, and a hammer was used to crack the glass. 2) The tape and glass were carefully peeled from the water-soil-LNAPL system. 3) Remaining frozen sample was placed in an acetate sleeve. 4) 1-in "hockey puck" samples were cut with a circular saw following methods described in Kialahosseinni et al., (2016). 5) "Hockey puck" samples were quartered and used for analysis of hydrocarbons, methane, total iron sulfate, and microbiome analysis (DNA and RNA). Figure SA.3 shows subsampling procedures in detail; photographs of frozen column sampling procedures are provided in Supplemental Material.

3.4.8. Geochemical Analyses

Differences Saturated soil samples (10-20g) were placed in a 120-ml jar containing 50 ml of HPLC grade methanol for hydrocarbon analysis as described in Kialahosseinni et al., (2016). Total petroleum hydrocarbon (TPH), gasoline range organics (GRO), and diesel range organics (DRO) concentrations were determined via GC with a flame ionization detector (FID) following Irianni-Renno et al., (2016). Tetradecane, dodecane, naphthalene and benzene concentrations were determined via GC coupled to a mass spectrophotometer (MS) following previously described methods (Bojan et al., 2021).

Soil samples (10-20 g) were placed in 120-ml glass jars with caps with a Teflon™-lined septa for methane, iron, and sulfate analysis. Methane analysis was performed using a purge and trap sampler coupled to a GC-FID, and iron analysis was performed via inductively coupled plasma mass spectrometry (ICP-MS). Sulfate analysis for soil was done as described in section 3.4.6. Details on these analyses are described by Olson et al., (2017).

3.4.9. Microbiome Analysis

Approximately 50 g of the cryogenically preserved soil sample were wrapped in aluminum foil and immediately placed on dry ice for DNA and RNA preservation. DNA and RNA were extracted from each soil sample and analyzed for present and active microbial taxa via targeting both 16S rRNA genes (DNA) and transcripts (RNA). DNA and RNA were extracted following methods described in Irianni-Renno et al., (2021). 16S rRNA gene and transcript amplicon sequencing was conducted following the Earth Microbiome Project Protocol and methods described by Rico et al., (2019). Total present and active bacteria and archaea were quantified via quantitative polymerase chain reaction (qPCR) and reverse transcription qPCR (RT-qPCR) targeting archaeal and bacterial 16S rRNA genes and transcripts, as described in Suzuki et al., (2000). Additional qPCR and RT-qPCR targets analyzed for included *mcrA, alkB,* and *assA* genes and transcripts (Irianni-Renno et al., 2021).

Amplicon sequencing data analysis was conducted using QIIME2 V2020.8. Demultiplexed reads from the Illumina MiSeq platform were processed using DADA2 (Callahan et al., 2016). Taxonomy was assigned to the 16S rRNA gene amplicon sequence variants (100% similarity) with Naive Bayes classifiers trained on the Silva v.138 database (Quast et al., 2012). Differences in the community structures were visualized via 3D-principal component analysis (PCoA) with UniFrac distance weighted plots using the Emperor tool (Rico et al., 2019).

3.4.10. Data Visualization and Analyses

gINT™ was used to display biogeochemical analytes and measured parameters from the cryogenically preserved columns following methods described by Roads (2020). Soil ORP data collected every 30 minutes for the 6 columns were represented with one GAS (Sale et al., 2021) plot per column. Details on this analysis were reported previously (Sale et al., 2021).

3.5. Results

3.5.1. Soil Phase Hydrocarbon Analysis

Data suggest that total petroleum hydrocarbon (TPH) degradation was greater in enhanced systems than in unenhanced methanogenic systems, particularly for SL and AL columns, although statistical comparison of enhancements was not possible (due to lack of true replication) (Figure 3.2). Additionally, results show that individual target hydrocarbons were affected differently by different treatments.

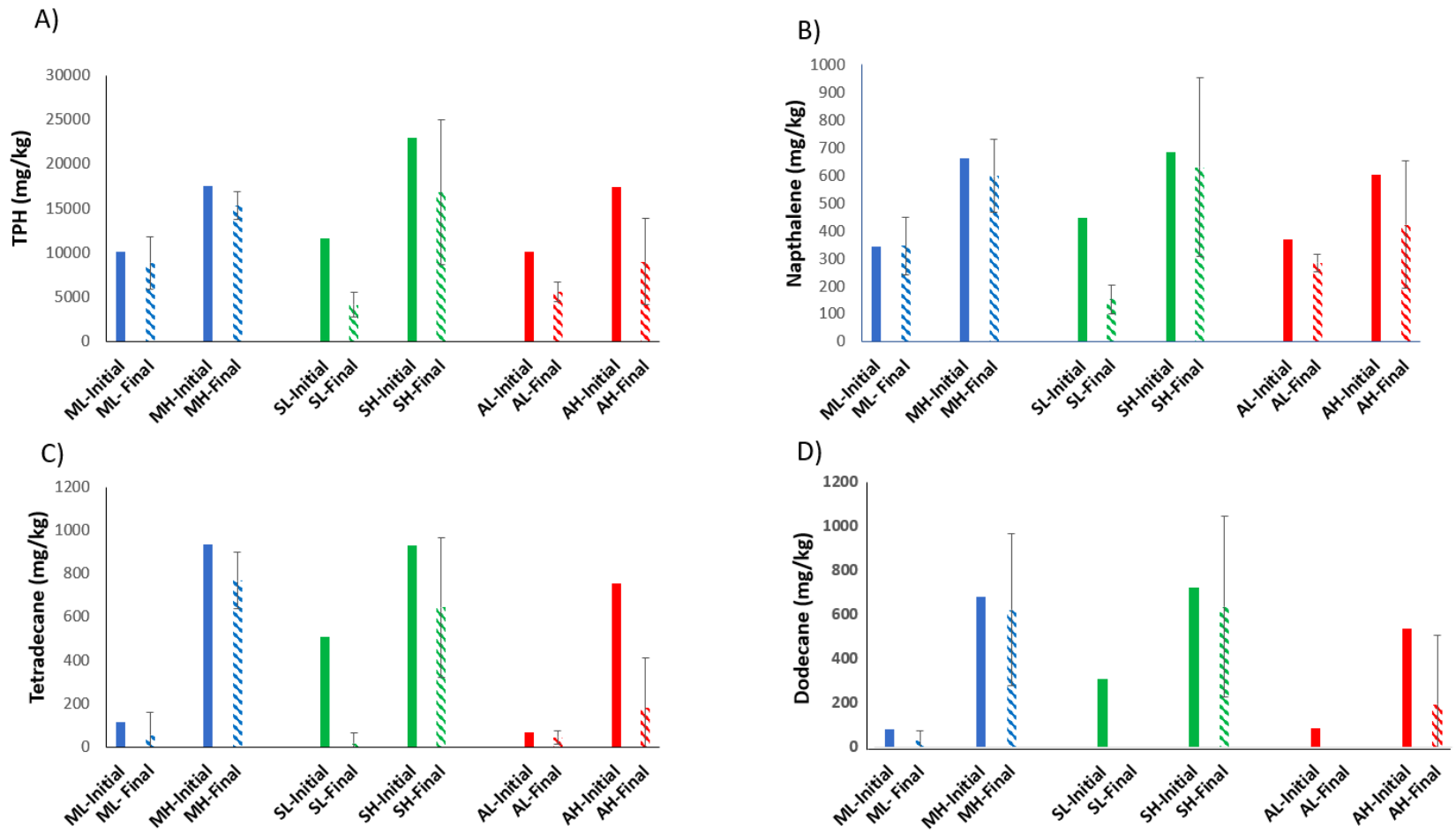

Figure 3.2. Hydrocarbon degradation in methanogenic and enhanced columns. Initial (solid bars) and final (stripped bars). Blue corresponds to methanogenic columns (operated for 567 days); green corresponds to sulfate addition enhanced columns (operation time post enhancement was 280 days); red corresponds to columns enhanced via pulsed air sparging (operation time post enhancement was 129 days). Initial concentrations were for the homogenized soil used to pack each column. Final concentrations were for samples collected at different column depths (20, 30, 40 ,50 and 60 cm from the top). Error bars correspond to standard deviations for the 5 samples from different depths.

Naphthalene degradation was affected by the redox environment. Under methanogenic conditions (ML and MH), naphthalene removal was minimal or not observed. In column ML, naphthalene depletion was not observed, while a slight decrease in concentration (from 664 to 599 (+/- 130) mg/kg) was observed in column MH. Surprisingly, although substantial naphthalene degradation was measured in column SL, enhanced via periodic sulfate addition, little naphthalene degradation was observed in column SH, which received the same treatment as column SL. Naphthalene concentration in column SL changed from 449 to 154.9 (+/- 51) mg/kg, while naphthalene concentration only decreased from 683 to 631 (+/- 321) mg/kg in column SH. Naphthalene degradation likely occurred at some depths in both columns enhanced by pulsed air sparging. In column AL naphthalene concentration decreased from 369 to 285 (+/- 31) mg/kg and in column AH naphthalene concentration decreased from 605 to 423 (+/- 230) mg/kg.

The measured linear alkanes tetradecane and dodecane were more substantially degraded than the PAH naphthalene. Results suggested alkane degradation occurred under every redox regime studied, although depletion increased with the addition of electron acceptors. Tetradecane removal under methanogenic conditions was greater in column MH than in column ML. Tetradecane decreased from 118 to 57 (+/- 25) mg/kg in column ML, while it decreased from 934 to 767 (+/- 25) mg/kg in column MH. More tetradecane was removed under sulfate reducing conditions than was removed under methanogenic conditions. In column SL, the tetradecane concentration decreased from 511 to only 18 mg/kg (+/-18). In column SH, the concentration decreased from 929 to 645 (+/- 546) mg/kg. Tetradecane depletion was also observed in systems enhanced via pulsed air sparging. In column AL, the measured tetradecane concentration decreased from 67 to 47 (+/- 15) mg/kg, and in column AH, tetradecane concentration decreased from 755 to 180 (+/- 230) mg/kg.

Similarly, results suggested dodecane degradation for all three redox regimes with depletion affected by addition of electron acceptors. Columns ML and MH degraded similar masses of dodecane. Dodecane concentration decreased from 84 to 29 (+/- 45) mg/kg in column ML, and it decreased from 682 to 622 (+/- 344) mg/kg in column MH. Dodecane was completely depleted in column SL, which contained an initial dodecane concentration of 310 mg/kg. In column SH, less dodecane was degraded with a decrease from 724 to 636 (+/-409) mg/kg. In column AL, which contained an initial concentration of 87 mg/kg, dodecane was entirely depleted (to below the detection limit). A similar response was observed in AH, where dodecane decreased from 536 to 195 (+/- 310) mg/kg.

3.5.2. Aqueous and Gaseous Phase Analyses

In aqueous samples collected from columns not treated via sulfate addition, sulfate was always below 100 mg/L. Directly after sulfate addition, aqueous sulfate concentrations were always above 1000 mg/L in both SL and SH columns. Sulfate consumption was observed in both SL and SH, but the amount of sulfate consumption differed between the two columns, with more reduction observed in SH (80 mmoles) compared to SL (27 mmoles) over 192 days (Figure 3.3). Further, column SL consumed on average 127 (+/- 8) µmoles of sulfate per day while column SH consumed 424 (+/- 183) µmoles per day. Interestingly, in the column that reduced less sulfate (i.e., SL), greater degradation was observed for TPH and individual targeted hydrocarbons (naphthalene, tetradecane and dodecane).

Differences in gas production were observed among the treatments and within treatments, between the L and H columns. Sulfate addition and pulsed air sparging eliminated methane production in the SL but only reduced methane production in the SH, AL, and AH columns (gas production data are shown in Figures SA.4 and SA.5). Carbon dioxide production was also

affected by the enhancements. More carbon dioxide mass was detected in column ML than in column MH, and more carbon dioxide mass was detected in column AL than in column AH. In contrast, in the sulfate reducing columns, SL produced less carbon dioxide mass than SH as expected, given than column SL consumed less sulfate than column SH.

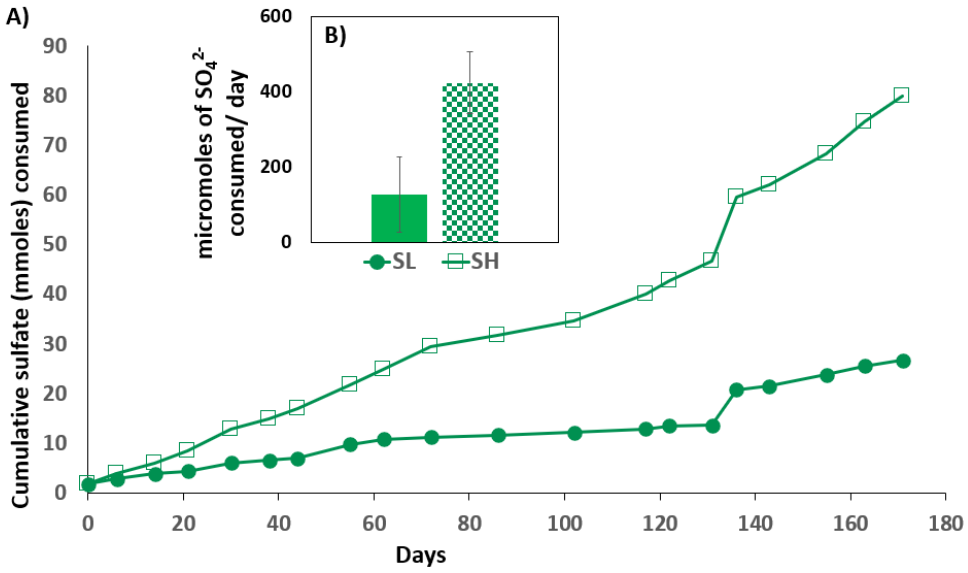

Figure 3.3. Sulfate reduction in columns SL and SH. A) Sulfate consumed in the columns (SH & SL) for the duration of the sulfate addition enhancement period. B) Average daily sulfate reduction rate, for columns SL (solid) and SH (checkers). Errors bars represent the standard deviation of 20 sulfate reduction values, calculated as the sulfate consumed between periodic applications.

Interestingly the column with lower initial hydrocarbon mass (SL) consumed less sulfate than the column with higher hydrocarbon mass (SH). Average measured sulfate reduction rate is 3.3 times higher for column SH than for column SL. Additionally, column SL degraded more mass than column SH. Column SH produced five times the amount of carbon dioxide than column SL.

3.5.3. Continuous Soil ORP

Peaks in ORP readings coincided with periodic addition of sulfate or air to the systems that can be observed as sharp increases in the continuous ORP data graphs (Figure 3.4). ORP peak magnitudes were greater for the columns that were air sparged than for the columns that were treated via periodic sulfate addition consistent with expected redox changes. Methanogenic columns ML and MH experienced ORP fluctuations with higher frequency, but smaller magnitude, than the ORP fluctuations induced by the enhancements. These small ORP reading peaks corresponded to observed gas volume increases in the Tedlar™ gas collection bags, consistent with ebullition causing these peaks. Figure SA.6 shows soil redox at only the column centers vs. time for all columns, with enhancement dates indicated, and corresponding gas volume produced.

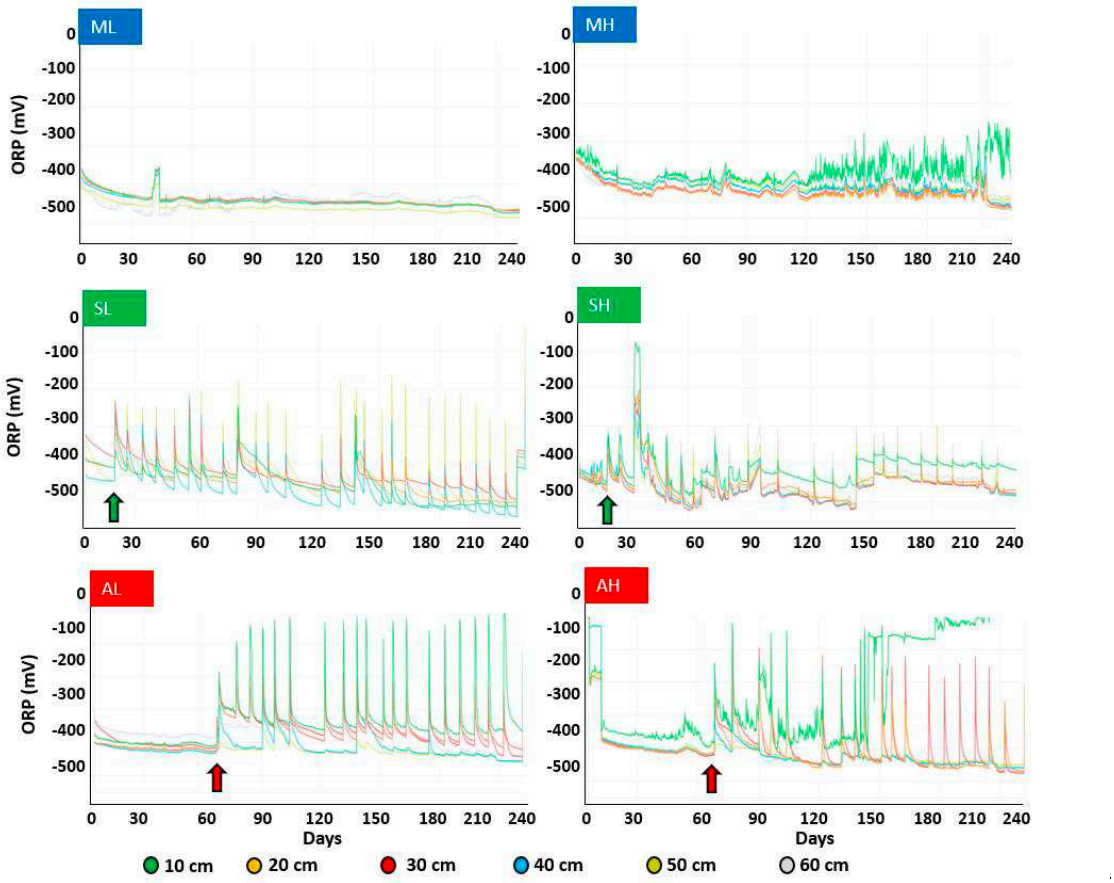

Figure 3.4. ORP (mV) readings through times in all columns. Blue boxes indicate methanogenic columns (ML and MH). Green boxes indicate columns enhanced via periodic sulfate addition (SL and SH); and red boxes indicate columns that were pulsed air sparged (AL and AH). Arrows indicate when enhancement treatment commenced. Each series color represents ORP measurements collected at a different column depth. Green is 10 cm from the top, orange is 20 cm from the top, red is 30 cm from the top, blue is 40 cm from the top, mustard is 50 cm from the top and grey is 60 cm from the top.

As expected, time averaged ORP readings for methanogenic and sulfate reducing columns were similar (Figure 3.5), and higher ORP reading averages were recorded for air sparged columns above the air addition point (samples collected at or above 30 cm from column top). Additionally, methanogenic and sulfate reducing columns had smaller standard deviations, while columns exposed to air showed larger variation above the enhancement addition point (located between 30 and 40 cm from the column top). Summary statistics for the continuous data

indicates that he closer the redox regime is to methanogenesis the smaller the range of the data spread (i.e., enhancing the system via sulfate addition has a smaller effect than perturbing the system via air sparging) (Figures 3.4 and 3.5 and Table 3.1). Interestingly, columns exposed to the same treatment conditions, but containing different initial TPH concentrations, showed different ORP patterns (Figure 3.4). Columns SH and SL behaved similarly at their centers (e.g., 30cm and 40cm positions); however, there are also appreciable differences between SL and SH ORP readings. For example, ORP readings differ in the magnitude of the increases and the smoothness of the reading values between ORP peaks (Figure 3.4). Column SL showed a smoother behavior than column SH between enhancement application. This is potentially due to biogenic gas ebullition occurring in SH. Peak ORP values achieved by pulsed air sparging are almost identical in columns AL and AH at the center (40 cm from the column top); however, ORP remained higher at the center of AL than at the center of AH in between air pulses. In column AH, the sensor 10 cm from the column top showed a step increase towards values that stabilize around -/+ 10 mV. This increase could have been due to air coalescing from the pore space and accumulating around the column top. Alternatively, this increase could have been only a “phantom” reading caused by a sensor connection failure given the low magnitude of the change + 10 mV.; those ORP readings likely coincided with an electrical disconnection of the system observed subsequently.

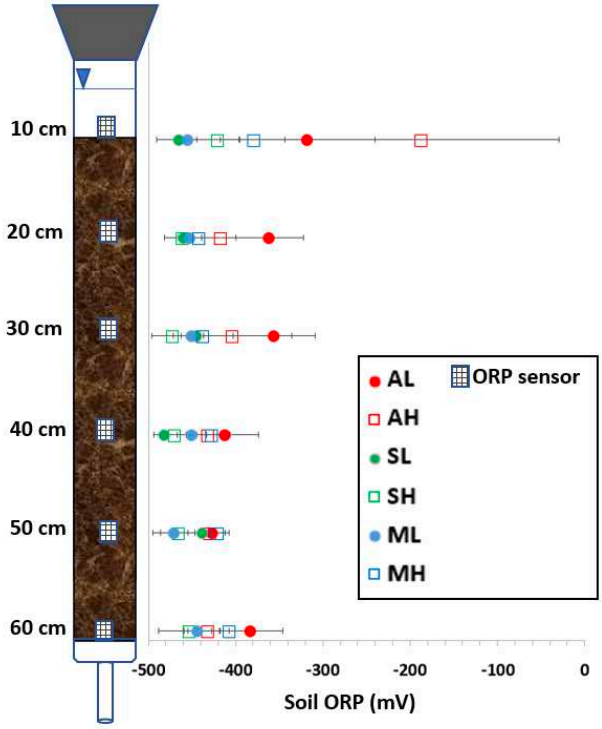

Figure 3.5. Average ORP (mV) for all columns. Values calculated over the duration of the enhancement experiment. Values are shown at each sensor depth, with corresponding standard deviations.

Table 3.1. Average ORP (mV) for all columns. Values were calculated for the duration of the enhancement experiment. Values are shown for each sensor depth, with corresponding standard deviation.

	ML		MH		SL		SH		AL		AH	
[1]Sensor	average	std dev	average	std dev	average	std dev	average	std dev	average	std dev	average	std dev
10 cm	-454.0	7.9	-378.0	36.8	-464.2	49.7	-419.7	24.3	-318.1	77.6	-186.2	157.4
20 cm	-452.2	6.2	-441.6	13.7	-459.5	37.5	-460.3	20.9	-361.0	38.5	-416.1	52.1
30 cm	-449.8	8.2	-436.4	12.7	-444.3	27.2	-471.9	23.9	-356.1	47.2	-403.5	67.4
40 cm	-450.2	8.1	-426.3	16.5	-481.7	43.6	-469.5	24.9	-412.0	37.7	-431.4	25.5
50 cm	-470.1	7.0	-419.4	15.9	-437.7	51.9	-464.6	29.8	-426.8	19.8	-429.3	17.4
60 cm	-443.4	14.0	-406.7	15.7	NA	NA	-452.6	35.3	-382.5	36.7	-430.9	23.3

3.5.4. Microbial Community Characterization

Microbial community composition analysis revealed differences between the enhancements, as well as between active microbial communities and the overall microbial communities present (Figure 3.6). Characterized microbial communities were relatively similar at the beginning of the study (Figure 3.6 A). Over the course of the study, and due to enhancements, the microbial communities diverged and clustered generally by treatment (Figure 3.6 B). Differences observed in microbial communities were much greater at the RNA level than at the DNA level, indicating RNA based analyses were required in this study to capture the dynamics of microbial community activity.

Methanogenic and sulfate-enhanced columns show limited differences in characterized active microbial communities with respect to column depth (Figure 3.6 B). In contrast, for columns AL and AH, the samples collected closer to the bottom of the column (below the air injection point) cluster together, while the samples collected closer to the top of the column (at or above the air injection point) plot relatively far from this cluster. Further, the 50-cm samples also cluster closer to the microbial communities in methanogenic columns ML and MH. Thus, data suggest air did not reach locations below the injection points resulting in methanogenic conditions remaining at these depths.

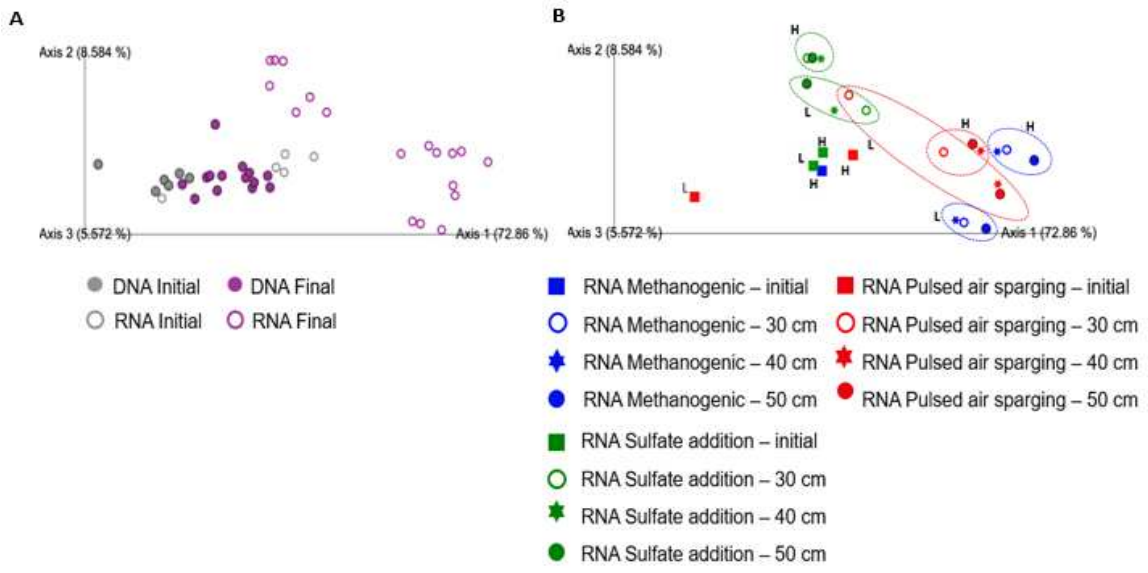

Figure 3.6. PCoA analysis showing column microbiomes. A) Microbial community characterization is shown at the DNA (filled circles) and the RNA (open circles) level for initial pre-enhancement (grey) and final (purple) samples. Initial samples correspond to one composite sample per column. At the final time point, the columns were sampled at three different depths (30, 40 and 50 cm from column top). B) RNA-level microbial community characterization as a function of treatment, analyzed pre-enhancement (grey) and post enhancement (blue: methanogenic, green: periodic sulfate addition and red: pulsed air sparging). Pre-enhancement samples correspond to one composite sample per column. The columns were sampled post-enhancements, at three depths (30 (rings), 40 (stars) and 50 (circles) cm from column top). Dashed ellipses were added to indicate samples collected from the same column.

In general, both ML and MH columns had similar relative microbial compositions when characterized via 16S rRNA gene sequencing analyses (DNA) and when characterized via 16S rRNA transcript sequencing analyses (RNA) (Figure 3.7); however, some key differences were observed between overall microbial community compositions and the active portion of the microbial communities. Gene sequencing analyses identified microorganisms that included methanogens, syntrophs, iron and sulfur cyclers, and methane oxidizers that can either use nitrate or oxygen as the electron acceptor. No major differences were observed across depths in either column ML or MH. Additionally, Microbial community data obtained via gene sequencing analysis, indicate potential for higher redox processes to occur in the methanogenic systems,

including sulfate reduction evidenced by the identification the genera *Desulfovibri*o (Morais-Silva et al., 2014) and *Desulfoprunum* (Junghare & Schink, 2015), iron reduction as suggested by the presence of organisms belonging to the genus *Chlorobium* (Li et al., 2021), nitrate reduction as suggested by the presence of the genus *Candidatus woesebacteria* (Chaudhari et al., 2021) and aerobic processes as evidenced by the presence of members belonging to the family *Methylopilacea* (Beck et al., 2015). In contrast, when characterized based on transcript sequencing analyses, organisms associated with higher redox processes than methanogenesis compose less than 2% of the total active community in most samples collected from both columns. An exception is the sample collected from column ML at 40 cm; *Methylopilaceae*, a family associated with aerobic methane oxidation and methanol degradation (Redmond et al., 2010) composed 3.9% of the active microbial community.

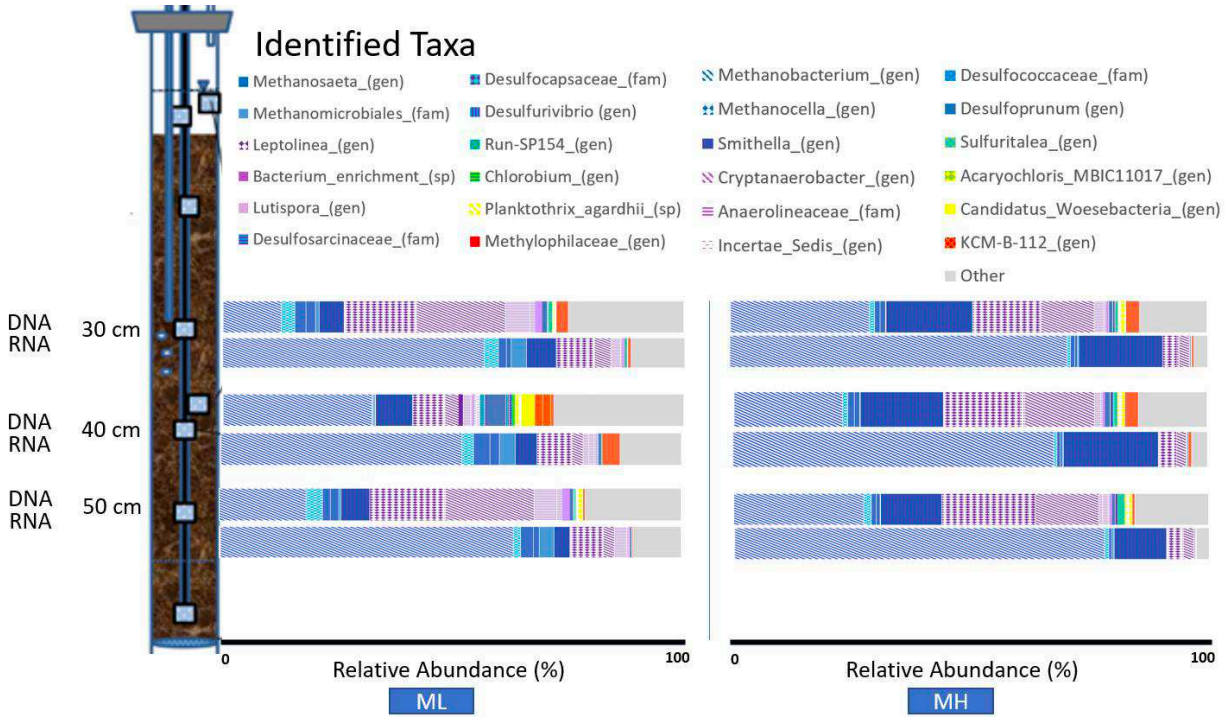

Figure 3.7. Microbiome structure of methanogenic columns. Relative abundances of bacteria and archaea identified at sampled depths (30, 40 and 50 cm from column top) in methanogenic columns ML and MH are shown.

Active microbial communities were also similar between columns ML and MH. For both methanogenic columns, 60 to 74% of all the active taxa identified at the 3 sampled depths correspond to methanogens, and approximately 90% of the active methanogens detected in both columns, across all depths, belong to the genus *Methanobacterium* (Sheng et al., 2016). Other identified active methanogens include members of the genus *Methanosarcina (*Maeder et al., 2006), members of the acetoclastic genus *Methanosaeta* and the hydrogenotrophic genus *Methanocella* (Sakai et al., 2011). Consistent with observed methane production, RT-qPCR targeting *mcrA* transcripts provided another confirmatory line of evidence that methanogens were active and indicate that methanogenesis was more active in column MH than in column ML (Figure SA.8 and Figure SA.9 and/or Table SA.2 and Table SA.3). *mcrA* transcription was detected only in the top sample collected from column ML, but it was detected in all three samples collected from column MH (Figure SA.14 and Figure SA.15). It is likely that in column ML readily degradable hydrocarbons were consumed and remaining hydrocarbons were not easily degraded in the absence of electron acceptor. In contrast column MH, likely still contained readily degradable hydrocarbons that were being metabolized via methanogenic processes at the time of sampling.

In columns SL and SH, the identified communities via gene (DNA) sequencing analysis were composed mainly of methanogens belonging to the *Methanobacterium, Methanosaeta,* and *Methanocella* genera, fermenters belonging to the *Smithella* and *Leptolinea* genera, and sulfate reducers, which were mainly represented by members of the *Desulfoprunum a*nd *Desulfovibrio* genera (Figure 3.8). Organisms associated with nitrate (*Planktothrix agardhil* and *Candidatus Wosebacteria*) (Chaudhari et al., 2021) and iron reduction (*Chlorobium*) (Li et al., 2021) were also identified at the DNA level but composed less than 5% of the characterized community.

Although the potential for aerobic processes to occur was detected in both sulfate reducing columns, in column SL, less than 2% of the organisms detected via gene sequencing were associated with aerobic processes, while in column SH, less than 1% of the organisms detected via gene sequencing were associated with aerobic processes. No major differences were observed across depths for either sulfate enhanced column.

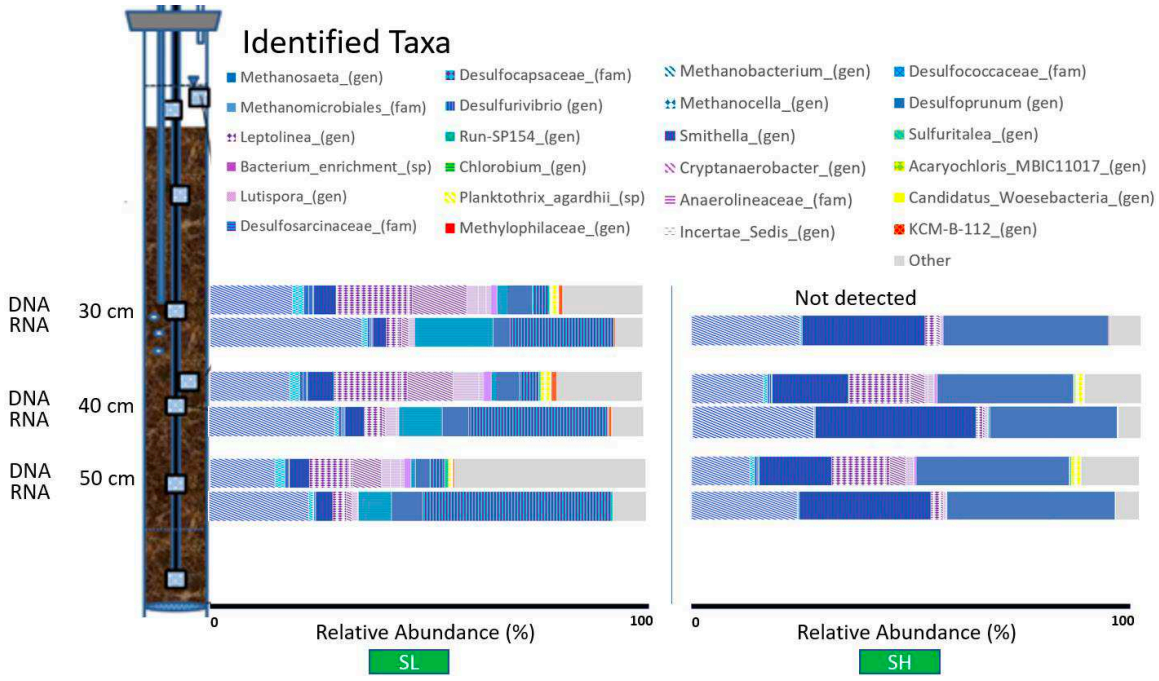

Figure 3.8. Microbiome structure of sulfate reducing columns. Relative abundances of bacteria and archaea identified at sampled depths (30, 40 and 50 cm from column top) in columns enhanced via periodic sulfate addition (columns SL and SH) are shown. The DNA sample collected at 30 cm from the column top for column SH failed to amplify.

RNA sequencing analysis revealed that both sulfate reducing systems, at every surveyed depth, contained active methanogens (between 20 and 30% of the active community, depending on the sample location). However, active methanogenesis as indicated via RT-qPCR of *mcrA* was only detected in column SH and not in column SL (Figure SA.17 and Figure SA.18), consistent with continued methane production in column SH after sulfate enhancements. Active

sulfate reducers were identified in both SL and SH including *Desulfosarcinaceae, Desulfovibrio,* and *Desulfoprunum.*

Although both sulfate reducers and methanogens were found to be active in every sample collected from SL and SH, interesting but subtle differences were detected between the sulfate reducing columns, when microbiomes were characterized based on transcript sequencing analysis. In column SL, sulfate reducers composed between 46 and 58% of the active microbial communities, with the genus *Desulfovibrio* being the predominant feature in every SL sample (70 % of the active sulfate reducers) (Gieg et al., 2014). Other identified sulfate reducers in column SL included members of the family *Desulfosarcinaceae;* members of this family have been associated with alkane degradation under anaerobic conditions (Lueders, 2017). *Desulfoprunum* represented less than 12% of the active sulfate reducer community. In contrast, in column SH *Desulfoprunum* represented approximately 98% of the active sulfate reducers and *Desulfovibrio* represented less than 2% of the active identified sulfate reducers. Another predominant difference between SL and SH was found for the genus *Smithella.* In column SH, *Smithella* represented between 27 and 35% of the active microbial community, while in column SL, *Smithella* represented, at most, 4.5% of the active microbial community. Members of the genus *Smithella* have been identified as fermenters in the syntrophic degradation of n-alkanes; a recent study described *Smithella* spp. as the dominant bacteria in alkane enriched environments (Ji et al., 2020). *Smithella* are known to outcompete other organisms in environments where n-alkanes are present (Ma et al., 2017).

In columns AL and AH microbial communities characterized via gene sequencing analysis were remarkably similar to those identified in their methanogenic counterparts (ML and MH) (Figure 3.9). Methanogens were detected in all samples collected from the air sparged

columns. Microorganisms associated with sulfur, iron and nitrate cycles were also detected. Additionally, methane oxidizers that can utilize oxygen, as well as sulfur and nitrate, as electron acceptors were identified. No major differences were observed between columns AL and AH in the microbiomes characterized via gene analysis.

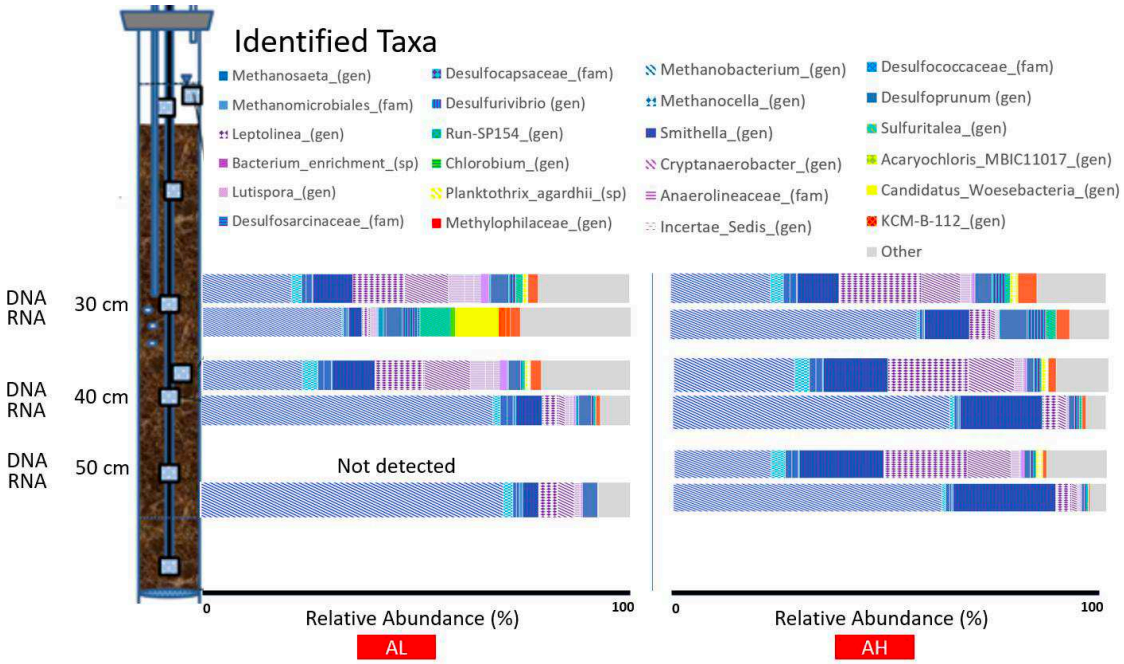

Figure 3.9. Microbiome structure of air sparged columns. Relative abundances of bacteria and archaea identified at sampled depths (30, 40 and 50 cm from column top) in columns enhanced via pulsed air sparging (columns AL and AH).

In general, between columns AL and AH, active microbial community compositions were similar as well. Surprisingly, despite receiving an air pulse immediately (1 hour) prior to being sampled, for both columns AL and AH, active methanogens were detected at every surveyed depth. For both columns, the sample analyzed above the air injection point (30 cm from the top) contained a lower relative abundance of active methanogens than the samples collected below the air injection point (40 and 50 cm from the top). Above the air injection point, a larger relative number of active microbes were related to higher redox processes, including sulfur

oxidation (*Sulfuritalea* spp. (7.3%)), iron (*Desulfovibrio* spp. (3.6%)) and aerobic methane oxidation (*Methylophilaceae* spp. (2.4%)).

Although active microbial communities were similar between AL and AH, differences were observed with depth in both columns. Methanogens belonging to the genus *Methanobacterium* composed 30% of the active microbial community identified at 30 cm in column AL. However, other active microbes detected at 30 cm were associated with higher redox metabolisms. For example, *Desulfovibrio* and *Desulfoprunum* represented 5% of the active genera. Facultative sulfur cyclers, represented by members of the genus *Sulfuritalea* (Sperfeld et al., 2018), were also found (7%) in column ML at this depth; *Sulfuritalea* have been associated with hydrogenotrophy in LNAPL environments. Also at 30 cm, putative aerobic hydrocarbon oxidizers (2.8%) were identified; these included microorganisms belonging to the genus *KCMB-112* (Puthiyapurayil, 2020) and methane and other smaller alkanes oxidizers belonging to the genus *Methylophilaceae* (2.3%) (Zheng et al., 2020). Similarly, the active microbial community above the air injection point in column AH was composed of microorganisms belonging to the genus *Sulfuritalea* (2.4%) and putative methane oxidizers *Methylophilaceae* (3%). By contrast, samples collected below the air injection points (40 and 50 cm) contained similar active microbial communities as those identified in the methanogenic columns ML and MH. As expected, in both columns at these lower depths, active methanogens showed greater relative abundances (50-60%) than above the injection points.

3.6. Discussion

Herein we demonstrated application of continuous multi-level redox sensors in conjunction with microbiome characterization via sequencing analyses of genes and transcripts for exploring the impact of three hydrocarbon remediation treatments: NSZD, periodic sulfate

addition, and pulsed air sparging. High spatial and temporal resolution sensor data allowed the effects of NSZD enhancements to be observed in real time and provided insights regarding the complex biogeochemical processes occurring post enhancement. Observations drawn based on continuous redox sensing were further supported by endpoint microbial analyses and geochemical soil characterization.

Results showed expected impacts on redox and microbiome composition as a function of treatment. Estimated TPH degradation rates (Table SA.1) suggested enhancements had the desired effect (i.e., inducing a higher redox environmet increased degradation rates) as reported in previous work. For the baseline NSZD case, without enhancement, redox was in the expected range for methanogenesis (-455 mV) (Sale et al., 2021) and methane was detected throughout the study. Microbiomes (ML and MH) at both the DNA and RNA levels were dominated by methanogens, and hydrocarbon biodegradation rates were lowest (Table SA.1). In columns enhanced via periodic sulfate addition (SL and SH), redox increased immediately after sulfate addition. Redox values at the center of the columns rose to the expected range (-411 mV) (Sale et al., 2021) or higher but returned to lower values generally within ten days after each treatment. An increase in the sulfate reducer populations in these columns was also observed both at the DNA and the RNA level. However, in general this increase was more pronounced at the RNA level than at the DNA level. TPH biodegradation rates under sulfate reducing conditions (40.7 mg/day- SL and 32.9 mg/day-SH) were roughly one order of magnitude higher than what was observed for baseline methanogenic conditions (2.3- mg/day- ML and 4.2 mg/day- MH) (Table SA.1). For pulsed air sparging, soil redox increased, albeit not to levels consistent with fully aerobic conditions (Sale et al., 2021). Microbiomes showed increases in phylotypes associated with more energetic redox processes (e.g., iron reduction), and estimated TPH biodegradation

rates (41.9 mg/day-AL and 114.9 mg/day AH) were higher than what was observed for baseline NSZD or sulfate addition columns.

Microbiome results were generally consistent with results of the redox sensors, particularly at the RNA level, indicating that these sensors provide useful and reliable real-time data for predicting general microbial activities (e.g., methanogenesis vs. aerobic metabolism). However, it is worth noting that when microbial processes occurring are too close in the redox ladder (i.e., sulfate reduction and methanogenesis), redox measurements alone might be insufficient to characterize the predominant degradation pathway. Nevertheless, IoT redox sensors provide relevant information regarding dynamic subsurface processes and can be deployed at low cost, and high spatial and temporal resolution data can be uploaded to the cloud, allowing practitioners affordable access to actionable information. Thus, we suggest that when a comprehensive conceptual site model based on a robust biogeochemical baseline characterization of the subsurface exists, continuous multi-level redox sensors can be an ideal and practical tool for monitoring putative degradation processes during NSZD and ENSZD remedies, quantifying their effectiveness, and guiding real-time adjustments in ENSZD remediation design and implementation.

Further, results revealed critical detail regarding the specific redox levels achieved and the dynamic nature of redox impacts. In practice, sulfate addition is performed with a goal of achieving sulfate-reducing redox levels (e.g., -411 mv at neutral pH) (Sale et al., 2021); however, in the absence of continuous redox measurements, the dynamics and longevity of sulfate enhancements on subsurface biogeochemistry can remain unknown (Shebl et al., 1996). Here, an average dose of 1.3 +/- 0.6 g to 0.7 L of sulfate every seven to thirty days resulted in only a transient increase in redox suggesting failure to realize the full potential benefits of sulfate

addition. Microbiology supported this conclusion; while active sulfate reducers were identified in columns SL and SH, active methanogens were also identified. It is worth noticing that active methanogenesis via functional RT-qPCR was only detected in column SH and our data points to the fact that methanogenic activity should be screened via application of functional assays (*mcrA* transcript detection) rather than solely inferred from 16S rRNA transcript data. Interestingly, redox plummeted after a few days despite pore water sulfate concentrations remaining high (on average 2,138 +/- 1,110 mg/L) indicating that this electron acceptor had not been entirely consumed. Then during the subsequent sulfate dose addition, redox increased again to the prior high level. Thus, it is likely that the replacement of pore water with sulfate-saturated water led to removal of hydrocarbon degradation by-products such as methane, and hydrogen, in solution or trapped as bubbles in the pore space, creating a transient increase in ORP to values expected in strictly sulfate-reducing conditions. However, as sulfate was utilized, and metabolites (e.g., volatile fatty acids, carbon dioxide, methane and hydrogen) were generated, ORP values returned to those expected in methanogenic systems, or lower (Huang et al., 2016). Further, redox transiently dropped below methanogenic conditions into a hydrogen production regime. As an example, in SL on day 176, upon sulfate enhancement application, ORP values rose from -522 mV to values around -500 mV; then, over a one-and-a-half-day period values returned to -500 mV, indicating presence of hydrogen gas. Generation of hydrogen occurs during sulfate reduction coupled to hydrocarbon oxidation (Cord-Ruwisch et al., 1987; Chen et al., 2023), and hydrogen-enriched environments are even more reduced than methane-enriched environments (Shin et al., 2019). Hydrogen generated can react with sulfide present or be scavenged by hydrogenotrophic methanogens and used to produce methane (Feldewert & Brune, 2020). Here, both active hydrogenotrophic methanogens and sulfate reducers were identified, likely

explaining the transient nature of the low ORP readings (-570 mV) in columns SL and SH. Continuously measuring ORP allowed for these redox cycles to be identified. Although, redox cycling in sulfate-reducing environments might differ between laboratory columns and in the field, due to differences in flow regimes, field deployment of redox sensors would likewise provide the real time information to guide engineering decision making around sulfate addition dosing and timing.

In practice, pulsed air sparging is done to stimulate aerobic biodegradation processes; however, data elucidating the impact of pulsed air sparging on subsurface redox and microbial processes has been lacking. Here, pulsed air sparging appeared to lead to expected increases in biodegradation (Table SA.1), but not via aerobic biodegradation processes (Figure 3.9). Rather, data suggested that oxygen supplied may have led to iron and sulfur mineral cycling that in turn stimulated use of iron and sulfur-based molecules (i.e., elemental sulfur, sulfate and thiosulfate) as electron acceptors, in the oxidation of hydrocarbons. Some use of oxygen by methanotrophic organisms was also observed (Figure 3.9). However, active methane oxidizers composed a very small percentage of the active microbial communities in AL and AH (Figure 3.9). Clearly, real-time redox data could have informed changes to the remediation design if used to guide decision-making in the field (e.g., increasing frequency of air doses or air volumes).

While redox sensors provide critical information that constrains predicted microbial processes to a given redox range, various microbial processes are possible. Combining microbiome characterization with application of continuous redox sensors provided insights into specific microbial metabolism; in particular, RNA-based analysis provided insight regarding the activities stimulated by the treatments when they were most effective (e.g., 1 hr after sulfate addition or air sparging). Interestingly, sulfate addition led to distinct impacts on column

microbiomes between SL and SH, likely due to the higher total mass of alkanes in the SH column. In our study we observed that, in SL, *Desulfovibrio* spp. dominated the active microbial community, where naphthalene degradation was observed, alkanes were depleted, and methane was not detected. Further, while *Desulfoprunum* spp. was active in both columns SH and SL, *Desulfovibrio* spp. was only significantly active in column SL. Members of the genus *Desulfovibrio* have been reported to degrade naphthalene under sulfate-reducing conditions(Qian et al., 2021; Sakaguchi et al., 2002). In contrast, while hydrocarbon-degrading, sulfate-reducing microbes were stimulated in column SH (containing higher levels of hydrocarbons) naphthalene degradation was not observed and methane continued to be produced throughout the experiment. This result may be explained by the higher levels of alkanes in SH, which favored growth of *Smithella*. *Smithella* spp. have been reported to thrive in methane rich environments (Ji et al., 2020). Modelling of syntrophic communities predicted that in alkane rich environments, *Smithella* generate hydrogen and acetate from alkanes (Embree et al., 2015). Thus, it appears likely that in alkane rich environments, like column SH, alkanes are consumed by fermenters such as members of the genus *Smithella,* who syntrophically interact with hydrogenotrophic methanogens.

Our study, like others (Embree et al., 2015; Shin et al., 2019), highlights the complexity associated with hydrocarbon degradation under sulfate addition and shows system response also can depend on contaminant composition. Shin et al., (2019) compared hydrocarbon degradation under sulfate-reducing conditions for two different compounds (hexane- a linear alkane and phenanthrene- a model PAH); similarly, Shin et al., (2019) found that hydrocarbon substrate shapes the sulfate-reducing community; over 55% of the RNA based sequences in the culture grown with phenanthrene as the sole carbon source belonged to the genus *Desulfatiglans* while

in the sulfate reducing culture grown with hexane as the sole carbon source, identified sulfate reducers were members of the genera *Desulfococcus* and *Desulfosarcina.* While Shin et al., (2019) were able to associate sulfate reducing phenanthrene and hexane degradation pathways to different genera, they were not able to fully elucidate the mechanisms by which these pathways occur. Shin et al., (2019) point to syntrophic processes as likely degradation mechanisms for both hydrocarbons studied. Recently, a study investigating anaerobic benzene biodegradation in freshwater aquifers also found an association between hydrocarbon composition and the system response to sulfate addition (Edwards et al., 2021). In their study, Edwards et al., (2021) hypothesize that the growth of anaerobic benzene degraders could be inhibited by competition with other organisms for nutrients and cofactors. Similarly, naphthalene degraders may have competed poorly for nutrients and cofactors in column SH, where concentrations of alkanes were high. Characterization of active microbes as a function of treatment can inform development of remediation models for predicting which contaminants are likely to be efficiently degraded. However, more work is needed to elucidate the relationship between microbial ecology and biochemical mechanisms of hydrocarbon degradation under sulfate-reducing conditions at a range of diverse field sites.

3.7. Conclusions

Progress of NSZD and ENSZD were evaluated in parallel under three LNAPL site-relevant biogeochemical conditions, utilizing laboratory columns. Herein, microbial activity was directly correlated to continuous soil-ORP readings. Combining continuous redox sensing with microbiome analysis provided insights beyond those possible with either monitoring tool alone. Upon enhancement via periodic sulfate addition, two distinct hydrocarbon degrading communities were observed with varying hydrocarbon distribution. When alkanes were present

naphthalene degradation was not observed, likely due to the fact that naphthalene degraders were outcompeted. *Desulfovibrio* spp. were directly associated with naphthalene degradation, and *Smithella* spp. were enriched in sulfate enhanced soils containing alkanes. Additionally, the implemented pulse air sparging regime (1 mole of air to 0.7 L of soil every two weeks) did not result in fully aerobic conditions suggesting that observed improvements in biodegradation can be explained by alternative anaerobic metabolisms (e.g., iron and sulfur reduction due to air oxidizing reduced iron and sulfur minerals); higher subsurface oxygen delivery would be needed to achieve aerobic metabolism. Recent development of sensor based IoT technology applied to restoration of LNAPL sites can complement the existing NSZD toolbox in further supporting NSZD and ENSZD as key technologies for LNAPL site restoration. Herein, the synergy achieved between microbiome characterization and soil redox continuous sensing illustrates how combining both provides insight into complex biogeochemical systems. Further understanding of these technologies will lead to improved predictions on remediation outcomes.

CHAPTER 4. IMPLEMENTING AN EXPANDED TOOLBOX FOR CHARACTERIZATION AND MONITORING OF NSZD AT A MID-TO-LATE STAGE LNAPL RELEASE SITE

4.1. Chapter Synopsis

The emergence of new technologies that facilitate characterization and monitoring of NSZD provide a basis for rethinking best practices for managing legacy releases of petroleum liquids (i.e., light non-aqueous phase liquids or LNAPL) in soils and groundwater. A former refinery tank farm was investigated to evaluate the integration of new emerging technologies with respect to characterization of subsurface conditions and best practices for monitoring NSZD in a mid- to late-stage LNAPL site. Herein cryogenic coring techniques and continuous internet -of-things (IoT) temperature and oxidation-reduction potential (ORP) sensors are combined with microbiome characterization to develop a conceptual site model (CSM) that can serve as a site baseline and can be informed over time by continuous monitoring. High resolution cryogenic core analysis in combination with next generation sequencing (NGS) documents active microbially-mediated NSZD through impacted intervals. Additionally, three-dimensional arrays of IoT temperature and ORP sensors registered NSZD losses on the order of 20,000 L/hectare/year. The CSM developed here is one that can evolve with the site as the site matures, as collected continuous data and periodic sample collection allow for the model to be informed as time goes by. A conceptual vision based on modern site characterization tools illustrates opportunities to improve best practices for managing legacy subsurface releases of petroleum liquids.

4.2. Introduction

Inadvertent releases of petroleum liquids (i.e., light non-aqueous phase liquids [LNAPL]) to soil and water pose human health and environmental risks (Sale et al., 2018; Sookhak Lari et al., 2024). However, under appropriate hydrogeologic and geochemical conditions, petroleum liquids in soils and groundwater can in some cases be effectively managed via natural processes referred to as natural source zone depletion (NSZD) (Garg et al., 2017; Sihota et al., 2011). Key processes that control NSZD include physicochemical processes (i.e., dissolution, volatilization, and vaporization) and biodegradation processes (Garg et al., 2017). Biodegradation processes have been shown to fully mineralize hydrocarbons; however, heterogeneity of subsurface biogeochemical conditions, as well as compositional differences of LNAPL, influence hydrocarbon mineralization pathways which complicates the assessment and understanding of NSZD and governing processes.

Although NSZD is gaining acceptance as a remediation technology for mid- to late-stage LNAPL sites (Karimi Askarani & Sale, 2020; Sale et al., 2018), challenges remain for broader regulatory adoption of NSZD as the sole remedy for LNAPL-containing zones (Pishgar et al., 2022). Central to adopting NSZD as a remedy is verifying that NSZD is occurring. NSZD is an efficient and cost-effective solution for LNAPL zones, but acceptance of this bioremediation technology relies on a multiple-lines-of-evidence approach that requires effective monitoring. Emerging use of *in situ* oxidation-reduction potential (ORP) sensors shows promise to resolve spatial and temporal redox dynamics during NSZD processes (Sale et al., 2021). Further, next generation sequencing (NGS) of microbial communities that are present and active can provide insights regarding subsurface biogeochemistry, associated elemental cycling utilized in electron transport (e.g., N, Mn, Fe, S), and the potential for biodegradation (Bojan et al., 2021; Irianni-

Renno et al., 2023; Key et al., 2022). Although recent work (Irianni-Renno et al., 2023; Yin et al., 2021) demonstrated expected relationships between soil redox and microbial dynamics, to date continuous redox sensing and active microbial processes characterization via microbiome analyses have not been fully tested together under field relevant conditions.

Herein, a case study is presented that advances integration of multiple nascent technologies for characterizing mid- and late-stage LNAPL sites including: 1) cryogenic coring, 2) multiple level internet of things (IoT) redox and temperature sensors in soil, and 3) application of DNA- and RNA-based molecular biological tools (MBTs) for site characterization. Factors motivating the use of cryogenic coring techniques include *in situ* retention of pore fluids, preservation of volatile compounds, preservation of RNA (Irianni-Renno et al., 2022; Johnson & Jackson, 2013), and increased reliability for LNAPL mass-in-place determination. Cryogenic coring also can provide more representative soil samples by preventing losses of unconsolidated soil during sampling recovery and temporally freezing the formation of the sampled intervals, helping to stabilize flowing sands (Kiaalhosseini et al., 2016). Additionally, multiple level temperature sensors can measure heat generated through NSZD (Karimi Askarani et al., 2018), where the oxidation of methane produced during anaerobic biodegradation of petroleum hydrocarbons (PHCs) generates heat (i.e., exothermic reaction), and can be used to calculate NSZD rates (Karimi Askarani et al., 2018; Karimi Askarani et al., 2024). Further, ORP data serve as an indication of the geochemical environment, which when used in conjunction with other subsurface biogeochemical data allow for elucidation of governing LNAPL biodegradation processes (Sale et al., 2021). Lastly, endogenous microorganisms that are capable of biodegrading contaminants can be detected via the implementation of MBTs, such as NGS. Evaluating and understanding the presence, abundance, and activity of microorganisms

associated with PHC biodegradation (e.g., methanogens, sulfate reducers, methanotrophs) as a function of other geochemical parameters (e.g., methane, sulfate, oxygen) can provide mechanistic data to support occurrence and progress of NSZD (Key et al., 2022).

4.3. Research Objectives

The objectives of this study are: 1) to explore the application of recently developed assessment technologies to an LNAPL site to demonstrate how the integration of these technologies can facilitate the construction of a robust CSM that supports NSZD, and 2) to show how better characterization and NSZD progress monitoring at mid- and late-stage LNAPL sites can serve as a multiple-line-of-evidence approach to fully support NSZD.

4.4. Materials and Methods

4.4.1. Site Overview

The case study area is a decommissioned 12-hectare tank farm, within a closed refinery. Crude oil refining and bulk storage of petroleum liquids occurred at the site from 1917 to the 1990s. During the operational history, gasoline, diesel, and other petroleum liquids were inadvertently released to soils and groundwater. The site lies within the flood plain of a large river in the central United States and is 2 km west of the river. Fluvial sediments underlying the site grade from fine to coarse with depth. Low permeability overbank deposits of silt and fine sand are encountered from 0 to ~6 m below ground surface (bgs). Overbank deposits are underlain by ~ 30 m of transmissive alluvium that include point bar deposits of well-sorted medium-sand, channel deposits of coarser grained sands, and glacial valley train deposits of sand and gravel (Bergstrom & Walker, 1956).

The hydrogeology of the site has been recorded for over the past half century. Records show river stages have varied seasonally and annually between 118 to 131 m above mean sea

level (amsl). Levies prevent flooding of the site, which has a surface elevation of ~124 m amsl. In the 1950s, high capacity municipal and industrial water wells in the vicinity of the site completed in the transmissive zone produced between 380,000 and 420,000 m^3 per day (Bergstrom and Walker, 1956). Industrial pumping created as much as 15 m of groundwater drawdown in the transmissive zone in the 1960s (Schicht, 1992). By the 1990s, municipal and industrial groundwater production ceased due to impacts to groundwater from multiple nearby industrial operations and groundwater levels have returned to pre-industrial levels (Schicht & Buck, 1995). Further, since closure, the tank farm has undergone a natural transition back to bottomland forest including diverse grasses, shrubs, and hardwood trees including oak, elm, and hickory. Average precipitation and pan evaporation rates are 1000 and 800 mm/year, respectively (Weather Underground and NASA).

4.4.2. Historical Site Characterization

Site characterization and remediation efforts span three decades. Monitoring wells have been the primary groundwater characterization tool. A total of 125 active monitoring wells are present at the site. Forty-two of the monitoring wells are within the tank farm study area. Screened intervals range between 3 and 6 m bgs. Following conventional practices, primary data from wells include quarterly to annual water levels, LNAPL thicknesses in wells, and concentrations of PHCs in groundwater.

An image of the tank farm study area, including locations of laser induced fluorescence (LIF) borings, cryogenic coring locations, and sensor strings, is shown in Figure 4.1. Representative LIF profile images adjacent to cryogenic coring locations are provided in supplemental information (SI). Also provided in SI are images of cryogenic coring, and core processing, IoT sensors, and as-built drawings for sensor strings.

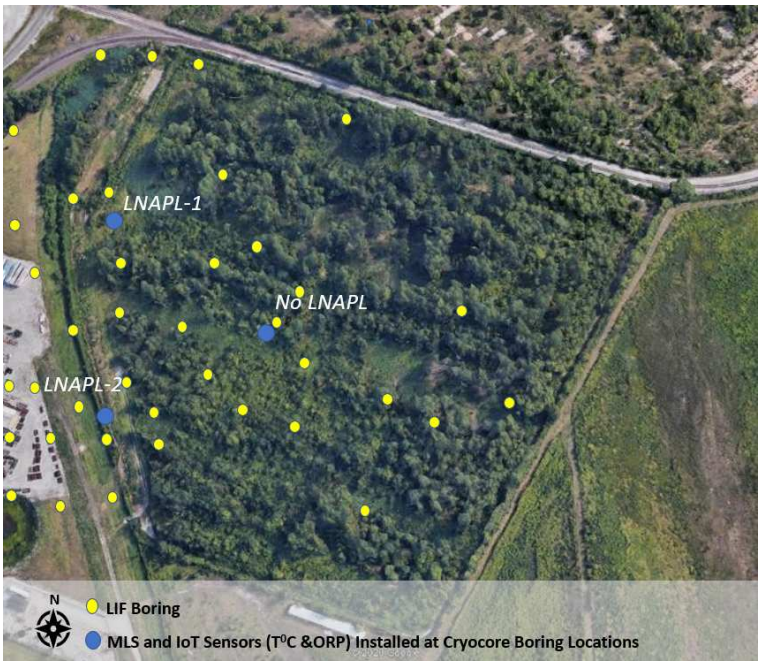

Figure 4.1. Locations of LIF borings, cryogenic coring locations, and sensor strings in the former tank farm study area.

4.4.3. Laser Induced Fluorescence (LIF)

In 2018, Dakota Technologies (Fargo, North Dakota) completed 43 direct push LIF test holes to depths of 15 m bgs in the tank farm (Figure 4.1). All LIF test holes were pushed through impacted material according to published methods (Bujewski & Rutherford, 1997)

4.4.4. Cryogenic Core Collection

Approximately 20 m of cryogenic soil cores were collected at the site from three borings with total depths ranging from 6.1-7.6 m bgs, each. Descriptive labels for cryogenic coring locations include *No LNAPL*, *LNAPL-1* and *LNAPL*-2. Respectively, *No LNAPL*, *LANPL-1* , and *LNAPL-2* labels refer to borings that had no LNAPL, LNAPL about the capillary fringe only, and LNAPL present from the capillary fringe through the overbank deposits. Coring locations were selected based on LIF data and a desire to study locations that reflect the range of conditions at the site.

Cryogenic coring was conducted by Drilling Engineers (Fort Collins, Colorado) using a CME-55 drill rig and hollow stem augers (11 cm inner diameter (ID), 23 cm outer diameter (OD)). Cores were collected in clear 5.7-cm ID polyvinyl chloride (PVC) liners in continuous drives of 67 cm using a modified CME continuous sample barrel. Sample barrel modifications included an insulated internal dual wall cooling barrel and insulated lines for fully contained delivery and exhaust of liquid nitrogen. Rotating hollow stem augers with a fixed sample barrel were advanced leading to "overcut" cores being pushed into soil liners.

After the core samples were in the liners, liquid nitrogen was circulated through the dual wall cooling barrel for 4-6 minutes. Liquid nitrogen was supplied via portable 100-L dewars. After *in situ* freezing: 1) the lined sample barrel containing the frozen core was brought to the surface, 2) the liner containing the frozen core was pulled from the sample barrel, 3) the liner containing the core was capped, 4) sample recovery was recorded (length recovered/length of the drive), and 5) core was placed in onsite coolers filled with dry ice (-78 C^o). Frozen cores were shipped overnight on dry ice to Colorado State University and promptly transferred to a -80^{o}C freezer.

4.4.5. Multilevel Sampling (MLS) Wells and Sensor Installation

Multiple Level Temperature and ORP Sensors, composed of strings of 12 to 15 multiple level temperature and ORP sensors, were installed in the cryogenic coring holes to depths of 7.5 m bgs. Intervals between sensors ranged from 0.15 to 1.22 m (SI).

Sensor hardware was provided by S3NSE Technologies Inc. (Fort Collins, Colorado). Modification to methods described in Karimi Askarani & Sale (2020) and Sale et al., (2021) include the following: each string had collocated digital temperature sensors (±0.5 °C; DS18B20, Adafruit Industries) and ORP sensors (an expanded titanium mesh coated with tantalum-iridium

mixed metal oxides (Corrpro Industries – Elgard™ Ribbon Mesh)). All sensors were on a single four-strand data wire. Sensors were mounted on 5.08-cm ID PVC pipe with a 30.5-cm section of 0.25-mm slotted well screen at the bottom. Annular space between the PVC pipe and the boring wall was backfilled with a uniform fine-grained quartz sand with a 1-meter hydrated bentonite plug at the top. The voltage potential of the Pd-$PdCl_2$ electrode was essentially the same as an Ag-AgCl reference electrode.

Data from each sensor was uploaded hourly via cellular connection to Ubidots™; a cloud-based data storage, analytics, and visualization platform. Data collection and wireless communication is controlled by a Particle Electron™ microprocessor (Particle Electron, E260KIT, Particle Industries, Inc.). Methods for calculating temperature based daily NSZD rates are described in Karimi Askarani & Sale (2020). ORP data analysis methods are presented in Sale et al., (2021).

Additionally sampling ports for aqueous and gas samples were also added to the MLS systems. Following methods described in Irianni-Renno et al., (2016), aqueous samples were analyzed for dissolved hydrocarbons, and for GRO, methane and common ions. Gas samples were analyzed for oxygen, carbon dioxide, and methane. Details on the location of sensors and sampling ports can be found in supplemental information (Figures SB.6, SB.7 and SB.9). Aqueous and gas samples were collected 40 days after MLSs were installed.

4.4.6. Cryogenic Core Subsampling and Analyses

Frozen cores were cut into 150 2.6 cm-thick subsamples (hockey pucks) at intervals of 7.5 to 15 cm. The cores were cut using a chop saw (DeWalt) equipped with a circular 36-cm diamond-tipped masonry blade. Core subsamples were: 1) visually logged by a professional geologist, 2) photographed under visible and UV light, 3) used to measure physical properties

including porosity and fluid saturations, and 4) analyzed to quantify total concentrations of methane, benzene, total petroleum hydrocarbons (TPH) gasoline range organics (TPH-GRO), and total petroleum hydrocarbons diesel range organic (TPH-DRO). Further details regarding collection and analysis of cryogenic cores are described in Kiaalhosseini et al., (2016), Sale et al., (2016), and Olson et al., (2017).

4.4.7. Microbiome Analyses

In addition, select core subsamples were analyzed to characterize microbiomes present and active with depth bgs; sample locations had varying levels of LNAPL. Five, four, and three subsamples were analyzed from the *No LNAPL*, *LNAPL-1*, and *LNAPL-2* locations, respectively. DNA and RNA extraction methods were followed as described in Irianni-Renno et al., (2022). 16S rRNA gene amplicon sequencing was conducted following the Earth Microbiome Protocol and methods described by Rico et al., (2021). Microbial community analysis was conducted using the QIIME2 V2020.8 software pipeline. Demultiplexed reads from the Illumina MiSeq platform were processed using the DADA2 algorithm (Callahan et al., 2016). Taxonomy was assigned to 16S rRNA amplicon sequence variants (100% similarity) with naïve Bayes classifiers trained on the Silva v.138 database (Quast et al., 2012).

Color coding for ORP values, introduced by Sale et al., (2021), was used to represent the microbial ecology data analyzed herein. Sale et al., (2021) used the visual color spectra to codify ORP (mV) values at neutral pHs. In their paper, the colors correspond to ORP ranges at which different redox couples are in equilibrium at pH 7; for example, solid red represents the coexistence of oxygen and carbon dioxide at pH 7 and corresponds to ORP value ranges above 450 mV when the measurements are referenced to a Ag/AgCl electrode. Considering the biogeochemical data collected for each sample, analyzed for microbial ecology, inferences on

microbial processes were made for each represented taxa within a sample. Colors were assigned to each taxa as per Sale et al.'s code to match the redox value of the environment at which each inferred microbial process would occur. Thus, red represents aerobes, yellow represents nitrogen cyclers, green represents iron cyclers, blue represents methanogens and sulfate reducers, and purple represents hydrogenotrophic methanogens. Purple in the ORP color scale represents reducing environments at which hydrogen can exist. Tables showing the results of the microbial analyses are presented as supplemental information for this chapter in Appendix B (Tables SB.1 through Table SB.8). The color scheme and pattern to represent each identified taxa, are shown in Tables SB.1 and SB.2. Other data shown are sample depth, corresponding relative percent abundance (%) of each characterized taxa, inferred metabolic function for each taxa, and supporting literature reference for each process assignment.

4.5. Results

4.5.1. LIF Data

LIF data indicate an LNAPL distribution that is atypical of most LNAPL sites (Figure SB.1 through Figure SB.5). LNAPL buoyancy limits the extent of LNAPL distribution to the immediate vicinity of the capillary fringe and spreading of LNAPL about the water table. LNAPL spreading on the water table tends to form laterally extensive LNAPL bodies about the capillary fringe. Additionally, LNAPL entrapments in vadose pore spaces appears to have occurred, potentially due to water table fluctuations (Newell et al., 1995) Shallow LNAPL (in immediate vicinity of the capillary fringe) is present across 20% of the tank farm, and LNAPL from near surface to 12 m below the capillary fringe beneath 30% of the tank farm.

4.5.2. Cryogenic Core Analyses

Core recovery (percent of material recovered with respect to material present within sampled interval) via cryogenic coring was 97, 99, and 96% for the *No LNAPL*, *LNAPL-1*, and *LNAPL-2* locations, respectively. Dark colors of soil, in the first column of Figure 4.2 were interpreted as an indication of reducing conditions associated with anaerobic biodegradation of organics (e.g., natural organic matter and LNAPL). Individual sediment beds range in thickness from 0.5 to 3.0 m and grade with depth from silt, silt with fine sand, to fine sand. Comparison of the geologic logs from the three cryogenic cores suggests interbeds in the overbank deposits are largely laterally discontinuous at the ~100 m spacing between the cryogenic coring locations. The mean porosity of all samples was 0.50.

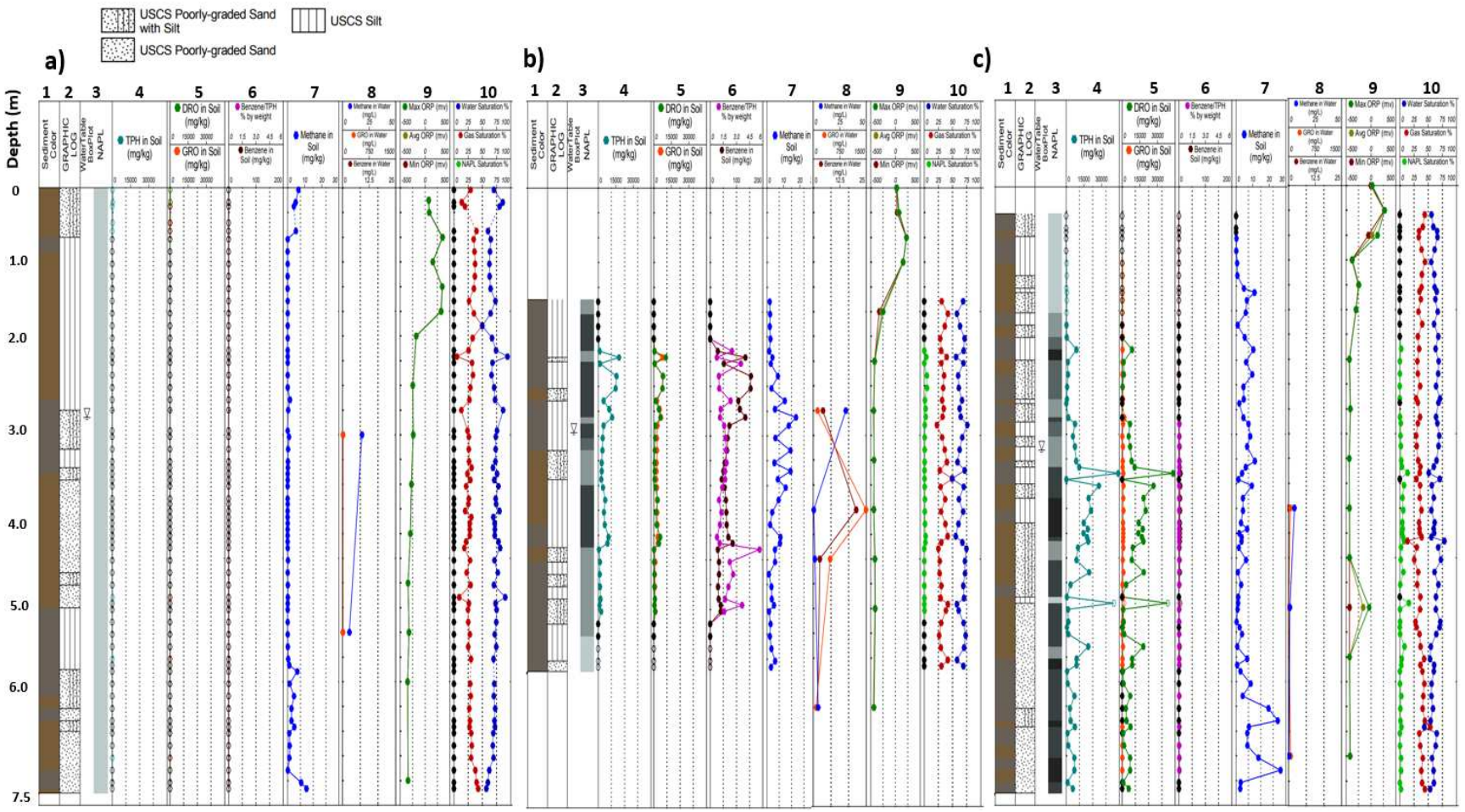

Figure 4.2. gINTTM plots of cryogenic core data.a) No LNAPL location, b) LNAPL-1 location and c) LNAPL-2 location. 1) Sediment color, 2) Graphic log, 3) Water table elevation and LNAPL, 4) TPH in soil (mg/kg), 5) TPH-DRO and TPH-GRO in soil (mg/kg), 6) Benzene distribution in soil (%-pink, mg/kg- brown, 7) Methane in soil (mg/kg), 8) Aqueous concentrations (mg/L) methane (blue), TPH-GRO (red), and Benzene in (brown), 9) ORP (mV), maximum recorded value (emerald green), Average value (military green), minimum ORP value in red and 10) Fluid saturations, water (blue), gas (red) and LNAPL (green). The vertical position of subsamples is indicated by open circle symbols in each column. The first column illustrates true soil colors ranging from brown to gray. The second column provides unified soil classification symbols (USCS) for encountered sediments.

The observed distribution of LNAPL, based on cryocore analysis (Figure 4.2, columns 3 (Visual LNAPL), 4 (TPH) and 5 (TPH-GRO, TPH-DRO)), is consistent with the 2018 LIF data (Figure SB.1 through SB.5). Average/maximum TPH concentrations at the *LNAPL-1* and *LNAPL-2* locations, are 4,180/17,800 and 7,110/44,200 mg TPH/kg dry soil, respectively (Figure 4.2, column 4). Similarly, average/maximum LNAPL saturations, at the *LNAPL-1* and *LNAPL-2* location, range from 2.2/16.0 to 1.0/5.0 %, respectively (Figure 4.2, column 10). Additionally, LNAPL composition at the *LNAPL* locations is different. While at the *LNAPL-1* location, LNAPL is composed of TPH-DRO and TPH-GRO (including benzene), no TPH-GRO was detected at the *LNAPL-2* location.

Methane in vadose zone gases coincides with LNAPL presence and below the water table methane co-exists in groundwater with TPH (Figure SB.9, Figure SB.10 and Figure SB.11).

4.5.3. MLS Port Gas and Aqueous Samples

The gas and aqueous data collected during the study indicate that at the *No LNAPL* location oxygen was detected at the deepest gas port located at 1.2 m bgs; however, oxygen present was considerably less than the port located at 0.6 m bgs where measured methane concentrations were close to 0% v/v. Given the gas data collected, it is estimated that at the time of sampling the methane oxidation front was located between 0.6 and 1 m bgs. Aqueous sulfate was detected at 1.5 m bgs and 2.4 m bgs at concentrations between 200 and 250 mg/L, respectively (Figure SB.9). Sulfate was not detected in the samples collected at both 3.9 m bgs and 5.18 m bgs. Ferrous iron was only detected in the samples collected at 3.9 m bgs and 5.18 m bgs, indicating at these depths available ferric iron was reduced associated with anaerobic biodegradation of TPH.

At the *LNAPL-1* location, a similar analysis placed the methane oxidation front around 1.8 m bgs. A low sulfate concentration (<20 mg/L) was detected at 2.7 m bgs, and no sulfate was detected at deeper sampling ports located at 4, 4.6 and 5.2 m bgs. Ferrous iron and dissolved manganese increased with depth, indicating these minerals were likely reduced at the sample depths.

At the *LNAPL-2* location, methane was detected at 0.3, 0.9 and 1.8 m bgs in the same concentration (10 % v/v). Further, oxygen was only detected at 0.3 m bgs, indicating the methane oxidation front at the time of sampling was located between 0.3 and 0.9 m bgs. Sulfate was not detected at any depth and ferrous iron was detected at every depth in concentrations greater than 50 mg/L. At the time of sampling, these data collectively indicate that at the *LNAPL-2* location below the methane oxidation front, biodegradation processes likely occur via syntrophic processes with methanogenesis.

gINT^{TM} plots showing water quality and gas data from samples collected from the MLS ports in all cryocoring locations (Figure SB.10 and Figure SB.11) serve as a line of evidence for PHC biodegradation.

4.5.4. Multilevel Temperature Data

The average subsurface temperature from 1 to 3 m bgs at the *LNAPL-1*, and *LNAPL-2* locations are 0.4 and 0.9 C^{o} warmer than the *No LNAPL* locations, respectively (Figure 4.3 a, b, and c). This finding is consistent with heat generation from methane oxidation. Monthly NSZD rates were calculated from temperature measurements based on methods advanced in Karimi Askarani & Sale (2020) (Figure 4.3 d, e, and f). As expected, the average biodegradation rates at the *No LNAPL* locations are ~0 L/hectare/year, whereas at the *LNAPL-1* and *LNAPL-2* locations, average biodegradation rates are ~20,000 L/hectare/year.

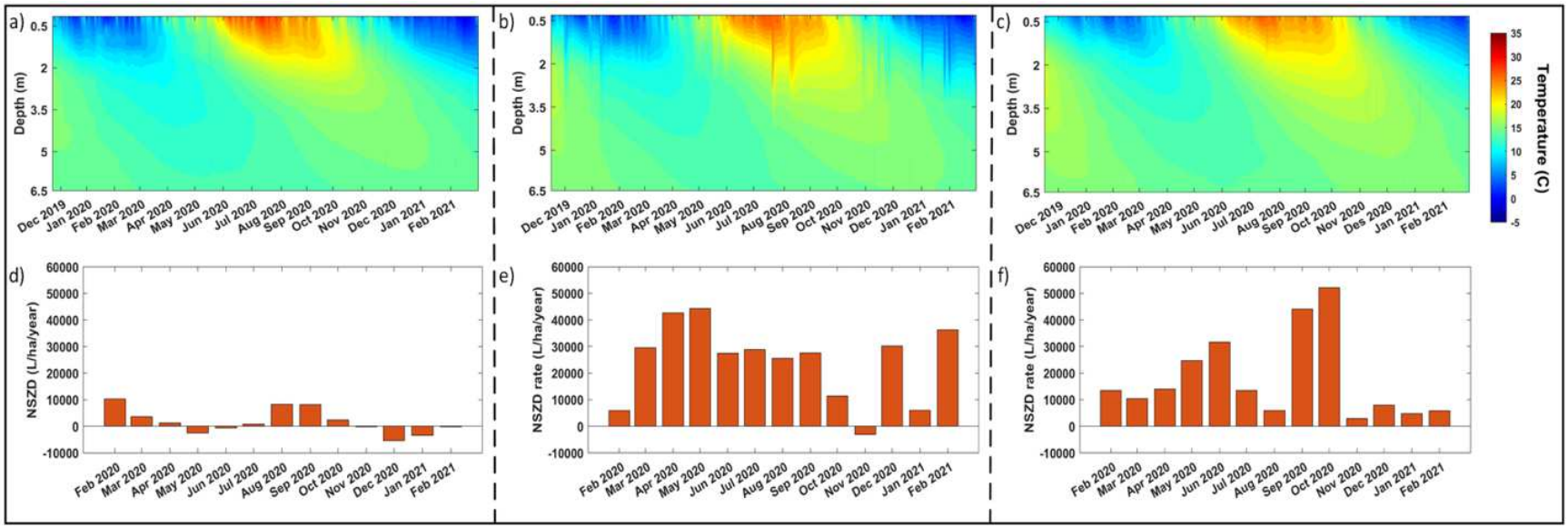

Figure 4.3. Heat maps of temperature as a function of depth and time with higher mean temperatures with LNAPL at a) No LNAPL, b) LNAPL-1, and c) LNAPL-2 locations. Monthly NSZD rates at d) No LNAPL, e) LNAPL-1, and f) LNAPL-2 locations. Figures 4.3a, 4.3b, and 4.3c, plot 500,000 temperature measurements for the period from February 2020 to February 2021, as a function of time (x-axis) and depth (y-axis), for the No, LNAPL-1, and LNAPL-2 locations. Temperatures are presented using the visible light spectrum (red to violet) indicating temperatures ranging from – 5 to 35 0C

4.5.5. Multilevel ORP Data

ORP readings collected with the continuous sensors were averaged and represented next to the cryocoring results (Figure 4.2, column 9). Groundwater without the presence of TPH had average ORP values in the overbank deposits ranging from -250 to -350mV, while where TPH was present in groundwater, average ORP values ranged between -500 and -450 mV. ORP values are shown in more detail in Figure 4.4. Within LNAPL-impacted soils, redox values in the vadose zone are depressed by 200 to 300 mV as compared to the *No LNAPL* location (Figure 4.4). Descending through the vadose zone, ORP values indicate redox conditions associated with nitrogen, iron, and methane redox couples. Below the water table, in LNAPL-impacted zones, redox conditions range from -400 to -500 mV, consistent with active methanogenic NSZD. Reducing conditions identified in the *No LNAPL* location could be attributed to naturally low redox associated with swamp-like overbank deposits; however, no organic carbon analysis was performed to test this hypothesis. Unfortunately, the naturally low redox in the overbank deposits constrain the use of ORP to be able to discern between LNAPL biodegradation and the biodegradation of natural organic matter (NOM).

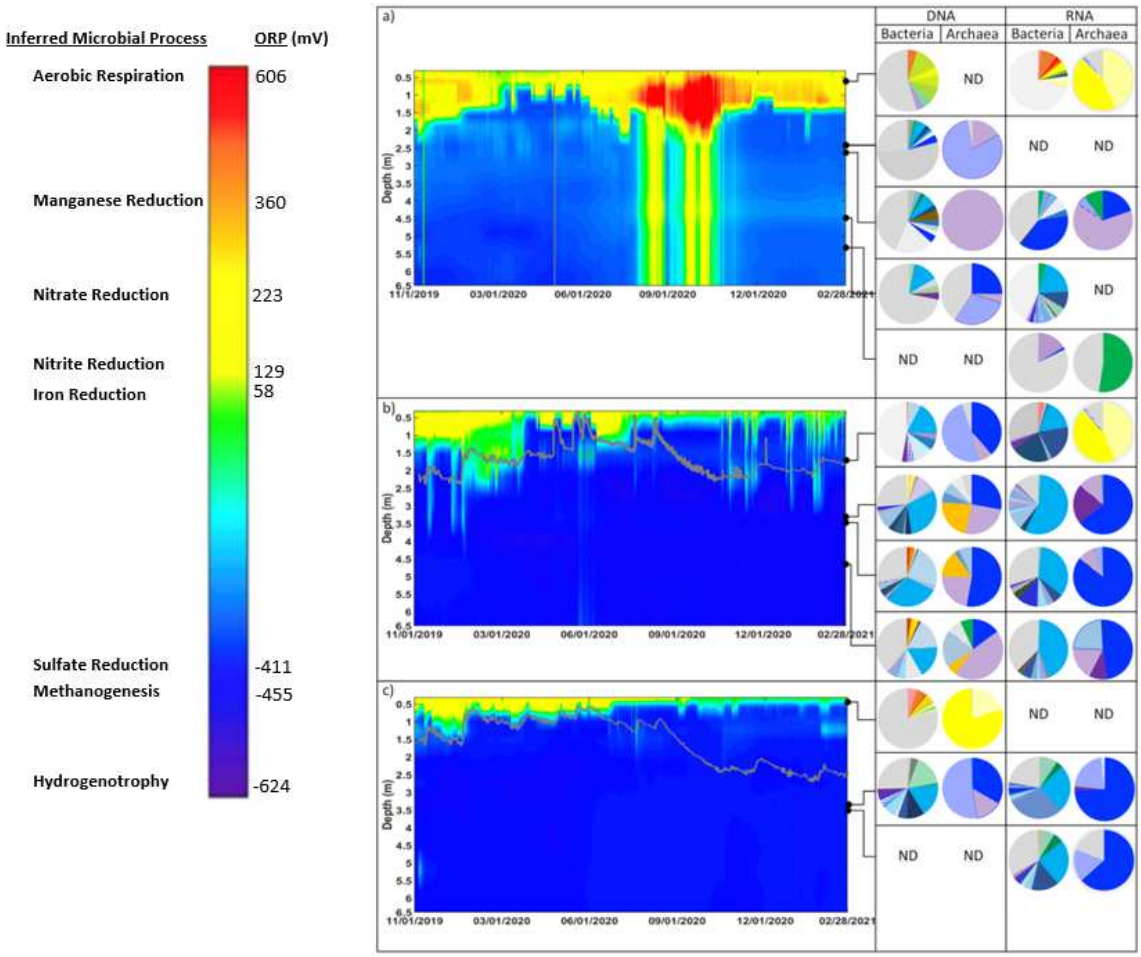

Figure 4.4. Continuous ORP data with microbial ecology data from the cryocore samples. Continuous data was collected between 11/2019 and 2/2021.Microbial ecology data was collected from cryogenic cores sampled on 09/2019 at a) No LNAPL, b) LNAPL-1, and c) LNAPL-2 locations. Panels b and c include experimental water level data shown as a grey line. A detailed key for the microbial data with specific phylotypes detected is provided in SI. ND indicates "non detect" based on failure of DNA or cDNA amplification prior to next generation sequencing. For the period of November 2019 to February 2021, 500,000 hourly ORP values are shown for the No LNAPL and LNAPL-1, LNAPL-2 locations. ORP is plotted as a function of time (x-axis) and depth (y-axis) using the visible light spectrum to illustrate redox conditions ranging from red (oxygen, +600 mV) to violet (hydrogen, -600 mV), assuming pH 7. Following color coding for ORP values introduced by Sale et al., (2021), the colors for inferred microbial processes include red for aerobes using oxygen, yellow for nitrogen reducers, green for iron reducers, blue for methanogens and sulfate reducers, and purple for hydrogenotrophic methanogens.

Episodic downward spikes in redox likely from shifts in oxygen, nitrate, and ferrous iron availability are seen in the vadose and groundwater zones. At the *No LNAPL* location, a spike of

increased ORP (i.e., more oxic conditions) across all depths (0.5-6.5 m bgs) was seen in August-October 2020. Smaller spikes of more oxidizing conditions into the formation (i.e., up to ~4 m bgs) are also seen at the *LNAPL-1* and *LNAPL-2* locations throughout the period of record (11/01/2019 – 02/28/2021). Following Sale et al., (2021), cycling ORP values in LNAPL zones may be due to barometric pumping of soil gases and/or biogas ebullition events in the groundwater zone. Further investigations are needed to resolve incomplete understandings of these apparent "downward spikes" in oxidizing conditions.

4.5.6. Microbiome Characterization

Characterized microbiomes (in all three core locations) agree well with the ORP data. Microbial ecology data including bacterial and archaeal microbiome characterization is shown and subtle differences between DNA- (present) and RNA-based (present and active) characterization were observed at locations where ORP values fluctuate, potentially due to these dynamic subsurface conditions in these locations.

Key attributes of microbial results include the following. First, microbial activity was detected via NGS of 16S rRNA transcripts at every sampled location that contained LNAPL, which supports occurrence of LNAPL biodegradation. While active microbes were detected at the *No LNAPL* location, transcript numbers were lower compared to the *LNAPL-1* and *LNAPL-2* locations. Second, microbiomes characterized in LNAPL zones (both at the DNA and the RNA level) indicate sulfate reduction and methanogenesis (Figures 4.4 panels b and c) are likely key processes that support biodegradation. Thirdly, microbes in the *No LNAPL* location vary with depth from 0.56 m to 4.35 m bgs. In contrast, in the *LNAPL-1* and *LNAPL-2* locations, microbial communities are different in the samples analyzed closer to the surface than those analyzed at deeper locations; however, below 2 m bgs, microbes show less variance with depth.

4.5.6.1. *No LNAPL* Location

At the *No LNAPL* location (Table SB.3 (DNA) and SB.4 (RNA)), in the sample collected at 0.64 m bgs, small differences were observed when biological processes are inferred utilizing DNA-based data versus RNA-based data. Identified microbiomes at the DNA level support the inference of a community composed mainly of bacteria involved in electron accepting processes ranging from iron reduction (members of the family *Gemmatimonadaceae* (Ma et al., 2019) and members of the genus *Vicinamibactrales* (Gong et al., 2021)) to aerobic processes (member of the genus *Methylobacter* (Smith et al., 2018)). Although putative iron reducers were identified at the DNA level, RNA microbial characterization at the time of sample collection suggests mainly aerobic and nitrate reducing organisms were active at 0.64 m bgs at the time of sampling. Active methanogens (as detected by the RNA analysis) at this depth compose only 2% of the community and have been identified as organisms belonging to the genus *Methanobacterium.* *Methanobacterium* spp. are methanogens, but these organisms are resilient to oxygen induced stresses (Zhou et al., 2021) and are often found in transition environments such as root zones. Eighty eight percent of the active archaeal community at 0.63 m bgs, has been identified as organisms belonging to the *Nitrososphaera* family. Most organisms of the *Nitrososphaera* family have been associated with the nitrogen cycle in the root zone of plants (Baskaran et al., 2021). At this location, the microbiology data agree well with the soil redox readings, which ranged from 129 to 329 mV associated with the nitrogen cycle redox processes. Although based on the RNA NGS analysis, active processes (at the time of sampling) range from nitrate reducing to aerobic processes, DNA analysis indicates that processes range from iron reducing to aerobic processes. Both datasets (microbial characterization and ORP measurements) characterize the soil sample

collected at 0.64 m bgs as a redox environment that fluctuates between iron reducing to aerobic processes.

Microbes identified at deeper locations at this boring were associated with iron reducing, sulfate reducing, fermentation and methanogenic processes. Active methanogens were only detected via RNA-based NGS at 2.62 m bgs. At the 2.62 m bgs *No LNAPL* location, 64% of the archaeal community detected belongs to the genus *Candidatus Methanomethylicus*. Members of the genus *Candidatus Methanomethylicus* are methylotrophic methanogens and have been found to inhabit iron reducing and sulfate reducing environments (Jia et al., 2021). Also, active organisms belonging to the archaeal class Bathyarchaeia were detected in the soil collected at 2.62 m bgs in the *No LNAPL* location, members of the *Bathyarchaeia* class have been identified as iron reducing organisms (Rios Del Toro et al., 2018). Members of the class *Bathyarchaeia* composed over 50% of the active archaeal community detected in the sample collected at 4.83 m bgs at the *No LNAPL* location.

4.5.6.2. *LNAPL-1* Location

The *LNAPL-1* location was sampled for microbial ecology at 1.55 m bgs, at 3 m, at 3.32 m bgs, and at 4.4 m bgs. These samples contained LNAPL and benzene. The active bacterial community identified at 1.55 m bgs was mainly composed of fermenting organisms such as members of the genus *Smithella* (17%) that have been associated with syntrophic alkane biodegradation under hydrogenotrophic methanogenesis conditions (Wawrik et al., 2016) and members of the order *Syntrophales* (4%) that have also been identified as fermenters in syntrophic methanogenic communities (Langwig et al., 2022). Active sulfate reducers of the genus *Desulfoprunum* were detected at 1.55 m bgs (21%). Members of the genus *Desulfoprunum* are known benzoate degraders and have been identified at LNAPL sites where benzene was

present (Bin Hudari et al., 2020). Members of the genus *Methalocystis* were also present at this sample location. Organisms belonging to the genus *Methalocystis* are known to oxidize methane in the presence of oxygen and have been associated with oxidizing methane under nitrate reducing conditions (Jung et al., 2020). Active archaea detected at 1.55 m bgs at the *LNAPL* location were predominantly methanogens. Both acetoclastic methanogens belonging to the genus *Methanosaeta* (69.5%) (Ito et al., 2011) and hydrogenotrophic methanogens belonging to the genus *Methanoregula* (6%) were detected. Approximately 20% of the active archaeal community, at 1.55 m bgs at the *LNAPL-1* location, was identified as being composed of members of the genus *Methanobacterium*. The identified active bacterial and archaeal communities at 1.55 m bgs at the *LNAPL-1* location indicate an anoxic redox environment where sulfate reduction and methanogenesis occur.

Microbial community characterization at the DNA level (Table SB.5) in combination with the RNA-based counterpart (Table SB.6) agrees with seasonally fluctuating ORP data that describes the soil environment at 1.55 m bgs at the *LNAPL-1* location as a redox environment that transitions episodically from iron reducing to sulfate reducing to methanogenic. Analysis of the samples collected at the remaining surveyed depths (3 m bgs, 3.32 m bgs, and 4.4 m bgs) at the *LNAPL-1* location identified active bacterial and archaeal communities associated with sulfate reducing and methanogenic processes. The microbial ecology characterization performed via DNA analysis supports the observations recorded via RNA analysis but also shows the presence of putative iron reducing and nitrate reducing organisms and thus the potential for iron and nitrate reducing processes to occur. The presence of putative iron and putative nitrate reducers at depths suggests, that at times, conditions at the site could favor these electron

accepting processes. Active organisms and complimentary chemical data suggest that at the time of sampling methanogenesis prevailed.

4.5.6.3. *LNAPL-2* Location

At the *LNAPL-2* location, microbiomes (Tables SB.7 and SB.8) were characterized in the samples collected at 0.33 m bgs, 3.39 m bgs, and 3.45 m bgs. Active organisms including fermenters such as *Smithella* spp. (over 30%) and methanogens such as *Methanosaeta* spp. (over 45%) were detected at every sampled depth, but the sample collected closest to the surface. At the time of sampling, this location (0.33 m bgs) was below the water table. The DNA-based microbial ecology characterization in combination with the continuous ORP data suggests that the redox environment at 0.33 m bgs in the *LNAPL-2* location fluctuates from nitrate reducing to iron reducing, and sometimes to sulfate reducing, conditions. It is likely that the presence of LNAPL in combination with a high-water table resulted in more reducing conditions, such as those found in methanogenic environments, which are likely unfavorable conditions for organisms found close to the surface. Thus, despite the potential for higher redox-based biodegradation to occur at this location, no activity was detected based on no detection in the RNA analysis at the time of sampling. In contrast, the samples collected deeper at this same boring location revealed the presence of active methanogens and active sulfate reducers based on RNA-based NGS analysis.

4.6. Discussion

4.6.1. Amount and Distribution of LNAPL

Cryogenic coring quantified specific LNAPL volumes of 2.7 and 7.5 cm per sampling area for the *LNAPL-1* and *LNAPL-2* locations, respectively. The importance of the smaller amount of LNAPL revealed by cryogenic coring is that the limited amounts of LNAPL

remaining can likely be addressed by NSZD in a few decades provided NSZD rates do not decrease from those shown in Figure 4.3, that is if biodegradation rates are zero order as proposed by Emerson (2016).

Data from cryogenic coring show low LNAPL presence in fine-grained soils, as described by Adamski et al., (2003), and as measured during our work, LNAPL biodegradation occurs in shallow and deep zones. Given the measured biodegradation rates of approximately 2,000 L/Ha/year (Figure 4.3) likely due to detected microbial activity, the largely immobile remaining LNAPL is likely to decrease. While cryogenic coring analyses are complimentary to LIF data to characterize LNAPL presence and distribution, estimation of LNAPL depletion timeframe at the site can only be accomplished with data generated through cryogenic coring, that allow us to quantify mass in place and combining this mass in place estimations with the measured degradation rates.

4.6.2. Verifying Processes Driving NSZD

Central to adopting NSZD as a remedy is verifying that NSZD is occurring. As with MNA of dissolved phase hydrocarbons in plumes, multiple lines of evidence can be used to demonstrate and document occurrence and rates of NSZD. MBTs are now more often used at the field-scale to provide lines of evidence for biodegradation in hydrocarbon plumes or for degradation of other contaminants (Gedalanga et al., 2016; Lu et al., 2006; Madison et al., 2023; Taggart & Key, 2023; Wilson et al., 2019, Wu et al., 2019). While MBTs can directly assay microorganisms responsible for biodegradation, there is additional value that can be unlocked through continuous monitoring with real-time data. Thus, monitoring other parameters (e.g., redox) that can be measured continuously can be coupled with MBTs to provide both continuous monitoring and mechanistic data to provide robust lines of evidence to demonstrate the

occurrence of NSZD. Herein, we show that continuous ORP data are consistent with microbial ecology data, providing evidence for using ORP sensors to track microbial processes associated with NSZD.

Microbial ecology data (i.e., MBTs) at this site document an active and diverse community of microbes driving NSZD through processes that include methanogenesis, sulfate reduction, iron cycling, and methane oxidation (Figure 4.4). RNA-based NGS provides evidence of these processes, occurring, further supported by biodegradation. rates calculated from temperature measurements that are based on methods advanced in Karimi Askarani & Sale (2020). Additionally, microorganisms can serve as redox indicators for complex soil-water environments (Irianni-Renno et al., 2023; Yin et al., 2021). Herein, the measured redox in the surveyed subsurface agrees well with inferred microbial metabolism. In general, microbial analysis at the DNA and RNA level show similar redox trends as those depicted by the soil-redox measurements collected via continuous sensing. Differences in characterized microbiomes at the DNA vs. the RNA level were observed in dynamic zones like the methane oxidation front. At this location, for example in the Continuous LNAPL location, based on the microbial analysis performed at the DNA level, an aerobic and nitrate-reducing community was inferred but no activity was detected based on RNA analysis. It is likely that at this location oxygen levels fluctuate and that is why, despite the fact that higher redox processes can occur at that location, absent oxygen no activity is detected.

Elevated temperatures due to exothermic biological processes provide a direct line of evidence for NSZD. ORP data provide continuous documentation of ongoing NSZD via sulfate reduction and methanogenesis in LNAPL zones and iron and oxygen cycling conditions in the

vadose zone. The detection of active microbes and analysis of LNAPL in place allow for accurate and corroborated interpretation of the continuous data.

A key challenge with the ORP data is that overbank floodplain deposits have NOM and reducing conditions that are similar to LNAPL zones; methane produced at these locations will be oxidized by microbes present in the vadose generating a temperature increase that indicates biodegradation. The biogeochemical characterization produced via the analyses of the cryogenically collected samples, coupled to periodic water chemistry analyses and gas analyses collected from the multilevel sampling ports installed along the continuous sensors, allows us to discern the type of biodegradation being measured by the other monitored parameters (for example NOM vs. PHC). Combining various tools (i.e., temperature profiling, ORP sensors, and MBTs) to generate complementary datasets increases the weight of evidence to demonstrate the occurrence of NSZD and associated biological processes at this site.

4.6.3. Conceptual Site Model (CSM)

A CSM (Figure 4.5) that describes the three cryocoring locations was developed by integrating the findings produced by the analysis of the collected data. A summary of the datasets included in the analysis are listed on Table 4.1. Data sets utilized are: biogeochemical data collected from the cryogenic core samples including microbiome analysis, water and gas chemistry collected from the MLS ports installed at each cryocore boring, and the continuous temperature and ORP data collected via remote sensing.

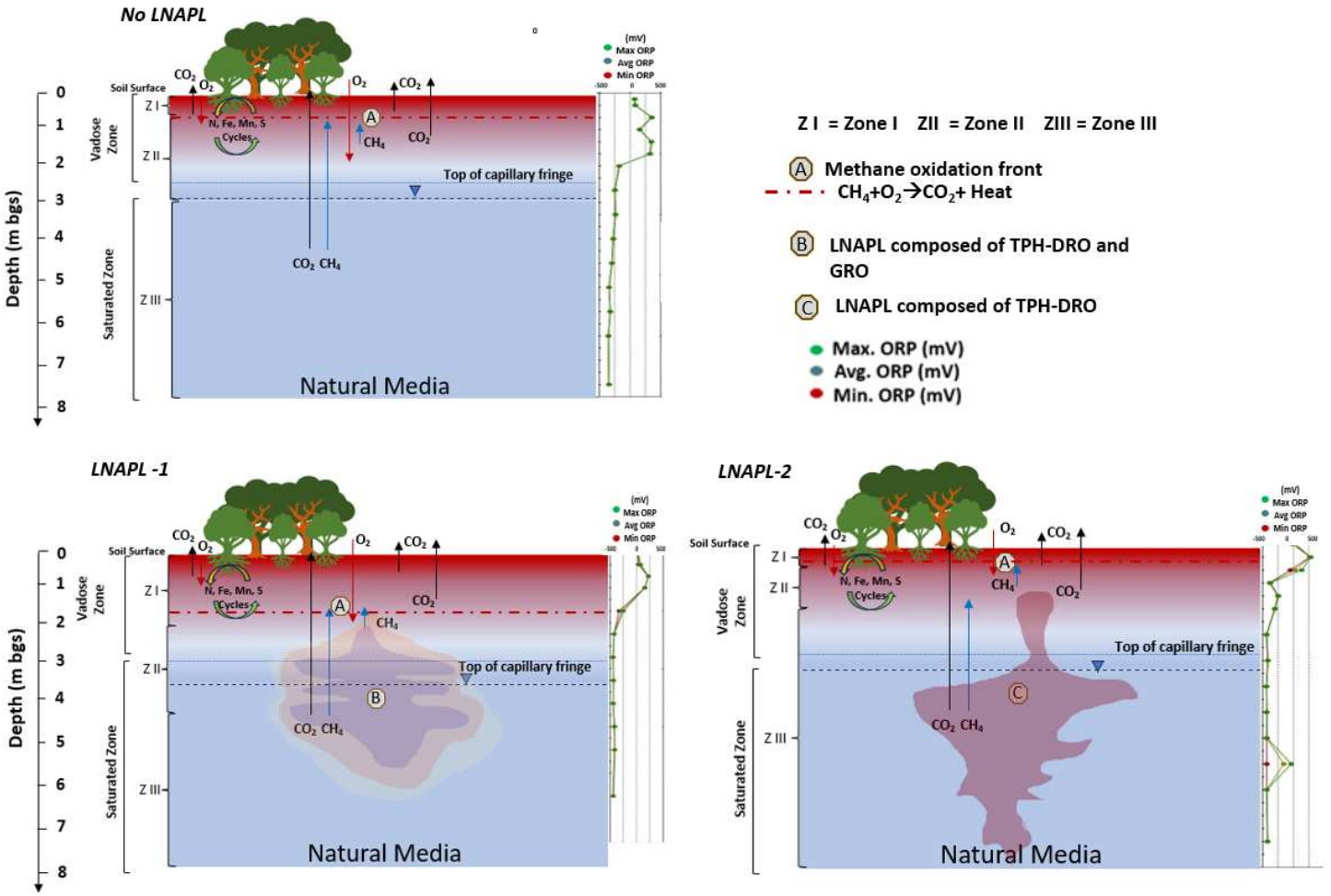

Figure 4.5. Site conceptual model showing three studied locations (*No LNAPL*, *LNAPL-1* and *LNAPL-2*) Dynamic data sets are integrated by showing maximum, minimum, and average ORP on the side of each location's model. Zone I is aerobic; Zone II is considered to have alternative electron acceptors available; Zone III is strictly methanogenic. The methane oxidation front at each location is identified by the letter A. B and C are used to denote the presence and type of LNAPL

Table 4.1. Summary of the data sets integrated in the CSM.

Tool implemented	Data set produced	One time sampling	Periodic sampling	
			Discrete	Continuous
Cryogenic coring	Hydrocarbon distribution	X		
	Pore water chemistry	X		
	Microbial ecology	X		
	Fluid saturations	X		
Multi level sampler	Gas composition		X	
	Water chemistry		X	
Temperature sensor	Temperature			X
	Degradation rates			X
Soil redox sensors	Redox			X

The *No LNAPL* location is conceptualized as having three zones. Zone I (0-0.6 m bgs) is an aerobic zone. Based on methane data collected in soil and gas samples, identified methane oxidizers (*Methylobacter* and *Methalocystis)*, and measured soil redox at 0.6 m bgs, likely the aerobic zone extends to that depth. Methane oxidation was also observed via the temperature-based method at 0.6 m bgs for the months of January, February, March, July, August, and September of 2020-2021. Although biodegradation was detected, all measurements were low when compared to those measured at the *LNAPL-1* and the *LNAPL-2* locations. Zone II (0.6-3 m bgs) has been conceptualized as a zone with ferric iron and sulfate available for degradation; methanogenesis and fermentation are also likely taking place at this location. At 1.5 m bgs, ORP decreases with depth support nitrate and iron reduction occurring. A pronounced dip in ORP can be seen at that location shifting from 400+ mV to 10 +mV. Based on the ORP readings with depth and the water quality data, iron and nitrate cycling associated with root zones are presumed to be occurring at this depth. Zone III was below 3 m bgs; active sulfate reducers, fermenters, and iron reducers were identified (Figure 4.4 and Table SB.1 and SB.4). Below 2 m bgs, ORP decreases steadily reaching sulfate-reducing and methanogenic values around 4.5 m bgs. Active

methanogens were only detected around 3 m bgs. Zone III is characterized as a reducing environment with no LNAPL biodegradation occurring. Low or no methanogenesis at this region of the subsurface agrees with the low biodegradation rates measured at this location and coincides with the absence of LNAPL detection via cryogenic coring methods.

The *LNAPL-1* location was also conceptualized as having three subsurface zones. According to the thermal data, recorded biodegradation is greatest at this location and was recorded for all months except for November (2020). Zone I (0-1.5 m bgs) is an aerobic zone and, based on the methane data collected in soil and gas samples, the methane oxidation front is likely located at 1.5 m bgs. No sample was analyzed for microbial analyses at this location. However, the characterized microbiome at the sample immediately below, collected above 2 m bgs, identified a low percentage of methane oxidizers *(Methalocystis*) and other anaerobic organisms composing the remainder of the active microbiome. Divergence between the maximum, minimum, and average recorded ORP was observed at the inferred location of the methane oxidation front. As noted by previous studies (Irianni-Renno et al., 2023; Sale et al., 2021) these variations are likely encountered in dynamic zones where redox cycling occurs. LNAPL composed of TPH-GRO and TPH-DRO was detected in Zone II (1.5 – 4.1 m bgs) extending as deep as 4.1 m bgs. Little to no ferrous iron was detected above 1.8 m bgs, but ferrous iron was detected below these depths indicating ferric iron is likely available at depths above 1.8 m bgs to be utilized as an electron acceptor. Iron reducing organisms were identified in Zone II as well. Zone III (below 4.1 m bgs) was characterized as a methanogenic zone with ORP readings below -400 mV. Active microbiomes characterized at these locations (3, 3.2 and 4.3 m bgs) included fermenters and methanogens.

The *LNAPL-2* location was conceptualized as having three main subsurface regions (Zone I, Zone II and Zone III) as well,. According to the thermal data, biodegradation occurred every month except for May 2021. Zone I (0-0.3 m bgs) was characterized as a shallow subsurface zone containing oxygen. The methane oxidation front was inferred to be at 0.3 m bgs as indicated by methane detected in soil and gas samples and oxygen measured in gas samples. At this location, ORP variations over time occur indicating a dynamic zone. In Zone II (0.3 -1.5 m bgs), ORP drops to ferric iron/nitrate reducing levels; at these depths processes associated with the root zone are likely to occur. ORP readings at the inferred zone depth reached -250 mV. In Zone III (below 1.5 m bgs), ferrous iron was detected at every aqueous sampling point and corresponding ORP values (below 1.54 m bgs) were at or below -450 mV indicating methanogenesis is the most likely process. Therefore, Zone III was inferred to be a strictly methanogenic zone.

4.7. Conclusions

Overall, this research suggested that combining continuous redox and temperature sensors with microbiome analysis (i.e., use of MBTs) can characterize *in situ* biodegradation occurrence and pathways better than the application of any of these tools alone. Soil redox data show episodic transitions in dynamic zones in the subsurface of the three boring locations. Microbial ecology data provide a similar description of the redox environment of the subsurface as illustrated by redox readings. The difference observed between the RNA-based characterization and the DNA-based characterization of the subsurface microbial ecology can be interpreted as the episodic fluctuations observed with the continuous temperature and ORP sensing. These data (temperature, ORP, and microbiome characterization) are complimentary lines of evidence that support the occurrence of NSZD processes at surveyed depths. The similar

description of the redox soil environment obtained by both NSZD characterization tools supports the use of continuous sensors as monitoring tools for biological processes. Sensors have the added advantage of providing real time feedback regarding the subsurface environment. Redox and temperature shifts can be associated with changes in other surface parameters (chemistry, water table fluctuations with barometric changes, etc.) besides biological processes. Therefore, understanding the environmental conditions where the sensors are deployed via cryogenic coring, or similar approaches, is critical to be able to interpret the redox evolution of surveyed environments via continuous sensing.

In this work we show how microorganisms can provide redox indicators in soil-water systems. Although similar observations were recorded by Yin et al., (2021) and by Irianni Renno et al., (2023), to our knowledge this study is the first to characterize active microbiomes in relation to *in situ* continuous ORP data at an LNAPL impacted site.

Further, we have shown how continuous multiple level temperature and ORP data coupled to microbiome characterization serve as complementary lines of evidence that collectively support and document the occurrence of NSZD. The modern tools tested herein for middle- and late-stage LNAPL sites offer opportunities to more effectively and efficiently manage legacy LNAPL sites.

CHAPTER 5. SUMMARY OF CONCLUSIONS AND FUTURE WORK

This work's major research findings are summarized and highlighted below. Lastly proposed future work based on this dissertation's key insights are outlined and briefly discussed.

5.1. Major Findings

NSZD of petroleum hydrocarbon has been established as an effective and practical remedy for mid to late-stage LNAPL sites, in the past decade (Karimi Askarani et al., 2024; Sale et al., 2018). However, broad technology adoption is lagging due to minimal advocacy, lack of process understanding and inadequate tools to monitor progress (Lari et al., 2019). In the work presented in Chapters 2, 3 and 4 of this dissertations, emerging NSZD monitoring tools are tested under laboratory conditions relevant to LNAPL impacted sites, and at field sites.

Despite the importance of being able to detect and characterize biological activity within LNAPL source zones, to date most RNA-based studies completed at hydrocarbon impacted sites involve analysis of samples containing plume levels of hydrocarbons. Examples of these include analysis of site water samples (Crisafi et al., 2016), analyses of culture media samples containing at most solubility levels of hydrocarbons (Canul-Chan et al., 2014), and analyses of soil samples containing less than 2,100 mg/kg of TPH per gram of soil (Fida et al., 2017). Until now, we have not seen RNA based analyses completed on samples containing petroleum liquid concentrations, such as those found in source zones. As part of this doctoral research, a new method was developed to allow for purification of RNA from LNAPL-impacted soils (Irianni-Renno et al., 2021). The new RNA extraction and purification method (Chapter 2) relies on a soil washing approach that has no adverse effects on RNA recovery but does improve RNA quality, by removing PCR inhibitors, which in turn allows for characterization of active microbial communities present in petroleum impacted soils. The new method was utilized in the research

presented in Chapters 3 and 4 of this dissertation, to gain key insights regarding the role of biodegradation in LNAPL zones.

Newly developed soil redox sensors for monitoring progress of NSZD and ENSZD were evaluated under biogeochemical conditions relevant to LNAPL-impacted sites, utilizing laboratory columns. The experiment evaluated the biogeochemical and soil redox responses of the LNAPL systems to two known enhancements (pulsed air sparging, and periodic sulfate addition). Although work relating hydrogeochemical data to continuous soil-ORP readings has been published previously (Sale et al., 2021), this is the first time that microbial activity was directly correlated to continuous soil-redox readings, utilizing IoT monitoring. Additionally, microbial work targeting 16S rRNA genes and transcripts provided key, novel insights regarding how LNAPL composition can drive sulfate utilization and the effects this has on hydrocarbon depletion rates. Although more work is needed to understand what drives different sulfate reduction pathways to be activated in LNAPL zones, this observation can help us understand how to monitor progress of ENSZD via sulfate addition.

Recent development of sensor based IoT technology applied to restoration of LNAPL sites can complement the existing NSZD toolbox in a way that would position NSZD above other technologies for LNAPL site restoration. Continuous IoT sensing is safer, more cost effective and more sustainable than other characterization and monitoring tools (Sale et al, 2021). Temperature based sensing has been established as an effective technology to measure hydrocarbon degradation rates (Karimi Askarani & Sale, 2020); and, lastly the RNA method developed as part of this dissertation (Irianni-Renno et al., 2021) allows for demonstrating NSZD activity (as shown with the measurement of *mcrA* transcripts in Chapter 3) in LNAPL soils. Chapter 4 of this dissertation combines the most recent technological advancements in NSZD

monitoring (applied continuous temperature and soil redox sensing, cryocoring and the recently developed RNA extraction method) to develop a high-resolution CSM that adds the dimension of time to capture natural depletion of hydrocarbon. The newly developed, dynamic CSM describes the site in detail and coupling to continuous IoT monitoring of temperature and ORP allows for the CSM to evolve as the site clean-up progresses. A more sustainable and effective approach to site restoration is envisioned for the site evaluated in this case study based on the novel characterization. Additionally, the combination of cryogenic coring with temperature-based degradation rates could allow for forecasting mass loss over time for this particular site.

5.2. Recommended Future Work

The results described herein suggest that NSZD and ENSZD could be greatly advanced as the main remedy for mature LNAPL sites. Key to achieving this lies in documenting the merits of such technology in ways that can be understood by both practitioners and regulators. Future research opportunities that should be pursued with the aim of establishing NSZD as a widely accepted remedy are outlined below.

Metatranscriptomic studies. Existing qPCR assays to identify genes encoding hydrocarbon degrading enzymes in environmental samples have limited applicability as the gene could be present but not expressed. A meta transcriptomics analysis of cryopreserved RNA samples of the experiment described in Chapter 3 can yield answers regarding hydrocarbon activated pathways during the enhancements. Insights gained via the proposed transcriptomic study could be used for the design of more relevant qPCR hydrocarbon degradation assays in a similar manner as performed in Rossmassler et al., (2019) work where a metagenomic analyses of o-xylene grown cultures provided sequences needed to design new primers for detecting o-xylene biodegradation.

Single compound sulfate reducing studies. Results presented in Chapter 3 suggest the presence of linear alkanes promotes sulfate utilization and sustains methanogenesis. Results presented in Chapter 3 also suggest that in the absence of linear alkanes, organotrophic sulfate reduction leads to sulfate reduction being the primary hydrocarbon depletion pathway halting methanogenesis. The omic studies suggested in the prior paragraph could be applied to sulfate enhanced hydrocarbon degrading cultures fed with sole carbon sources to elucidate the biodegradation pathways of each tested hydrocarbon.

Temporal variability in hydrocarbon mass as determined via cryocoring. The influence of different environmental factors on thermal determination of rates due to seasonal variations suggests the uncertainty in hydrocarbon depletion forecasts introduced in Chapter 4 could be further described and constrained. LNAPL depletion forecasts based on temperature should be verified with a long-term field study that would sample via cryocoring site soils to measure hydrocarbon depletion over time.

REFERENCES

Adams, J. A., & Ready, K. R. (2003). Extent of Benzene Biodegradation in Saturated Soil Column During Air Sparging. Groundwater Monitoring & Remediation, 23(3), 85–94. https://doi.org/10.1111/j.1745-6592.2003.tb00686.x

Adamski, M., Kremesec, V., & Charbeneau, R. J. (2003). Residual Saturation: What is it? How is it measured? How should we use it?. In Proceedings of the Petroleum Hydrocarbons and Organic Chemicals in Ground Water: Prevention, Assessment, and Remediation, 20th Conference and exposition, Costa mesa, CA.

Aitken, C., Jones, D., Maguire, M., Gray, N., Sherry, A., Bowler, B., Ditchfield, A., Larter, S., & Head, I. (2013). Evidence that crude oil alkane activation proceeds by different mechanisms under sulfate-reducing and methanogenic conditions. Geochim. Cosmochim. Acta, 109, 162–174.

Albers, C. N., Jensen, A., Bælum, J., & Jacobsen, C. S. (2013). Inhibition of DNA polymerases used in Q-PCR by structurally different soil-derived humic substances. Geomicrobiol. J., 30(8), 675–681.

American Petroleum Institute. (2017). Qualification of vapor phase-related natural source zone depletion processes. American Petroleum Institute.

Amos, R. T., Mayer, K. U., Bekins, B. A., Delin, G. N., & Williams, R. L. (2005). Use of dissolved and vapor-phase gases to investigate methanogenic degradation of petroleum hydrocarbon contamination in the subsurface. Water Resources Research, 41(2). https://doi.org/10.1029/2004WR003433.

An, D., Brown, D., Chatterjee, I., Dong, X., Ramos-Padron, E., Wilson, S., Bordenave, S., Caffrey, S. M., Gieg, L. M., & Sensen, C. W. (2013). Microbial community and potential

functional gene diversity involved in anaerobic hydrocarbon degradation and methanogenesis in an oil sands tailings pond. Genome, 56(10), 612–618.

Antonelli, F., Esposito, A., Galotta, G., Davidde Petriaggi, B., Piazza, S., Romagnoli, M., & Guerrieri, F. (2020). Microbiota in waterlogged archaeological wood: Use of Next-Generation Sequencing to evaluate the risk of biodegradation. Applied Sciences, 10(13), 4636.

Askarani, K. K., & Sale, T. C. (2020). Thermal estimation of natural source zone depletion rates without background correction. Water Res., 169, 115245.

Askarani, K. K., Stockwell, E. B., Piontek, K. R., & Sale, T. C. (2018). Thermal Monitoring of Natural Source Zone Depletion. Groundwater Monitoring & Remediation, 38(3), 43–52.

Atekwana, E. A., & Atekwana, E. A. (2010). Geophysical signatures of microbial activity at hydrocarbon contaminated sites: A review. Surveys in Geophysics, 31(2), 247–283.

Azubuike, C. C., Chikere, C. B., & Okpokwasili, G. C. (2016). Bioremediation techniques–classification based on site of application: Principles, advantages, limitations and prospects. World Journal of Microbiology and Biotechnology, 32(11), 180. https://doi.org/10.1007/s11274-016-2137-x

Baani, M., & Liesack, W. (2008). Two isozymes of particulate methane monooxygenase with different methane oxidation kinetics are found in Methylocystis sp. Strain SC2. Proceedings of the National Academy of Sciences, 105(29), 10203–10208.

Baskaran, S. M., Zakaria, M. R., Sabri, A. S. M. A., Mohamed, M. S., Wasoh, H., Toshinari, M., & Banat, I. M. (2021). Valorization of biodiesel side stream waste glycerol for rhamnolipids production by Pseudomonas aeruginosa RS6. Environmental Pollution, 276, 116742.

Beaver, C. L., Atekwana, E. A., Bekins, B. A., Ntarlagiannis, D., Slater, L. D., & Rossbach, S. (2021). Methanogens and their syntrophic partners dominate zones of enhanced magnetic susceptibility at a petroleum contaminated site. Frontiers in Earth Science, 9, 156.

Beck, D. A. C., McTaggart, T. L., Setboonsarng, U., Vorobev, A., Goodwin, L., Shapiro, N., Woyke, T., Kalyuzhnaya, M. G., Lidstrom, M. E., & Chistoserdova, L. (2015). Multiphyletic origins of methylotrophy in A lphaproteobacteria , exemplified by comparative genomics of L ake W ashington isolates. Environmental Microbiology, 17(3), 547–554. https://doi.org/10.1111/1462-2920.12736

Bergstrom, R. E., & Walker, T. R. (1956). Groundwater Geology of the East St. Louis Area, Illinois. Report of investigations no. 191.

Bhuvaneswar, C., Swathi, G., Bhaskar, B., Munichandrababu, T., & Rajendra, W. (2012). Effective synergetic biodegradation of diesel oil by bacteria. International Journal of Environmental Biology, 2(4), 195–199.

Bin Hudari, M. S., Vogt, C., & Richnow, H. H. (2020). Effect of Temperature on Acetate Mineralization Kinetics and Microbial Community Composition in a Hydrocarbon-Affected Microbial Community During a Shift from Oxic to Sulfidogenic Conditions. Frontiers in Microbiology, 11, 3183.

Bojan, O. K., Irianni-Renno, M., Hanson, A. J., Chen, H., Young, R. B., De Long, S. K., Borch, T., Sale, T. C., McKenna, A. M., & Blotevogel, J. (2021). Discovery of Oxygenated Hydrocarbon Biodegradation Products at a Late-Stage Petroleum Release Site. Energy & Fuels, 35(20), 16713–16723. https://doi.org/10.1021/acs.energyfuels.1c02642

Boll, M., Estelmann, S., & Heider, J. (2020). Anaerobic Degradation of Hydrocarbons: Mechanisms of Hydrocarbon Activation in the Absence of Oxygen. In M. Boll (Ed.),

Anaerobic Utilization of Hydrocarbons, Oils, and Lipids (pp. 3–29). Springer International Publishing. https://doi.org/10.1007/978-3-319-50391-2_2

Bouchard, D., Hunkeler, D., Madsen, E. L., Buscheck, T., Daniels, E., Kolhatkar, R., DeRito, C. M., Aravena, R., & Thomson, N. (2018). Application of Diagnostic Tools to Evaluate Remediation Performance at Petroleum Hydrocarbon-Impacted Sites. Groundwater Monitoring & Remediation, 38(4), 88–98. https://doi.org/10.1111/gwmr.12300

Bouchard, D., Marchesi, M., Madsen, E. L., DeRito, C. M., Thomson, N. R., Aravena, R., Barker, J. F., et al. (2018). Diagnostic tools to assess mass removal processes during pulsed air sparging of a petroleum hydrocarbon source zone. Groundwater Monitoring & Remediation, 38(4), 29-44.

Breukelen, B. M. (2015). Biodegradation: updating the concepts of control for microbial cleanup in contaminated aquifers. Environmental Science & Technology, 49(12), 7073-7081.

Bruce, L. G., & Biagi, C. Q. (1997). Capillary Control of Free Phase Oil Migration in the Shallow Subsurface: Review with Case Histories. Environmental Geosciences, 4(4), 177–185.

Bruckberger, M., Gleeson, D., Bastow, T., Morgan, M., Walsh, T., Rayner, J., Davis, G., & Puzon, G. (2021). Unravelling Microbial Communities Associated with Different Light Non-Aqueous Phase Liquid Types Undergoing Natural Source Zone Depletion Processes at a Legacy Petroleum Site. Water, 13(7), 898. https://doi.org/10.3390/w13070898

Bujewski, G., & Rutherford, B. (1997). The site characterization and analysis penetrometer system (SCAPs) laser-induced fluorescence (LIF) sensor and support system. Innovative Technology Verification Report.

Burge, S. R., Burge, R. G., & Hoffman, D. A. (2018). Microbial sensor system for the assessment of subsurface environments (Patent US 15/237,230).

Cai, Y., Shen, J. P., Di, H. J., Zhang, L. M., Zhang, C., & He, J. Z. (2020). Variation of soil nitrate and bacterial diversity along soil profiles in manure disposal maize field and adjacent woodland. Journal of Soils and Sediments, 20, 3557–3568.

Callahan, B. J., McMurdie, P. J., Rosen, M. J., Han, A. W., Johnson, A. J. A., & Holmes, S. P. (2016). DADA2: High-resolution sample inference from Illumina amplicon data. Nature Methods, 13(7), 581–583. https://doi.org/10.1038/nmeth.3869

Canul-Chan, M., Estrella-Gomez, N., Zepeda, A., Cabanias-Vargas, & Rojas-Herrera, R. (2014). A protocol for metagenomic RNA extraction from bacterial consortium in the presence of crude oil. Romanian Biotechnological Letters, 19(1).

Castelle, C. J., Wrighton, K. C., Thomas, B. C., Hug, L. A., Brown, C. T., Wilkins, M. J., & Banfield, J. F. (2015). Genomic expansion of domain archaea highlights roles for organisms from new phyla in anaerobic carbon cycling. Current Biology, 25(6), 690–701.

Cavaliere, M., Feng, S., Soyer, O. S., & Jiménez, J. I. (2017). Cooperation in microbial communities and their biotechnological applications. Environmental Microbiology, 19(8), 2949–2963.

Chapple, M. C., Vittorio Jr, L. F., Tucker, W. A., & Richey, M. G. (1998). Capillary influences on the operation and effectiveness of LNAPL interceptor trenches. Geological Society, London, Engineering Geology Special Publications, 14(1), 13–18.

Chaudhari, N. M., Overholt, W. A., Figueroa-Gonzalez, P. A., Taubert, M., Bornemann, T. L. V., Probst, A. J., Hölzer, M., Marz, M., & Küsel, K. (2021). The economical lifestyle of

CPR bacteria in groundwater allows little preference for environmental drivers. Environmental Microbiome, 16(1), 24. https://doi.org/10.1186/s40793-021-00395-w

Chen, H., Hao, S., Chen, Z., Sompong, O., Fan, J., Clark, J., & Zhang, S. (2020). Mesophilic and thermophilic anaerobic digestion of aqueous phase generated from hydrothermal liquefaction of cornstalk: Molecular and metabolic insights. Water Research, 168, 115199.

Chen, K.-F., Kao, C.-M., Chen, C.-W., Surampalli, R. Y., & Lee, M.-S. (2010). Control of petroleum-hydrocarbon contaminated groundwater by intrinsic and enhanced bioremediation. Journal of Environmental Sciences, 22(6), 864–871. https://doi.org/10.1016/S1001-0742(09)60190-X

Chen, M. Y., Wu, S. H., Lin, G. H., Lu, C. P., Lin, Y. T., Chang, W. C., & Tsay, S. S. (2004). Rubrobacter taiwanensis sp. Nov., a novel thermophilic, radiation-resistant species isolated from hot springs. International Journal of Systematic and Evolutionary Microbiology, 54(5), 1849–1855.

Chen, W., Li, T., Ren, Y., Wang, J., Chen, H., & Wang, Q. (2023). Biological hydrogen with industrial potential: Improvement and prospection in biohydrogen production. Journal of Cleaner Production, 387, 135777.

Clarke, A. N., Norris, R. D., & Wilson, D. J. (2017). Saturated Zone Remediation of VOCs Through Sparging. In D. J. Wilson & A. N. Clarke (Eds.), Hazardous Waste Site Soil Remediation (1st ed., pp. 433–455). CRC Press. https://doi.org/10.1201/9780203752258-8

Coates, J. D., Lonergan, D. J., Philips, E. J. P., Jenter, H., & Lovley, D. R. (1995). Desulfuromonas palmitatis sp nov, a marine dissimilatory Fe III reducer that can oxidize long-chain fatty acids. Archives of Microbiology, 164(6), 406–413.

Crisafi, F., Giuliano, L., Yakimov, M. M., Azzaro, M., & Denaro, R. (2016). Isolation and degradation potential of a cold-adapted oil/PAH-degrading marine bacterial consortium from Kongsfjorden (Arctic region). Rendiconti Lincei, 27(1), 261-270.

Daugulis, A. J., & McCracken, C. M. (2003). Microbial degradation of high and low molecular weight polyaromatic hydrocarbons in a two-phase partitioning bioreactor by two strains of Sphingomonas sp. Biotechnology Letters, 25(17), 1441–1444.

Davis, G. B., Rayner, J. L., & Donn, M. J. (2023). Advancing "Autonomous" sensing and prediction of the subsurface environment: a review and exploration of the challenges for soil and groundwater contamination. Environmental Science and Pollution Research, 30(8), 19520-19535.

Davis, G. B., Rayner, J. L., Donn, M. J., Johnston, C. D., Lukatelich, R., King, A., Bastow, T. P., & Bekele, E. (2022). Tracking NSZD mass removal rates over decades: Site-wide and local scale assessment of mass removal at a legacy petroleum site. Journal of Contaminant Hydrology, 248, 104007. https://doi.org/10.1016/j.jconhyd.2022.104007

DePoy, A. N., King, G. M., & Ohta, H. (2021). Anaerobic Carbon Monoxide Uptake by Microbial Communities in Volcanic Deposits at Different Stages of Successional Development on O-yama Volcano, Miyake-jima, Japan. Microorganisms, 9(1), 12.

Dojka, M. A., Hugenholtz, P., Haack, S. K., & Pace, N. R. (1998). Microbial diversity in a hydrocarbon-and chlorinated-solvent-contaminated aquifer undergoing intrinsic bioremediation. Applied and Environmental Microbiology, 64(10), 3869–3877.

Dong, H., Huang, L., Zhao, L., Zeng, Q., Liu, X., Sheng, Y., Shi, L., Wu, G., Jiang, H., Li, F., Zhang, L., Guo, D., Li, G., Hou, W., & Chen, H. (2022). A critical review of mineral–microbe interaction and co-evolution: Mechanisms and applications. National Science Review, 9(10), nwac128. https://doi.org/10.1093/nsr/nwac128

Edwards, E. A., Toth, C. R. A., Luo, F., Bawa, N., Webb, J., Guo, S., & Dworatzek, S. (2021). Anaerobic benzene biodegradation linked to the growth of highly specific bacterial clades. Environmental Science and Technology, 55(12).

Embree, M., Liu, J. K., Al-Bassam, M. M., & Zengler, K. (2015). Networks of energetic and metabolic interactions define dynamics in microbial communities. Proceedings of the National Academy of Sciences, 112(50), 15450–15455. https://doi.org/10.1073/pnas.1506034112

Emerson, E. (2016). Biotic Control of LNAPL Longevity Laboratory and Field-Scale Studies [MS thesis]. Colorado State University.

Feldewert, C., Lang, K., & Brune, A. (2020). The hydrogen threshold of obligately methyl-reducing methanogens. FEMS Microbiology Letters, 367(17), fnaa137.

Feng, L., Chen, J., Wang, F., Chen, Y., & Luo, J. (2019). Acidogenic fermentation facilitates anaerobic biodegradation of polycyclic aromatic hydrocarbons in waste activated sludge. ACS Sustainable Chemistry & Engineering, 7(5), 5404–5411.

Feng, W. M., Liu, P., Yan, H., Zhang, S., Shang, E. X., Yu, G., & Duan, J. A. (2021). Impact of Bacillus on Phthalides Accumulation in Angelica sinensis (Oliv.) by Stoichiometry and Microbial Diversity Analysis. Frontiers in Microbiology, 11, 3421.

Fida, T. T., Moreno-Forero, S. K., Breugelmans, P., Heipieper, H. J., Röling, W. F., & Springael, D. (2017). Physiological and transcriptome response of the polycyclic aromatic

hydrocarbon degrading Novosphingobium sp. LH128 after inoculation in soil. Environmental Science & Technology, 51(3), 1570-1579.

Gao, P., Tian, H., Li, G., Sun, H., & Ma, T. (2015). Microbial diversity and abundance in the Xinjiang Luliang long-term water-flooding petroleum reservoir. MicrobiologyOpen, 4(2), 332–342.

Garg, S., Newell, C. J., Kulkarni, P. R., King, D. C., Adamson, D. T., Renno, M. I., & Sale, T. (2017). Overview of Natural Source Zone Depletion: Processes, Controlling Factors, and Composition Change. Groundwater Monitoring & Remediation, 37(3), 62–81. https://doi.org/10.1111/gwmr.12219

Gedalanga, P., Madison, A., Miao, Y., Richards, T., Hatton, J., DiGuiseppi, W. H., Wilson, J., & Mahendra, S. (2016). A multiple lines of evidence framework to evaluate intrinsic biodegradation of 1,4-dioxane. Remediation Journal, 27(1), 93-114.

Gieg, L. M., Fowler, S. J., & Berdugo-Clavijo, C. (2014). Syntrophic biodegradation of hydrocarbon contaminants. Current Opinion in Biotechnology, 27, 21–29.

Gong, W.-J., Niu, Z.-F., Wang, X.-R., & Zhao, H.-P. (2021). How the Soil Microbial Communities and Activities Respond to Long-Term Heavy Metal Contamination in Electroplating Contaminated Site. Microorganisms, 9(2), 362.

Guo, G., Tian, F., Ding, K., Wang, L., Liu, T., & Yang, F. (2017). Effect of a bacterial consortium on the degradation of polycyclic aromatic hydrocarbons and bacterial community composition in Chinese soils. Int. Biodeterior. Biodegrad., 123, 56–62.

Gupta, A., Dutta, A., Panigrahi, M. K., & Sar, P. (2021). Geomicrobiology of mine tailings from malanjkhand copper project, India. Geomicrobiology Journal, 38(2), 97–114.

Haynes, W. M. (2014). CRC Handbook of Chemistry and Physics. CRC Press, Boca Raton, Florida.

Howard, A. K. (1986). Soil Classification Handbook: Unified Soil Classification System. Geotechnical Branch, Division of Research and Laboratory Services, Engineering and Research Center, Bureau of Reclamation, Denver, Colorado.

Hua, D., Fan, Q., Zhao, Y., Xu, H., Chen, L., Si, H., & Li, Y. (2020). Continuous anaerobic digestion of wood vinegar wastewater from pyrolysis: Microbial diversity and functional genes prediction. Frontiers in Bioengineering and Biotechnology, 8, 923.

Huang, R., Phan, H., Herng, T. S., Hu, P., Zeng, W., Dong, S. Q., ... & Wu, J. (2016). Higher order π-conjugated polycyclic hydrocarbons with open-shell singlet ground state: nonazethrene versus nonacene. Journal of the American Chemical Society, 138(32), 10323-10330.

Huang, W. H., Dong, C. D., Chen, C. W., Surampalli, R. Y., & Kao, C. M. (2017). Application of sulfate reduction mechanisms for the simultaneous bioremediation of toluene and copper contaminated groundwater. International Biodeterioration & Biodegradation, 124, 215-222.

Hunter, K. S., Wang, Y., & Van Cappellen, P. (1998). Kinetic modeling of microbially-driven redox chemistry of subsurface environments: Coupling transport, microbial metabolism and geochemistry. Journal of Hydrology, 209(1–4), 53–80. https://doi.org/10.1016/S0022-1694(98)00157-7

Huntley, D., & Beckett, G. D. (2002). Persistence of LNAPL sources: Relationship between risk reduction and LNAPL recovery. Journal of Contaminant Hydrology, 59(1–2), 3–26.

Irianni-Renno, M., Akhbari, D., Olson, M. R., Byrne, A. P., Lefevre, E., Zimbron, J., Lyverse, M., Sale, T. C., & Long, S. K. D. (2016). Comparison of bacterial and archaeal communities in depth-resolved zones in an LNAPL body. Applied Microbiology and Biotechnology, 100(7), 3347–3360.

Irianni-Renno, M., Rico, J. L., Key, T. A., & De Long, S. K. (2023). Evaluating NSZD and ENSZD in Laboratory Columns via Soil Redox Continuous Sensing and Microbiome Characterization.

Irianni-Renno, M., Sale, T. C., & De Long, S. K. (2021). Advanced methods for RNA recovery from petroleum impacted soils. MethodsX, 8, 101503. https://doi.org/10.1016/j.mex.2021.101503

Ito, T., Yoshiguchi, K., Ariesyady, H. D., & Okabe, S. (2011). Identification of a novel acetate-utilizing bacterium belonging to Synergistes group 4 in anaerobic digester sludge. The ISME Journal, 5(12), 1844–1856. https://doi.org/10.1038/ismej.2011.59

ITRC. (2009). Evaluating Natural Source Zone Depletion at Sites with LNAPL. Interstate Technology and Regulatory Council, Washington, DC.

ITRC. (2018). Light non-aqueous phase liquid (LNAPL) site management: LCSM evolution, decision process, and remedial technologies. https://lnapl-3.itrcweb.org

Ji, J.-H., Zhou, L., Mbadinga, S. M., Irfan, M., Liu, Y.-F., Pan, P., Qi, Z.-Z., Chen, J., Liu, J.-F., Yang, S.-Z., Gu, J.-D., & Mu, B.-Z. (2020). Methanogenic biodegradation of C9 to C12n-alkanes initiated by Smithella via fumarate addition mechanism. AMB Express, 10(1), 23. https://doi.org/10.1186/s13568-020-0956-5

Jia, Y., Kumar Khanal, S., Yin, L., Sun, L., & Lu, H. (2021). Influence of ibuprofen and its biotransformation products on different biological sludge systems and ecosystem. Environment International, 146, 106265.

Jiménez, N., Richnow, H. H., Vogt, C., Treude, T., & Krüger, M. (2016). Methanogenic hydrocarbon degradation: Evidence from field and laboratory studies. J. Mol. Microbiol. Biotechnol., 26(1–3), 227–242.

Jochum, L. M., Schreiber, L., Marshall, I. P., Jørgensen, B. B., Schramm, A., & Kjeldsen, K. U. (2018). Single-cell genomics reveals a diverse metabolic potential of uncultivated Desulfatiglans-related Deltaproteobacteria widely distributed in marine sediment. Frontiers in Microbiology, 9, 2038.

Johnson, P. C., Johnson, R. L., Bruce, C. L., & Leeson, A. (2001). Advances in In Situ Air Sparging/Biosparging. Bioremediation Journal, 5(4), 251–266. https://doi.org/10.1080/20018891079311

Johnson, P. C., Leeson, A., Johnson, R. L., Vogel, C. M., Hinchee, R. E., Marley, M., Peargin, T., Bruce, C. L., Amerson, I. L., Coonfare, C. T., & Gillespie, R. D. (2001). A Practical Approach for the Selection, Pilot Testing, Design, and Monitoring of In Situ Air Sparging/Biosparging Systems. Bioremediation Journal, 5(4), 267–281. https://doi.org/10.1080/20018891079320

Johnson, P., Lundegard, P., & Liu, Z. (2006). Source zone natural attenuation at petroleum hydrocarbon spill sites – I: site-specific assessment approach. Groundwater Monitoring & Remediation, 26(4), 82–92.

Johnson, S. J., & Jackson, R. N. (2013). Ski2-like RNA helicase structures: common themes and complex assemblies. RNA biology, 10(1), 33-43.

Jolivet, J., & Vasseur, G. (1982). Sur un essai de mesure directe du flux geothermique in situ. Ann. Geophys., 38, 225-239.

Jorgensen, K. (2011). In Situ Bioremediation. In E. Inc (Ed.), Comprehensive Biotechnology (2nd ed., Vol. 6, pp. 59–67). Elsevier Inc.

Jørgensen, K. S. (2007). In situ bioremediation. Advances in Applied Microbiology, 61, 285-305.

Jung, H., Koh, D. C., Kim, Y. S., Jeen, S. W., & Lee, J. (2020). Stable isotopes of water and nitrate for the identification of groundwater flowpaths: A review. Water, 12(1), 138.

Junghare, M., & Schink, B. (2015). Desulfoprunum benzoelyticum gen. Nov., sp. Nov., a Gram-stain-negative, benzoate-degrading, sulfate-reducing bacterium isolated from a wastewater treatment plant. International Journal of Systematic and Evolutionary Microbiology, 65(Pt_1), 77–84. https://doi.org/10.1099/ijs.0.066761-0

Juottonen, H., Galand, P. E., & Yrjälä, K. (2006). Detection of methanogenic Archaea in peat: Comparison of PCR primers targeting the mcrA gene. Res. Microbiol., 157(10), 914–921.

Jury, W. A., & Horton, R. (2004). Soil Physics. John Wiley & Sons, New York.

Kanaparthi, D., Pommerenke, B., Casper, P., & Dumont, M. G. (2013). Chemolithotrophic nitrate-dependent Fe (II)-oxidizing nature of actinobacterial subdivision lineage TM3. The ISME Journal, 7(8), 1582–1594.

Karimi Askarani, K., & Sale, T. C. (2020). Thermal estimation of natural source zone depletion rates without background correction. Water Research, 169, 115245.

Karimi Askarani, K., Sale, T., & Palaia, T. (2024). Natural Source Zone Depletion of Petroleum Hydrocarbon NAPL. In J. García-Rincón, E. Gatsios, R. J. Lenhard, E. A. Atekwana, & R. Naidu (Eds.), Advances in the Characterisation and Remediation of Sites

Contaminated with Petroleum Hydrocarbons (pp. 113–138). Springer International Publishing. https://doi.org/10.1007/978-3-031-34447-3_5

Karimi Askarani, K., Stockwell, E. B., Piontek, K. R., & Sale, T. C. (2018). Thermal Monitoring of Natural Source Zone Depletion. Groundwater Monitoring & Remediation, 38(3).

Key, T. A., Sorsby, S. J., Wang, Y., & Madison, A. S. (2022). Framework for field-scale application of molecular biological tools to support natural and enhanced bioremediation. Frontiers in Microbiology, 13, 958742. https://doi.org/10.3389/fmicb.2022.958742

Kiaalhosseini, S., Johnson, R. L., Rogers, R. C., Renno, M. I., Lyverse, M., & Sale, T. C. (2016). Cryogenic core collection (C3) from unconsolidated subsurface media. Groundwater Monitoring & Remediation, 36(4), 41–49.

Kim, S., Bae, J., Choi, O., Ju, D., Lee, J., Sung, H., & Um, Y. (2014). A pilot scale two-stage anaerobic digester treating food waste leachate (FWL): Performance and microbial structure analysis using pyrosequencing. Process Biochemistry, 49(2), 301–308.

King, G. M. (2006). Nitrate-dependent anaerobic carbon monoxide oxidation by aerobic CO-oxidizing bacteria. FEMS Microbiology Ecology, 56(1), 1–7.

Kleindienst, S., Herbst, F.-A., Stagars, M., Von Netzer, F., Von Bergen, M., Seifert, J., Peplies, J., et al. (2014). Diverse sulfate-reducing bacteria of the Desulfosarcina/Desulfococcus clade are the key alkane degraders at marine seeps. The ISME Journal, 8(10), 2029–2044.

Kolhatkar, R., & Schnobrich, M. (2017). Land Application of Sulfate Salts for Enhanced Natural Attenuation of Benzene in Groundwater: A Case Study. Groundwater Monitoring & Remediation, 37(2), 43–57. https://doi.org/10.1111/gwmr.12209

Kontanis, E. J., & Reed, F. A. (2006). Evaluation of real-time PCR amplification efficiencies to detect PCR inhibitors. Journal of Forensic Sciences, 51(4), 795–804.

Kraan, G. M. van der, Ridder, M. D., Lomans, B. P., & Muyzer, G. (2010). Sampling and nucleic extraction procedures from oil reservoir samples. In Applied microbiology and molecular biology in oilfield systems (pp. 7–16). Springer.

Kuever, J., Rainey, F. A., & Widdel, F. (2015). Desulfovirga. In Bergey's Manual of Systematics of Archaea and Bacteria (pp. 1–2).

Kulkarni, P. R., Newell, C. J., King, D. C., Molofsky, L. J., & Garg, S. (2020). Application of Four Measurement Techniques to Understand Natural Source Zone Depletion Processes at an LNAPL Site. Groundwater Monitoring & Remediation, 40(3), 75–88. https://doi.org/10.1111/gwmr.12398

Kümmel, S., Herbst, F.-A., Bahr, A., Duarte, M., Pieper, D. H., Jehmlich, N., Seifert, J., von Bergen, M., Bombach, P., Richnow, H. H., & Vogt, C. (2015). Anaerobic naphthalene degradation by sulfate-reducing Desulfobacteraceae from various anoxic aquifers. FEMS Microbiology Ecology, 91(3). https://doi.org/10.1093/femsec/fiv006

Laczi, K., Kis, E., Szilágyi, Á., Bounedjoum, N., Bodor, A., Vincze, G. E., et al. (2020). New frontiers of anaerobic hydrocarbon biodegradation in the multi-omics era. Frontiers in Microbiology, 11, 2886.

Langwig, M. V., De Anda, V., Dombrowski, N., Seitz, K. W., Rambo, I. M., Greening, C., Teske, A. P., & Baker, B. J. (2022). Large-scale protein level comparison of Deltaproteobacteria reveals cohesive metabolic groups. The ISME Journal, 16(1), 307–320. https://doi.org/10.1038/s41396-021-01057-y

Lari, K. S., Davis, G. B., Rayner, J. L., Bastow, T. P., & Puzon, G. J. (2019). Natural source zone depletion of LNAPL: A critical review supporting modelling approaches. Water Research, 157, 630–646.

Lee, J., Koo, T., Yulisa, A., & Hwang, S. (2019). Magnetite as an enhancer in methanogenic degradation of volatile fatty acids under ammonia-stressed condition. Journal of Environmental Management, 241, 418–426.

Lee, K., & Ulrich, A. (2021). Indigenous microbial communities in Albertan sediments are capable of anaerobic benzene biodegradation under methanogenic, sulfate-reducing, nitrate-reducing, and iron-reducing redox conditions. Water Environment Research, 93(4), 524–534.

Levar, C. E., Hoffman, C. L., Dunshee, A. J., Toner, B. M., & Bond, D. R. (2017). Redox potential as a master variable controlling pathways of metal reduction by Geobacter sulfurreducens. The ISME Journal, 11(3), 741–752. https://doi.org/10.1038/ismej.2016.146

Li, W., Cai, C., Song, Y., Ni, G., Zhang, X., & Lu, P. (2021). The Role of Crystalline Iron Oxides in Methane Mitigation through Anaerobic Oxidation of Methane. ACS ES&T Water, 1(5), 1153–1160. https://doi.org/10.1021/acsestwater.0c00199

Liang, B., Wang, L.-Y., Mbadinga, S. M., Liu, J.-F., Yang, S.-Z., Gu, J.-D., & Mu, B.-Z. (2015). Anaerolineaceae and Methanosaeta turned to be the dominant microorganisms in alkanes-dependent methanogenic culture after long-term of incubation. Amb Express, 5(1), 37.

Liang, L., Song, X., Kong, J., Shen, C., Huang, T., & Hu, Z. (2014). Anaerobic biodegradation of high-molecular-weight polycyclic aromatic hydrocarbons by a facultative anaerobe Pseudomonas sp. JP1. Biodegradation, 25(6), 825–833.

Linda, A., & Bouziane, A. (2012). Petroleum-oil biodegradation by Corynebacterium aquaticum and Pseudomonas aeruginosa strains isolated from the industrial rejection of the refinery of ARZEW-Algeria. World Appl. Sci, 18, 1119–1123.

Liu, Y. F., Qi, Z. Z., Shou, L. B., Liu, J. F., Yang, S. Z., Gu, J. D., & Mu, B. Z. (2019). Anaerobic hydrocarbon degradation in candidate phylum 'Atribacteria' (JS1) inferred from genomics. The ISME Journal, 13(9), 2377–2390.

Liu, Y., Balkwill, D. L., Aldrich, H. C., Drake, G. R., & Boone, D. R. (1999). Characterization of the anaerobic propionate-degrading syntrophs Smithella propionica gen. Nov., sp. Nov. And Syntrophobacter wolinii. International Journal of Systematic and Evolutionary Microbiology, 49(2), 545–556.

Livney, Y. D. (2010). Milk proteins as vehicles for bioactives. Current Opinion in Colloid & Interface Science, 15(1–2), 73–83.

Löffler, F. E., & Edwards, E. A. (2006). Harnessing microbial activities for environmental cleanup. Current Opinion in Biotechnology, 17(3), 274–284.

Lovley, D. R., Giovannoni, S. J., White, D. C., Champine, J. E., Phillips, E., Gorby, Y. A., & Goodwin, S. (1993). Geobacter metallireducens gen. Nov. Sp. Nov., a microorganism capable of coupling the complete oxidation of organic compounds to the reduction of iron and other metals. Arch. Microbiol., 159(4), 336–344.

Lu, L., Huggins, T., Jin, S., Zuo, Y., & Ren, Z. J. (2014). Microbial Metabolism and Community Structure in Response to Bioelectrochemically Enhanced Remediation of Petroleum Hydrocarbon-Contaminated Soil. Environmental Science & Technology, 48(7), 4021–4029. https://doi.org/10.1021/es4057906

Lu, X., Wilson, J. T., & Kampbell, D. H. (2006). Relationship between Dehalococcoides DNA in groundwater and rates of reductive dechlorination at field scale. Water Research, 40(16), 3131–3140.

Lueders, T. (2017). The ecology of anaerobic degraders of BTEX hydrocarbons in aquifers. FEMS Microbiology Ecology, 93(1), fiw220. https://doi.org/10.1093/femsec/fiw220

Lundegard, P. D., & Johnson, P. C. (2006). Source zone natural attenuation at petroleum hydrocarbon spill sites—II: Application to a former oil field. Groundwater Monitoring & Remediation, 26(4), 93–106.

Luo, H., Dahlen, P. R., Johnson, P. C., & Peargin, T. (2013). Proof-of-concept study of an aerobic vapor migration barrier beneath a building at a petroleum hydrocarbon-impacted site. Environmental Science & Technology, 47(4), 1977–1984.

Ma, S., Tong, M., Yuan, S., & Liu, H. (2019). Responses of the microbial community structure in Fe (II)-bearing sediments to oxygenation: The role of reactive oxygen species. ACS Earth and Space Chemistry, 3(5), 738–747.

Ma, T.-T., Liu, L.-Y., Rui, J.-P., Yuan, Q., Feng, D.-S., Zhou, Z., Dai, L.-R., Zeng, W.-Q., Zhang, H., & Cheng, L. (2017). Coexistence and competition of sulfate-reducing and methanogenic populations in an anaerobic hexadecane-degrading culture. Biotechnology for Biofuels, 10(1), 1-14.

Madison, A. S., Sorsby, S. J., Wang, Y., & Key, T. A. (2023). Increasing in situ bioremediation effectiveness through field-scale application of molecular biological tools. Frontiers in Microbiology, 13, 1005871.

Maeder, D. L., Anderson, I., Brettin, T. S., Bruce, D. C., Gilna, P., Han, C. S., ... & Sowers, K. R. (2006). The Methanosarcina barkeri genome: comparative analysis with

Methanosarcina acetivorans and Methanosarcina mazei reveals extensive rearrangement within methanosarcinal genomes. Journal of bacteriology, 188(22), 7922-7931.

Mancini, S. A., Ulrich, A. C., Lacrampe-Couloume, G., Sleep, B., Edwards, E. A., & Lollar, B. S. (2003). Carbon and Hydrogen Isotopic Fractionation during Anaerobic Biodegradation of Benzene. Applied and Environmental Microbiology, 69(1), 191–198. https://doi.org/10.1128/AEM.69.1.191-198.2003

McAlexander, B., & Sihota, N. (2019). Influence of Ambient Temperature, Precipitation, and Groundwater Level on Natural Source Zone Depletion Rates at a Large Semiarid LNAPL Site. Groundwater Monitoring & Remediation, 39(1), 54–65. https://doi.org/10.1111/gwmr.12309

McCoy, K., Zimbron, J., Sale, T., & Lyverse, M. (2015). Measurement of Natural Losses of LNAPL Using CO 2 Traps. Groundwater, 53(4), 658–667. https://doi.org/10.1111/gwat.12240

McGenity, T. J., Timmis, K. N., & Fernández, B. N. (2016). Hydrocarbon and lipid microbiology protocols. Springer.

Meckenstock, R. U., Elsner, M., Griebler, C., Lueders, T., Stumpp, C., Aamand, J., & van Breukelen, B. M. (2015). Biodegradation: Updating the concepts of control for microbial cleanup in contaminated aquifers. Environmental Science & Technology, 49(12), 7073–7081.

Merino, N. & others. (2020). Single-Cell Genomics of Novel Actinobacteria With the Wood–Ljungdahl Pathway Discovered in a Serpentinizing System. Frontiers in Microbiology, 11, 1031.

Meziti, A., Kormas, K. A., Pancucci-Papadopoulou, M. A., & Thessalou-Legaki, M. (2007). Bacterial phylotypes associated with the digestive tract of the sea urchin Paracentrotus lividus and the ascidian Microcosmus sp. Russian Journal of Marine Biology, 33(2), 84–91.

Michas, A., Harir, M., Lucio, M., Vestergaard, G., Himmelberg, A., Schmitt-Kopplin, P., Lueders, T., Hatzinikolaou, D. G., Schöler, A., Rabus, R., & Schloter, M. (2020). Sulfate Alters the Competition Among Microbiome Members of Sediments Chronically Exposed to Asphalt. Frontiers in Microbiology, 11, 556793. https://doi.org/10.3389/fmicb.2020.556793

Militon, C., Atkinson, A., Michotey, V., Jeziorski, C., Cravo-Laureau, C., Duran, R., ... & Cuny, P. (2016). Metatranscriptomes of oil-contaminated marine coastal sediment affected by oil addition and/or by the bioturbating activity of the marine polychaete Hediste diversicolor: Who are the microbial players?. Marine Genomics, 29, 55-59.

Molins, S., Mayer, K. U., Amos, R. T., & Bekins, B. A. (2010). Vadose zone attenuation of organic compounds at a crude oil spill site—Interactions between biogeochemical reactions and multi-component gas transport. Journal of Contaminant Hydrology, 112(1), 15-29.

Morais-Silva, F. O., Rezende, A. M., Pimentel, C., Santos, C. I., Clemente, C., Varela–Raposo, A., Resende, D. M., Da Silva, S. M., De Oliveira, L. M., Matos, M., Costa, D. A., Flores, O., Ruiz, J. C., & Rodrigues-Pousada, C. (2014). Genome sequence of the model sulfate reducer Desulfovibrio gigas: A comparative analysis within the Desulfovibrio genus. MicrobiologyOpen, 3(4), 513–530. https://doi.org/10.1002/mbo3.184

Moreira, D., Rodríguez-Valera, F., & López-García, P. (2006). Metagenomic analysis of mesopelagic Antarctic plankton reveals a novel deltaproteobacterial group. Microbiology, 152(2), 505–517.

Morris, B. E., Henneberger, R., Huber, H., & Moissl-Eichinger, C. (2013). Microbial syntrophy: Interaction for the common good. FEMS Microbiology Reviews, 37(3), 384–406.

Mussman, G., & Kessels, W. (1980). An in-situ thermal conductivity probe. In A. S. Strub & P. Ungemach (Eds.), Advances in European Geothermal Research, Second International seminar on the Results of EC Geothermal Energy Research (pp. 556-564). Dordrecht: D. Reidel Publishing.

Nakano, M. M., & Zuber, P. (1998). Anaerobic growth of a "strict aerobe" (Bacillus subtilis). Annual Review of Microbiology, 52(1), 165–190.

Nan, Q., Wang, C., Wang, H., Yi, Q., & Wu, W. (2020). Mitigating methane emission via annual biochar amendment pyrolyzed with rice straw from the same paddy field. Science of the Total Environment, 746, 141351.

Newell, C. J. (1995). Light nonaqueous phase liquids. United States Environmental Protection Agency, Office of Research and Development, [and] Office of Solid Waste and Emergency Response.

Ning, Z., Sheng, Y., Guo, C., Wang, S., Yang, S., & Zhang, M. (2022). Incorporating the Soil Gas Gradient Method and Functional Genes to Assess the Natural Source Zone Depletion at a Petroleum-Hydrocarbon-Contaminated Site of a Purification Plant in Northwest China. Life, 13(1), 114.

Nothaft, D. B., Templeton, A. S., Boyd, E. S., Matter, J. M., Stute, M., Paukert Vankeuren, A. N., & Team, O. D. P. S. (2021). Aqueous geochemical and microbial variation across

discrete depth intervals in a peridotite aquifer assessed using a packer system in the Samail Ophiolite, Oman. Journal of Geophysical Research: Biogeosciences, e2021JG006319.

Olson, M., Long, S. D., Irianni-Renno, M., Clayton, W., Sale, T., & Johnson, R. (2017). Evaluating Long-Term Impacts of Soil-Mixing Source-Zone Treatment using Cryogenic Core Collection. Trihydro Corporation.

Or, D., Smets, B. F., Wraith, J., Dechesne, A., & Friedman, S. (2007). Physical constraints affecting bacterial habitats and activity in unsaturated porous media – a review. Advances in Water Resources, 30(6–7), 1505–1527.

Ozuolmez, D., Stams, A. J., & Plugge, C. M. (2020). Propionate converting anaerobic microbial communities enriched from distinct biogeochemical zones of Aarhus Bay, Denmark under sulfidogenic and methanogenic conditions. Microorganisms, 8(3), 394.

Pagnozzi, G., Carroll, S., Reible, D. D., & Millerick, K. (2021). Powdered activated carbon (PAC) amendment enhances naphthalene biodegradation under strictly sulfate-reducing conditions. Environmental Pollution, 268, 115641.

Pannekens, M., Voskuhl, L., Meier, A., Müller, H., Haque, S., Frösler, J., Brauer, V. S., & Meckenstock, R. U. (2020). Densely populated water droplets in heavy-oil seeps. Applied and Environmental Microbiology, 86(11), e00164-20.

Patel, A. K., Singhania, R. R., Albarico, F. P. J. B., Pandey, A., Chen, C.-W., & Dong, C.-D. (2022). Organic wastes bioremediation and its changing prospects. Science of The Total Environment, 824, 153889. https://doi.org/10.1016/j.scitotenv.2022.153889

Peng, W., Li, X., Lin, M., & Fan, W. (2020). Microbiological analysis of cadmium-contaminated sediments during biostabilization with indigenous sulfate-reducing bacteria. Journal of Soils and Sediments, 20(1), 584–593.

Pester, M., Bittner, N., Deevong, P., Wagner, M., & Loy, A. (2010). A 'rare biosphere' microorganism contributes to sulfate reduction in a peatland. The ISME Journal, 4(12), 1591–1602.

Pishgar, R., Hettiaratchi, J. P., & Chu, A. (2022). Natural Source Zone Depletion (NSZD) Quantification Techniques: Innovations and Future Directions. Sustainability, 14(12), 7027. https://doi.org/10.3390/su14127027

Plyasunov, A. V., & Shock, E. L. (2000). Thermodynamic functions of hydration of hydrocarbons at 298.15 K and 0.1 MPa. Geochimica et Cosmochimica Acta, 64(3), 439-468. https://doi.org/10.1016/S0016-7037(99)00330-0.

Probst, A. J., & Moissl-Eichinger, C. (2015). "Altiarchaeales": Uncultivated archaea from the subsurface. Life, 5(2), 1381–1395.

Puthiyapurayil, H. K. (2020). Variability in Genomic Patterns of Bacterial Communities Related to Tarmats and Quantification of Hydrocarbon Present in the Tarmats Deposited along the Qatar Coast. [Master's thesis].

Qian, Y., Xu, M., Deng, T., Hu, W., He, Z., Yang, X., Wang, B., Song, D., Chen, L., Huang, Y., & Sun, G. (2021). Synergistic interactions of Desulfovibrio and Petrimonas for sulfate-reduction coupling polycyclic aromatic hydrocarbon degradation. Journal of Hazardous Materials, 407, 124385. https://doi.org/10.1016/j.jhazmat.2020.124385

Qiu, Y. L., Hanada, S., Ohashi, A., Harada, H., Kamagata, Y., & Sekiguchi, Y. (2008). Syntrophorhabdus aromaticivorans gen. Nov., sp. Nov., the first cultured anaerobe

capable of degrading phenol to acetate in obligate syntrophic associations with a hydrogenotrophic methanogen. Applied and Environmental Microbiology, 74(7), 2051–2058.

Quast, C., Pruesse, E., Yilmaz, P., Gerken, J., Schweer, T., Yarza, P., Peplies, J., & Glöckner, F. O. (2012). The SILVA ribosomal RNA gene database project: Improved data processing and web-based tools. Nucleic Acids Research, 41(D1), D590–D596. https://doi.org/10.1093/nar/gks1219

Rakoczy, J., Schleinitz, K. M., Müller, N., Richnow, H. H., & Vogt, C. (2011). Effects of hydrogen and acetate on benzene mineralisation under sulphate-reducing conditions. FEMS Microbiology Ecology, 77(2), 238–247.

Ramirez, J. A., Baird, A. J., Coulthard, T. J., & Waddington, J. M. (2015). Ebullition of methane from peatlands: does peat act as a signal shredder? Geophysical Research Letters, 42(9), 3371–3379.

Redmond, M. C., Valentine, D. L., & Sessions, A. L. (2010). Identification of novel methane-, ethane-, and propane-oxidizing bacteria at marine hydrocarbon seeps by stable isotope probing. Applied and Environmental Microbiology, 76(19), 6412-6422.

Rico, J. L., Reardon, K. F., & De Long, S. K. (2021). Inoculum microbiome composition impacts fatty acid product profile from cellulosic feedstock. Bioresource Technology, 323, 124532. https://doi.org/10.1016/j.biortech.2020.124532

Rios-Del Toro, E. E., Valenzuela, E. I., López-Lozano, N. E., Cortés-Martínez, M. G., Sánchez-Rodríguez, M. A., Calvario-Martínez, O., & Cervantes, F. J. (2018). Anaerobic ammonium oxidation linked to sulfate and ferric iron reduction fuels nitrogen loss in marine sediments. Biodegradation, 29(5), 429–442.

Riser-Roberts, E. (2020). Remediation of petroleum contaminated soils: Biological, physical, and chemical processes. CRC press.

Rojas, C. A., De Santiago Torio, A., Park, S., Bosak, T., & Klepac-Ceraj, V. (2021). Organic electron donors and terminal electron acceptors structure anaerobic microbial communities and interactions in a permanently stratified sulfidic lake. Frontiers in Microbiology, 12, 847.

Rossmassler, K., Snow, C. D., Taggart, D., Brown, C., & De Long, S. K. (2019). Advancing biomarkers for anaerobic o-xylene biodegradation via metagenomic analysis of a methanogenic consortium. Applied Microbiology and Biotechnology, 103, 4177-4192.

Rotaru, A. E., & Thamdrup, B. (2016). A new diet for methane oxidizers. Science, 351(6274), 658–658.

Rubin-Blum, M., Sisma-Ventura, G., Yudkovski, Y., Belkin, N., Kanari, M., Herut, B., & Rahav, E. (2021). Diversity, activity and abundance of benthic microbes in the southeastern Mediterranean Sea: A baseline for monitoring. bioRxiv, Preprint.

Sakaguchi, T., Arakaki, A., & Matsunaga, T. (2002). Desulfovibrio magneticus sp. Nov., a novel sulfate-reducing bacterium that produces intracellular single-domain-sized magnetite particles. International Journal of Systematic and Evolutionary Microbiology, 52(1), 215–221. https://doi.org/10.1099/00207713-52-1-215

Sakai, S., Takaki, Y., Shimamura, S., Sekine, M., Tajima, T., Kosugi, H., ... & Takai, K. (2011). Genome sequence of a mesophilic hydrogenotrophic methanogen Methanocella paludicola, the first cultivated representative of the order Methanocellales. PLoS One, 6(7), e22898.

Sale, T., Gallo, S., Askarani, K. K., Irianni-Renno, M., Lyverse, M., Hopkins, H., Blotevogel, J., & Burge, S. (2021). Real-time soil and groundwater monitoring via spatial and temporal resolution of biogeochemical potentials. Journal of Hazardous Materials, 408, 124403. https://doi.org/10.1016/j.jhazmat.2020.124403

Sale, T., H. Hopkins, and A. Kirkman. (2018). Managing Risks at LNAPL Sites. 2nd Edition Bulletin 18, American Petroleum Institute.

Sale, T.C., E.B. Stockwell, C.J. Newell, and P.R. Kulkarni. 2018. Devices and methods for measuring thermal flux and estimating rate of change of reactive material within a subsurface formation. U.S. Patent No. 10,094,719 filed February 18, 2015. Issued October 9, 2018.

Scherr, K. E., Lundaa, T., Klose, V., Bochmann, G., & Loibner, A. P. (2012). Changes in bacterial communities from anaerobic digesters during petroleum hydrocarbon degradation. J. Biotechnol., 157(4), 564–572.

Schicht, R. (1992). Ground-Water Investigation at Peoria, Illinois: Central Well-Field Area. ISWS Contract Report CR 537.

Schicht, R. J., & Buck, A. G. (1995). Ground-water levels and pumpage in the Metro-East area, Illinois, 1986-1990. Circular no. 180.

Shafieiyoun, S., Al-Raoush, R. I., Ngueleu, S. K., Rezanezhad, F., & Van Cappellen, P. (2020). Enhancement of Naphthalene Degradation by a Sequential Sulfate Injection Scenario in a (Semi)-Arid Coastal Soil: A Flow-Through Reactor Experiment. Water, Air, & Soil Pollution, 231(8), 421. https://doi.org/10.1007/s11270-020-04725-5

Shao, Z., & Wang, W. (2013). Enzymes and genes involved in aerobic alkane degradation. Frontiers in Microbiology, 4, 116.

Sharma, J. (2019). Advantages and limitations of in situ methods of bioremediation. Recent Adv Biol Med, 5, 10941.

Shebl, M. A., & Surdam, R. C. (1996). Redox reactions in hydrocarbon clastic reservoirs: experimental validation of this mechanism for porosity enhancement. Chemical Geology, 132(1-4), 103-117.

Shekhar, S. K., Godheja, J., & Modi, D. (2015). Hydrocarbon bioremediation efficiency by five indigenous bacterial strains isolated from contaminated soils. Int J Curr Microbiol App Sci, 4(3), 892–905.

Sheng, Y., Tian, X., Wang, G., Hao, C., & Liu, F. (2016). Bacterial diversity and biogeochemical processes of oil-contaminated groundwater, Baoding, North China. Geomicrobiology Journal, 33(6), 537-551.

Shin, B., Kim, M., Zengler, K., Chin, K.-J., Overholt, W. A., Gieg, L. M., Konstantinidis, K. T., & Kostka, J. E. (2019). Anaerobic degradation of hexadecane and phenanthrene coupled to sulfate reduction by enriched consortia from northern Gulf of Mexico seafloor sediment. Scientific Reports, 9(1), 1239. https://doi.org/10.1038/s41598-018-36567-x

Sidstedt, M., Rådström, P., & Hedman, J. (2020). PCR inhibition in qPCR, dPCR and MPS—mechanisms and solutions. Anal. Bioanal. Chem., 1–15.

Sieber, J. R., McInerney, M. J., & Gunsalus, R. P. (2012). Genomic insights into syntrophy: The paradigm for anaerobic metabolic cooperation. Annual Review of Microbiology, 66, 429–452.

Sihota, N. J., Mayer, K. U., Toso, M. A., & Atwater, J. F. (2013). Methane emissions and contaminant degradation rates at sites affected by accidental releases of denatured fuel-grade ethanol. Journal of Contaminant Hydrology, 151, 1–15.

Sihota, N. J., Singurindy, O., & Mayer, K. U. (2011). CO2-efflux measurements for evaluating source zone natural attenuation rates in a petroleum hydrocarbon contaminated aquifer. Environmental Science & Technology, 45(2), 482–488.

Sihota, N. J., Trost, J. J., Bekins, B. A., Berg, A., Delin, G. N., Mason, B., Warren, E., & Mayer, K. U. (2016). Seasonal variability in vadose zone biodegradation at a crude oil pipeline rupture site. Vadose Zone Journal, 15(5).

Sihota, N., McAlexander, B., Lyverse, M., & Mayer, K. U. (2018). Multi-year CO2 efflux measurements for assessing natural source zone depletion at a large hydrocarbon-impacted site. Journal of contaminant hydrology, 219, 50-60.

Smith, G. J., Angle, J. C., Solden, L. M., Borton, M. A., Morin, T. H., Daly, R. A., Johnston, M. D., & others. (2018). Members of the genus Methylobacter are inferred to account for the majority of aerobic methane oxidation in oxic soils from a freshwater wetland. MBio, 9(6), e00815-18.

Snousy, M. G. (2017). Prevalent Remediation Technologies for Organic Contaminants. SDRP Journal of Earth Sciences & Environmental Studies, 2(1). https://doi.org/10.25177/JESES.2.1.1

Sookhak Lari, K., Davis, G. B., Bastow, T., & Rayner, J. L. (2024). On quantifying global carbon emission from oil contaminated lands over centuries. Science of The Total Environment, 907, 168039. https://doi.org/10.1016/j.scitotenv.2023.168039

Sperfeld, M., Diekert, G., & Studenik, S. (2018). Anaerobic aromatic compound degradation in Sulfuritalea hydrogenivorans sk43H. FEMS Microbiology Ecology. https://doi.org/10.1093/femsec/fiy199

Sra, K. S., Ponsin, V., Kolhatkar, R., Hunkeler, D., Thomson, N. R., Madsen, E. L., & Buscheck, T. (2023). Sulfate Land Application Enhances Biodegradation in a Petroleum Hydrocarbon Smear Zone. Groundwater Monitoring & Remediation, 43(1), 44–59. https://doi.org/10.1111/gwmr.12547

Stams, A. J., Sousa, D. Z., Kleerebezem, R., & Plugge, C. M. (2012). Role of syntrophic microbial communities in high-rate methanogenic bioreactors. Water Science and Technology, 66(2), 352-362.

Statham, T. M., Summer, R., Hill, A. F., & Smith, J. W. (2023). Transitions from Active Remediation to Natural Source Zone Depletion (NSZD) at a LNAPL-Impacted Site, Supported by Sustainable Remediation Appraisal. Quarterly Journal of Engineering Geology and Hydrogeology.

Stockwell, E. (2015). Continuous NAPL loss rates using subsurface temperatures. [Master's thesis, Colorado State University].

Sui, X., & Ji, G. D. (2010). Impact of ultrasonic power density on elution of super heavy oil and its biomarkers from aging soils using Triton X-100 micellar solution. Journal of Hazardous Materials, 176(1–3), 473–480.

Sundberg, C., Al-Soud, W. A., Larsson, M., Alm, E., Yekta, S. S., Svensson, B. H., & Karlsson, A. (2013). 454 pyrosequencing analyses of bacterial and archaeal richness in 21 full-scale biogas digesters. FEMS Microbiology Ecology, 85(3), 612–626.

Suzuki, M. T., Taylor, L. T., & DeLong, E. F. (2000). Quantitative analysis of small-subunit rRNA genes in mixed microbial populations via 5′-nuclease assays. Appl. Environ. Microbiol., 66(11), 4605–4614.

Sweeney, R. E., & Ririe, G. T. (2014). Temperature as a tool to evaluate aerobic biodegradation in hydrocarbon contaminated soil. Groundwater Monitoring & Remediation, 34(3), 41-50.

Taggart, D. M., & Clark, K. (2021). Lessons learned from 20 years of molecular biological tools in petroleum hydrocarbon remediation. Remediation Journal, 31(4), 83–95.

Taggart, D. M., & Key, T. A. (2023). Molecular Biological Tools Used in Assessment and Remediation of Petroleum Hydrocarbons in Soil and Groundwater. In Advances in the Characterisation and Remediation of Sites Contaminated with Petroleum Hydrocarbons (pp. 329–359). Springer International Publishing.

Technology, I., & Council, R. (2009). Evaluating LNAPL remedial technologies for achieving project goals. Interstate Technology & Regulatory Council, LNAPLs Team.

Thawai, C., Tanasupawat, S., Itoh, T., & Kudo, T. (2006). Actinocatenispora thailandica gen. Nov., sp. Nov., a new member of the family Micromonosporaceae. International Journal of Systematic and Evolutionary Microbiology, 56(8), 1789–1794.

Tong, S., Zhu, H., & Bao, G. (2019). Magnetic iron oxide nanoparticles for disease detection and therapy. Materials Today, 31, 86–99.

Toni, L. S., Garcia, A. M., Jeffrey, D. A., Jiang, X., Stauffer, B. L., Miyamoto, S. D., & Sucharov, C. C. (2018). Optimization of phenol-chloroform RNA extraction. MethodsX, 5, 599–608.

Toth, C. R. A., Luo, F., Bawa, N., Webb, J., Guo, S., Dworatzek, S., & Edwards, E. A. (2021). Anaerobic Benzene Biodegradation Linked to the Growth of Highly Specific Bacterial Clades. Environmental Science & Technology, 55(12), 7970–7980. https://doi.org/10.1021/acs.est.1c00508

Vanwonterghem, I., Evans, P. N., Parks, D. H., Jensen, P. D., Woodcroft, B. J., Hugenholtz, P., & Tyson, G. W. (2016). Methylotrophic methanogenesis discovered in the archaeal phylum Verstraetearchaeota. Nature Microbiology, 1(12), 1–9.

Waals, M. J. van der, Atashgahi, S., Rocha, U. N. D., Zaan, B. M. van der, Smidt, H., & Gerritse, J. (2017). Benzene degradation in a denitrifying biofilm reactor: Activity and microbial community composition. Appl. Microbiol. Biotechnol., 101(12), 5175–5188.

Warren, E., & Bekins, B. B. (2015). Relating surface temperature changes to microbial activity at a crude oil-contaminated site. Journal of Contaminant Hydrology, 182, 183-193. https://doi.org/10.1016/j.jconhyd.2015.09.007

Wartell, B., Boufadel, M., & Rodriguez-Freire, L. (2021). An effort to understand and improve the anaerobic biodegradation of petroleum hydrocarbons: A literature review. International Biodeterioration & Biodegradation, 157, 105156. https://doi.org/10.1016/j.ibiod.2020.105156

Wawrik, B., Marks, C. R., Davidova, I. A., McInerney, M. J., Pruitt, S., Duncan, K. E., Suflita, J. M., & Callaghan, A. V. (2016). Methanogenic paraffin degradation proceeds via alkane addition to fumarate by 'Smithella' spp. Mediated by a syntrophic coupling with hydrogenotrophic methanogens. Environmental Microbiology, 18(8), 2604–2619.

Wei, Y., Thomson, N. R., Aravena, R., Marchesi, M., Barker, J. F., Madsen, E. L., Kolhatkar, R., Buscheck, T., Hunkeler, D., & DeRito, C. M. (2018). Infiltration of Sulfate to Enhance Sulfate-Reducing Biodegradation of Petroleum Hydrocarbons. Groundwater Monitoring & Remediation, 38(4), 73–87. https://doi.org/10.1111/gwmr.12298

Wiedemeier, T. H., Rifai, H. S., Newell, C. J., & Wilson, J. T. (1999). Natural attenuation of fuels and chlorinated solvents in the subsurface. John Wiley & Sons.

Wilson, J. T., Mills IV, J. C., Wilson, B. H., Ferrey, M. L., Freedman, D. L., & Taggart, D. (2019). Using qPCR assays to predict rates of cometabolism of TCE in aerobic groundwater. Groundwater Monitoring & Remediation, 39(2), 53-63.

Wu, S. L., Sun, J., Chen, X., Wei, W., Song, L., Dai, X., & Ni, B. J. (2020). Unveiling the mechanisms of medium-chain fatty acid production from waste activated sludge alkaline fermentation liquor through physiological, thermodynamic and metagenomic investigations. Water Research, 169, 115218.

Wu, Y.-J., Liu, P.-W. G., Hsu, Y.-S., Whang, L.-M., Lin, T.-F., Hung, W.-N., & Cho, K.-C. (2019). Application of molecular biological tools for monitoring efficiency of trichloroethylene remediation. Chemosphere, 233, 697-704.

Wyatt, D. E., Richers, D. M., & Pirkle, R. J. (1995). Barometric pumping effects on soil gas studies for geological and environmental characterization. Environmental Geology, 25(4), 243-250.

Yamada, T., & Sekiguchi, Y. (2015). Longilinea. Bergey's Manual of Systematics of Archaea and Bacteria, 1–3.

Yin, X., Hua, H., Burns, F., Fennell, D., Dyer, J., Landis, R., & Axe, L. (2021). Identifying redox transition zones in the subsurface of a site with historical contamination. Science of The Total Environment, 762, 143105. https://doi.org/10.1016/j.scitotenv.2020.143105

Zaitoun, M. A., & Lin, C. T. (1997). Chelating behavior between metal ions and EDTA in sol-gel matrix. Abstracts of Papers of the American Chemical Society, 213, 279-COLL.

Zeman, N. R., Renno, M. I., Olson, M. R., Wilson, L. P., Sale, T. C., & Susan, K. (2014). Temperature impacts on anaerobic biotransformation of LNAPL and concurrent shifts in microbial community structure. Biodegradation, 25(4), 569–585.

Zhang, N. & others. (2021). Coexistence between antibiotic resistance genes and metal resistance genes in manure-fertilized soils. Geoderma, 382, 114760.

Zhang, Z., Sun, J., Guo, H., Gong, X., Wang, C., & Wang, H. (2021). Investigation of anaerobic biodegradation of phenanthrene by a sulfate-dependent Geobacter sulfurreducens strain PheS2. Journal of Hazardous Materials, 409, 124522. https://doi.org/10.1016/j.jhazmat.2020.124522

Zheng, Y., Wang, H., Yu, Z., Haroon, F., Hernández, M. E., & Chistoserdova, L. (2020). Metagenomic insight into environmentally challenged methane-fed microbial communities. Microorganisms, 8(10), 1614.

Zhou, H., Xing, D., Xu, M., Su, Y., Ma, J., Angelidaki, I., & Zhang, Y. (2021). Optimization of a newly developed electromethanogenesis for the highest record of methane production. Journal of Hazardous Materials, 407, 124363.

APPENDIX A – SUPPORTING INFORMATION FOR CHAPTER 3

Sampling Equipment with Sensors and Particle Board

Figure SA.1 shows a diagram of the equipment installed in each column for monitoring of continuous ORP, Continuous temperature, water and gas sampling. Ag-AgCl reference electrodes (World Precision Instruments – DRIREF-5) were inserted at the bottom of each column. The water elevation of each soil column was approximately 5 cm from the column top. Additionally, all columns are equipped with a 1 L Tedlar™ bag (Restek, Bellafonte, PA) for gas collection. The Tedlar™ bag is connected to the system via a glass rod.

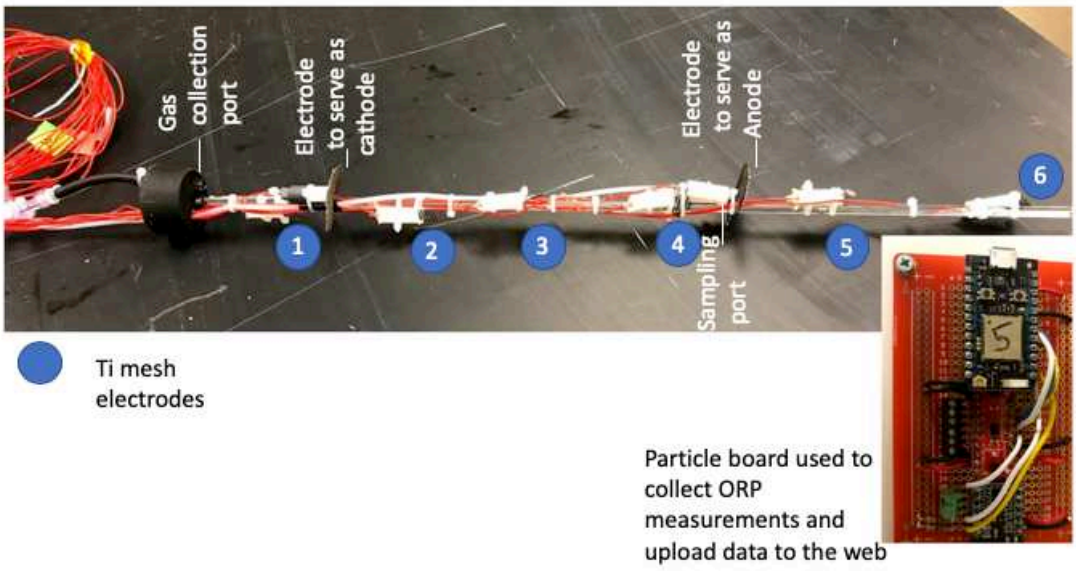

Figure SA.1. Sampling system with sensor and particle board.

Freeze Preservation of the Columns

Columns were disconnected from the sensor boards.

1- Valves and hoses were shut to prevent oxygen from entering the system and column fluids to exit the system.

2- Columns were wrapped with electrical tape as described in Emerson (2016) while still being vertically mounted on a rack.

3- Columns were placed vertically inside an insulated PVC pipe.

4- Pelleted dry ice was used to cover each column.

5- After 25 minutes elapsed, columns were laid horizontally inside a -80 ^{0}C freezer for storage until sampled.

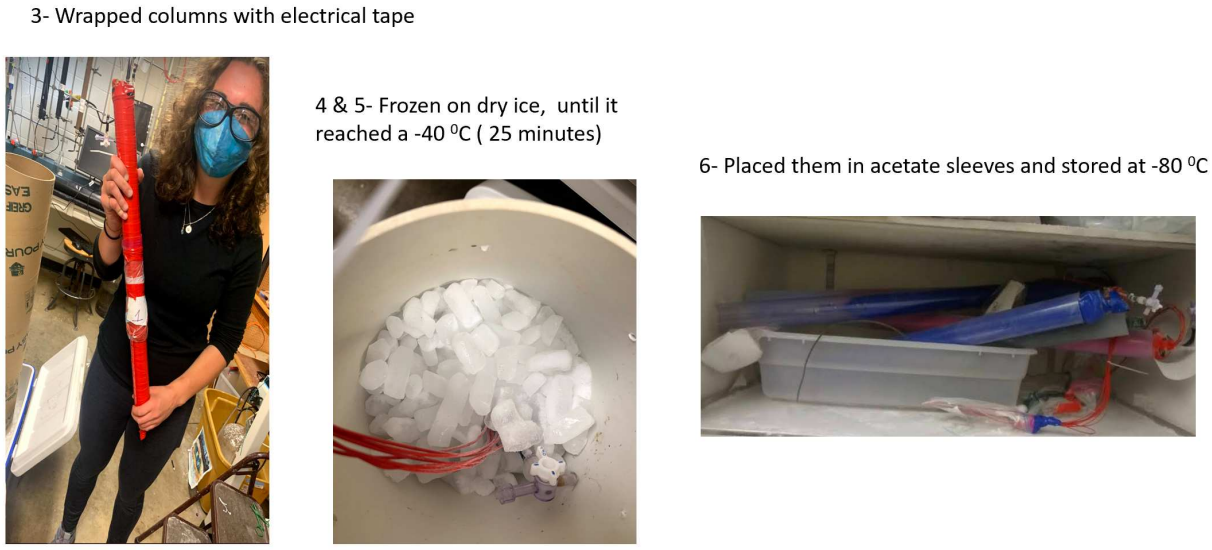

Figure SA.2. Schematic of freeze-preservation of columns.

Cryogenic sampling of the columns

All Columns were sampled the day after being frozen. Subsamples were collected around each sensor that was in contact with soil. Sample depths with respect to column top were as follows: 20 cm, 30 cm, 40 cm, 50 cm and 60 cm. The steps for obtaining the subsamples are outlined below and shown on Figure SA.3.

1- The glass from the column was removed by making a longitudinal cut through the electrical tape.

2- A hammer was used to crack the glass tape and glass were carefully peeled from the water-sediment-LNAPL system.

3- Remaining frozen sample was placed in an acetate sleeve.

4- 1" "hockey puck" samples were cut with a circular saw following methods described in Kiaalhosseini et al., (2016).

5- "Hockey puck" samples were quartered for collection and preservation of the following.

   a. One quarter was placed in a 120-ml jar containing 50-ml of Methanol for hydrocarbon analysis (Kiaalhosseini et al., 2016).

   b. Two quarters were wrapped in aluminum foil and immediately placed on dry ice for DNA and RNA analysis (Irianni-Renno et al., 2021)

   c. One quarter was placed in a 120 ml glass jar with a cap with a Teflon^{TM} lined septa for methane, iron, sulfate, formate, and acetate analysis (Olson et al., 2017).

d. The 2 mm x 2 mm titanium mesh sensing electrode located at the center of each “hockey puck” was recovered, wrapped in aluminum foil and placed on dry ice for future microscopic analysis.

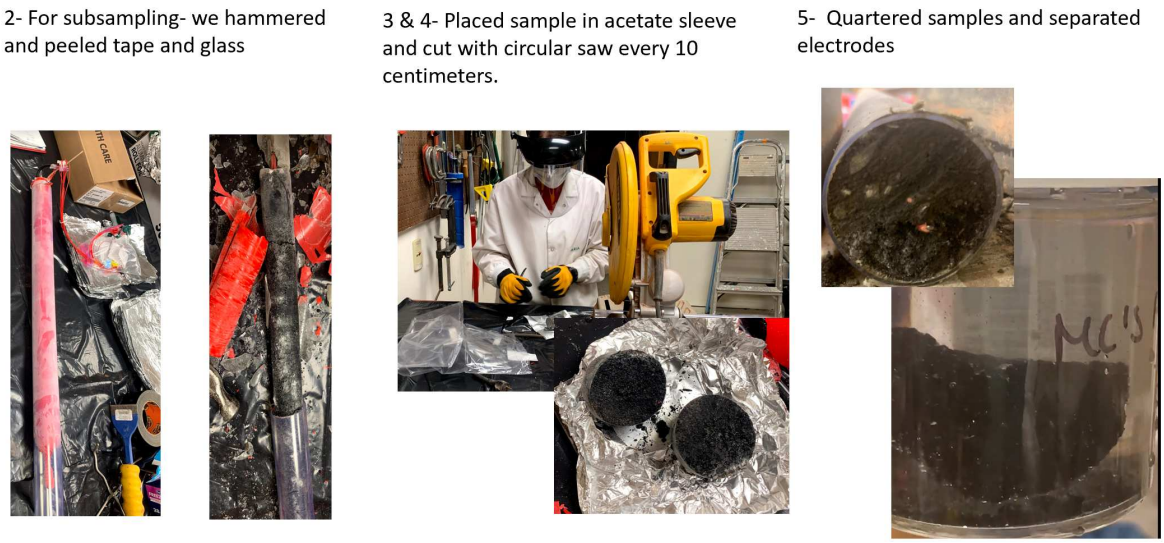

Figure SA.3. Schematic of cryocolumn subsampling.

Monitoring CH_4 and CO_2 production by the columns and continuous soil ORP

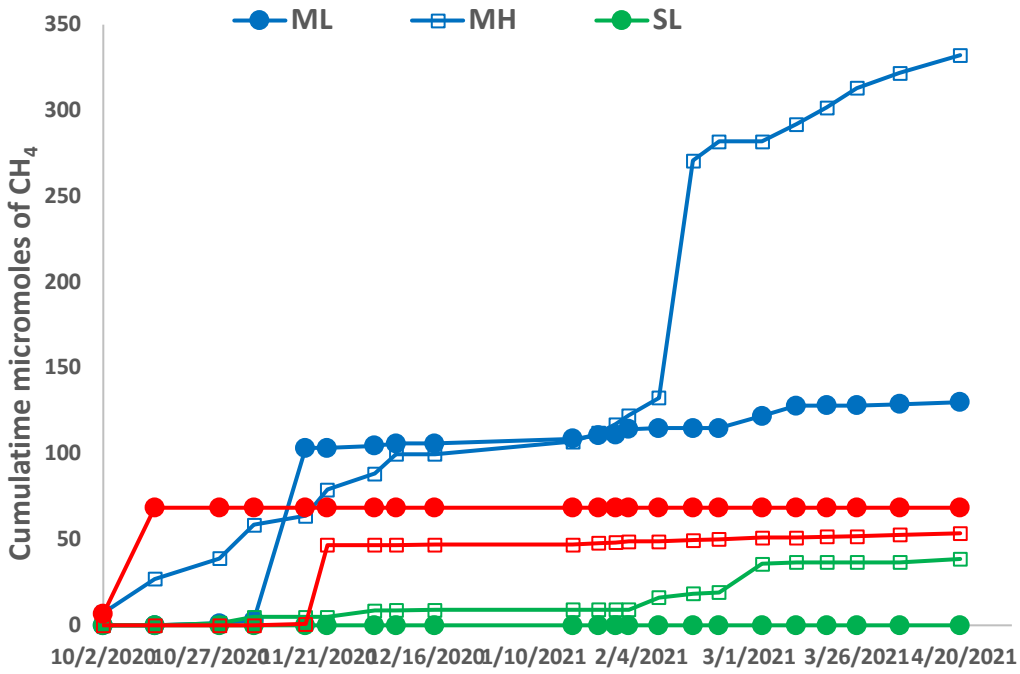

Figure SA.4. Cumulative CH_4 produced by the columns.

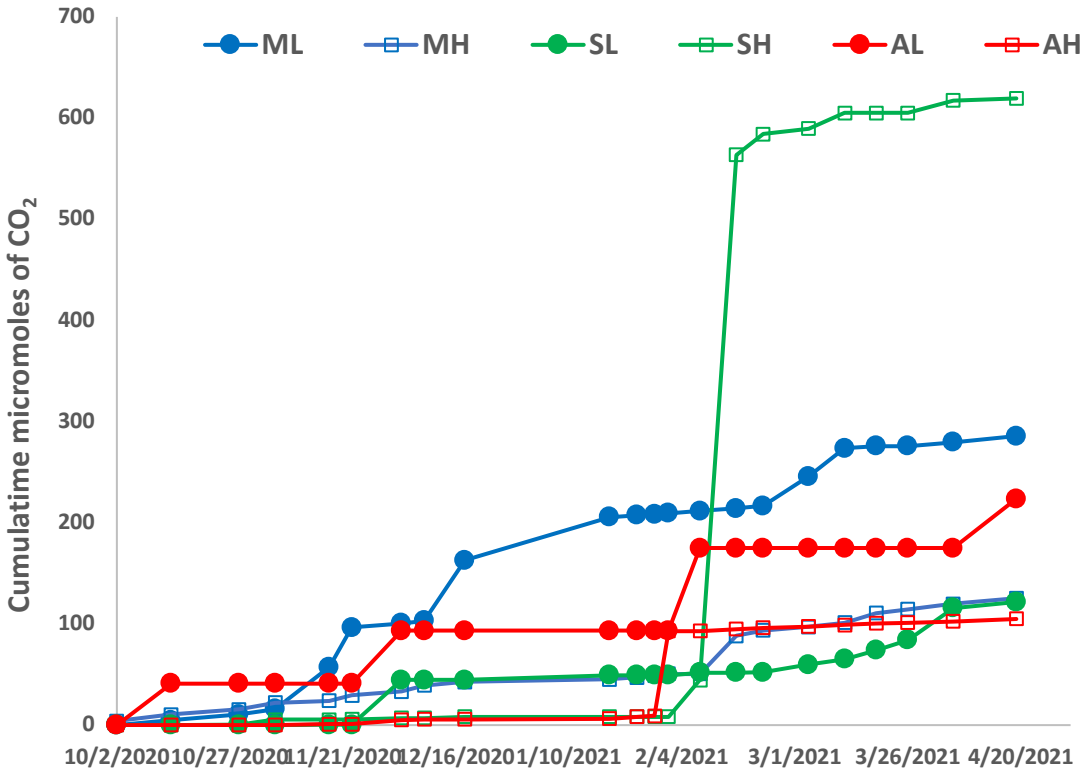

Figure SA.5. Cumulative CO_2 produced by the columns.

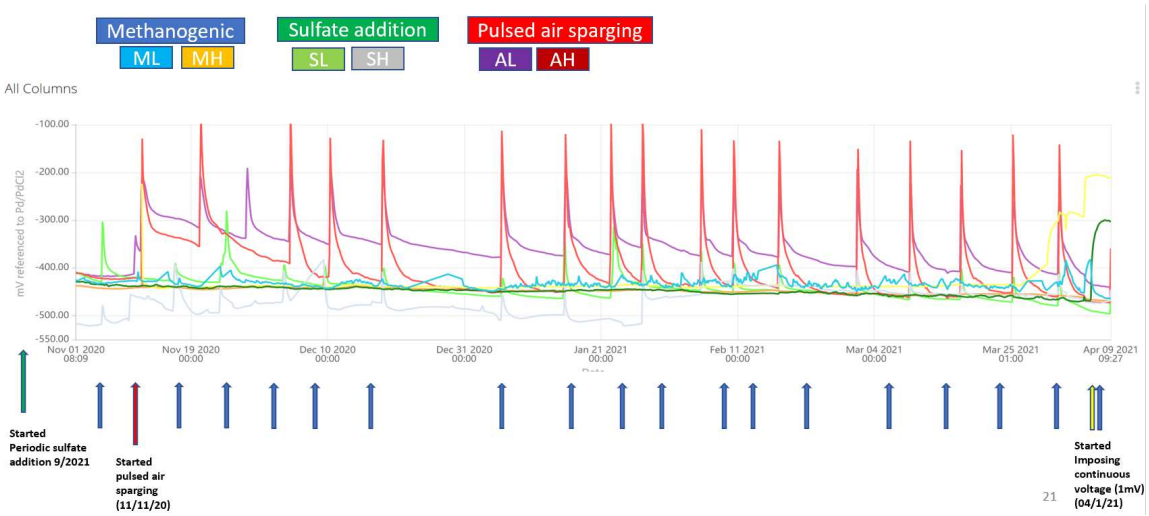

Figure SA.6. Continuous ORP recorded at the center of all columns. Methanogenic columns are turquoise (ML) and Orange (MH), Periodic sulfate addition are green (SL) and grey (SH) and pulsed air sparging are purple (AL) and red (AH). Blue arrows indicate time when enhancement was applied. Sulfate addition was started on 9/2/2020 and pulsed air sparging enhancement was started on 11/11/20.

Degradation rate calculations

Table SA.1. Estimated degradation rates under different treatments.

Column	Treatment	Duration of methanogenic conditions (days)	Treatment duration (days)	Estimated rate (mg/day) *
ML	Methanogenic	567	-	2.3
MH	Methanogenic	567	-	4.2
SL	Periodic sulfate addition	287	280	40.7
SH	Periodic sulfate addition	287	280	32.9
AL	Pulsed air sparging	438	129	41.9
AH	Pulsed air sparging	438	151	114.9

*Hydrocarbon degradation rates for the methanogenic columns were calculated as initial mass minus final mass over time. An average methanogenic rate was utilized to estimate initial mass for remaining columns at the beginning of the enhancement details on these calculations are shown in figure SA.7.

Calculations for rate estimations based on TPH removal

$$\text{methanogenic rate per day} = \frac{(TPH_0 - TPH_F)}{treatment\ duration}$$

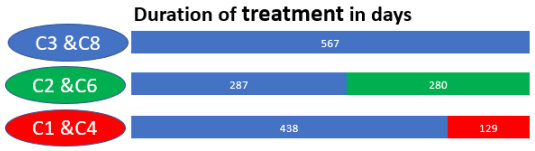

Estimation TPH removal rate due to sulfate addition

1- Average methanogenic degradation rated (C3 & C8)

2- Calculate mass remaining at the beginning of sulfate addition

$TPH_{sulfate\ t=287}$ = average methanogenic degradation rate x 287 days

3- $TPH_{removed\ due\ to\ sulfate\ addition} = (TPH_{sulfate\ t=287} - TPH_{sulfate\ final})$

4- Calculate removal rate due to treatment as:

$$\text{Sulfate addition rate per day} = \frac{TPH_{\text{removed due to sulfate addition}}}{treatment\ duration\ (280\ days)}$$

5- normalize estimated rate by soil volume

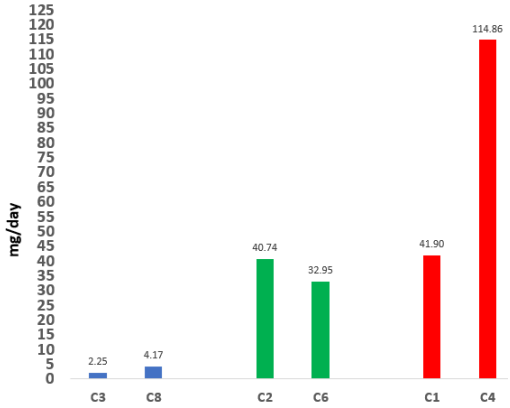

Figure SA.7. Calculation of degradation rates in the columns

gINT plots with aqueous data and additional microbiology analysis

Table SA.2. Methanogenic (Column ML). All Parameters

Depth (cm)	Sample ID	TPH (mg/kg)	Methane (mg/kg)	pH	Alkalinity (ppm CaCO3)	Sulfate (mg/kg)	Iron (mg/kg)	Acetate (mg/kg)	Formate (mg/kg)
20	32	4759.35	8.20	6.91	40.00	6.47	31.47	3.32	3.12
30	33	9424.88	10.01	7.10	40.00	1.56	22.35	1.02	0.90
40	34	8964.22	6.91	7.05	40.00	0.90	13.06	0.68	0.59
50	35	8402.96	9.84	7.33	40.00	0.86	4.79	0.43	0.77
60	36	13032.25	14.15	7.48	80.00	1.25	4.06	0.58	0.90

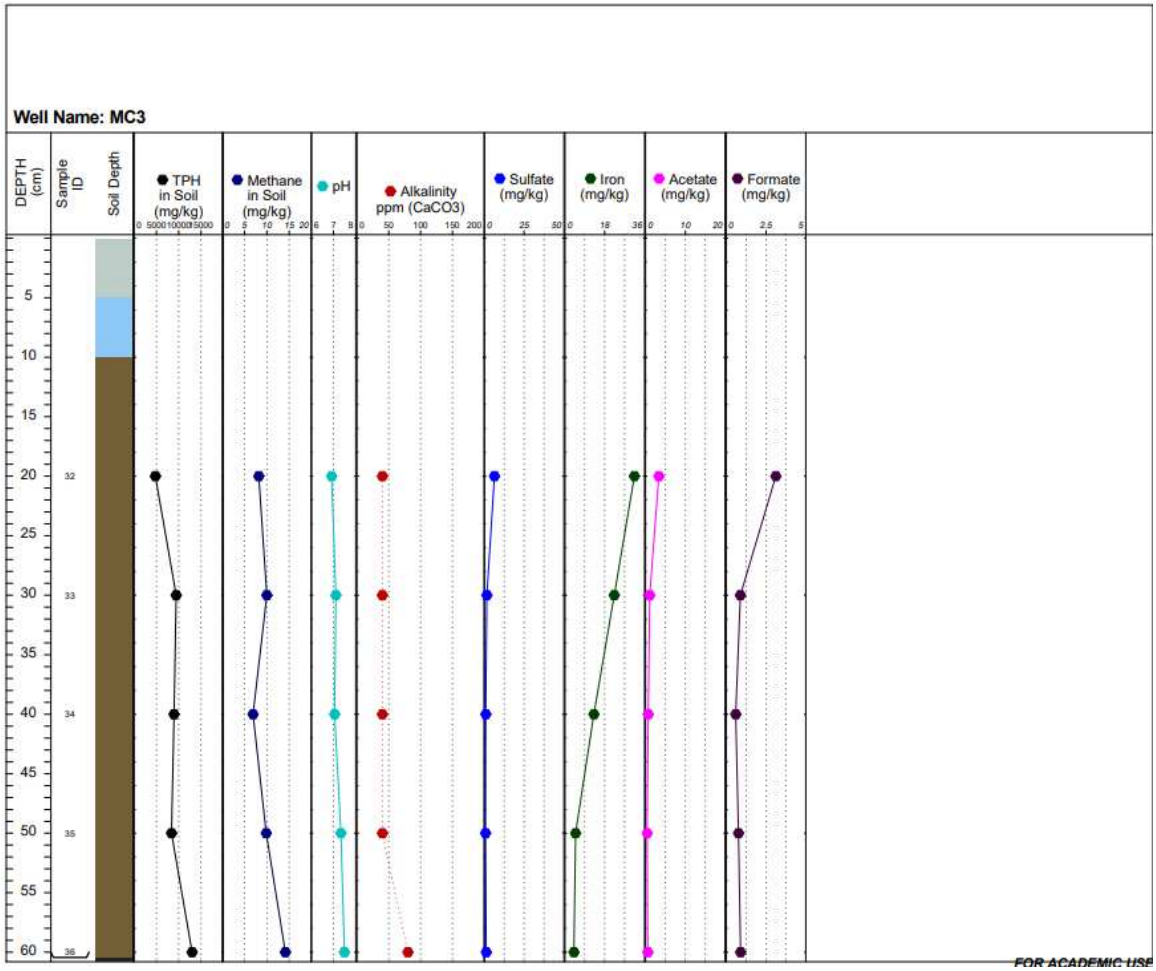

Figure SA.8. Methanogenic (Column ML) All Parameters

Table SA.3. Methanogenic (Column MH) All Parameters

Depth (cm)	Sample ID	TPH (mg/kg)	Methane (mg/kg)	pH	Alkalinity (ppm CaCO3)	Sulfate (mg/kg)	Iron (mg/kg)	Acetate (mg/kg)	Formate (mg/kg)
20	26	14284.43	10.35	7.06	40.00	1.70	6.54	0.55	0.87
30	27		14.65	6.83	40.00	1.66	8.85	0.77	1.21
40	28	13559.16	17.64	6.91	40.00	1.75	7.56	1.23	1.90
50	29	15991.92	17.14	6.99	40.00	2.00	5.85	1.75	1.81
60	30	17476.86	12.37	6.90	40.00	1.13	8.37	0.77	0.72

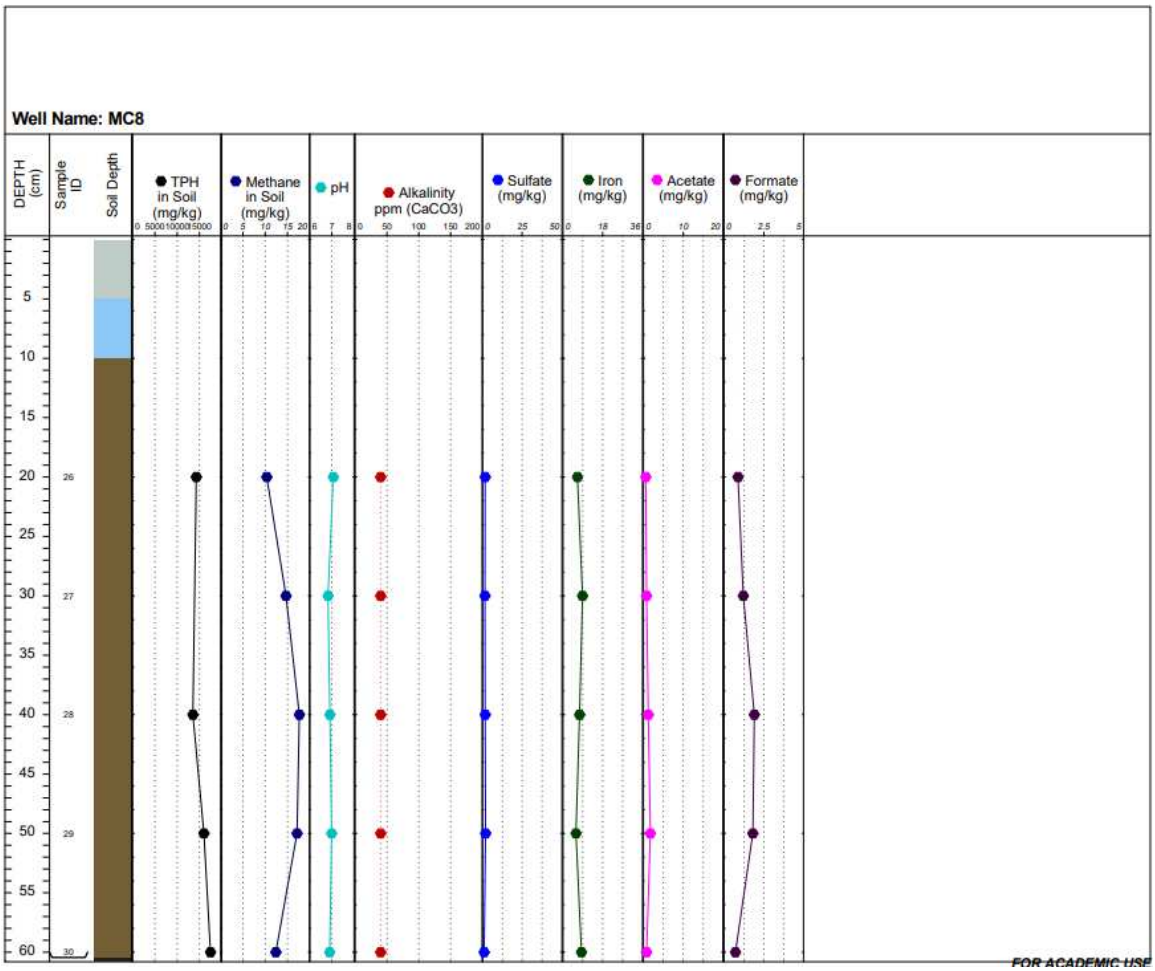

Figure SA.9. Control (Column 8) All Parameter

Table SA.4. Periodic Sulfate addition (Column SL) All Parameters

Depth (cm)	Sample ID	TPH (mg/kg)	Methane (mg/kg)	pH	Alkalinity (ppm CaCO3)	Sulfate (mg/kg)	Iron (mg/kg)	Acetate (mg/kg)	Formate (mg/kg)
20	14	4374.99	0.00	7.69	80.00	687.45	0.00	0.41	0.61
30	15	4173.10	0.00	7.64	120.00	640.00	0.00	0.09	0.19
40	16	2422.65	0.00	7.84	80.00	1087.68	0.00	0.29	0.62
50	17	6322.44	0.00	7.70	80.00	954.34	0.00	0.38	0.55
60	18	3648.74	0.00	7.61	80.00	1071.41	0.00	0.60	0.81

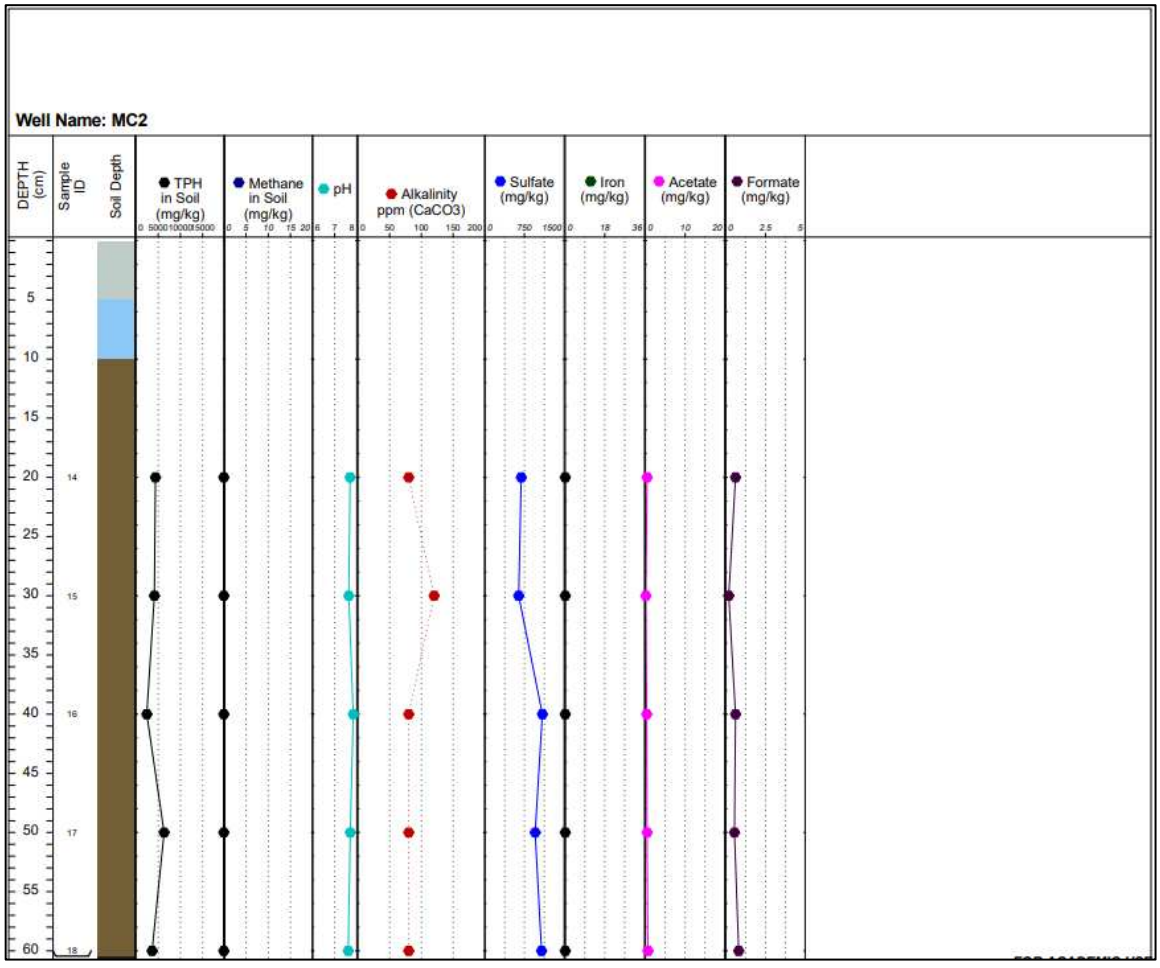

Figure SA.10. Periodic Sulfate (Column 2) All Parameters.

Table SA.5. Periodic Sulfate addition (Column SH) All Parameters

Depth (cm)	Sample ID	TPH (mg/kg)	Methane (mg/kg)	pH	Alkalinity (ppm CaCO3)	Sulfate (mg/kg)	Iron (mg/kg)	Acetate (mg/kg)	Formate (mg/kg)
10									
20	20	9005.70	0.64	7.82	180.00	3387.29	0.00	0.00	0.00
30	21	14650.45	0.00	7.74	180.00	513.02	0.00	0.23	0.47
40	22	10282.08	0.00	7.65	180.00	586.16	5.81	0.50	0.86
50	23	21892.29	0.00	7.65	120.00	1020.42	0.00	0.53	0.54
60	24	28399.83	0.00	7.53	120.00	1118.45	0.00	19.53	0.32

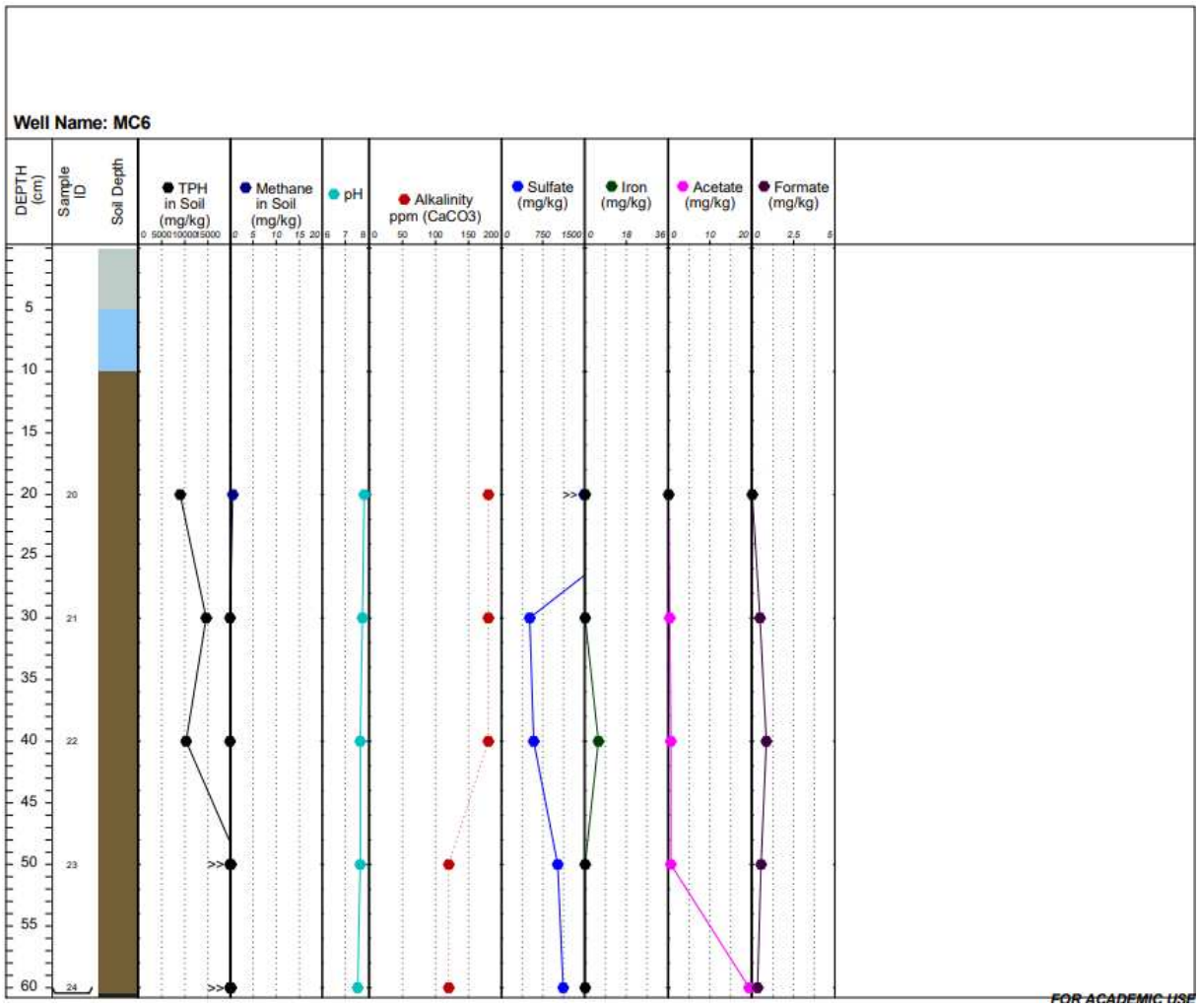

Figure SA.11. Periodic Sulfate (Column SL) All Parameters

Table SA.6. Pulsed Air Sparging (AL) All Parameters

Depth (cm)	Sample ID	TPH (mg/kg)	Methane (mg/kg)	pH	Alkalinity (ppm CaCO3)	Sulfate (mg/kg)	Iron (mg/kg)	Acetate (mg/kg)	Formate (mg/kg)
20	2	3888.58	0.00	7.57	80.00	9.51	0.00	0.77	1.36
30	3	6322.83	0.00	7.55	80.00	8.88	0.00	0.76	0.98
40	4	6735.03	0.00	7.43	80.00	8.24	0.00	1.35	1.24
50	5	5613.54	7.68	7.48	80.00	2.74	0.00	0.85	1.39
60	6	5719.94	4.18	7.85	80.00	2.57	0.00	0.73	2.14

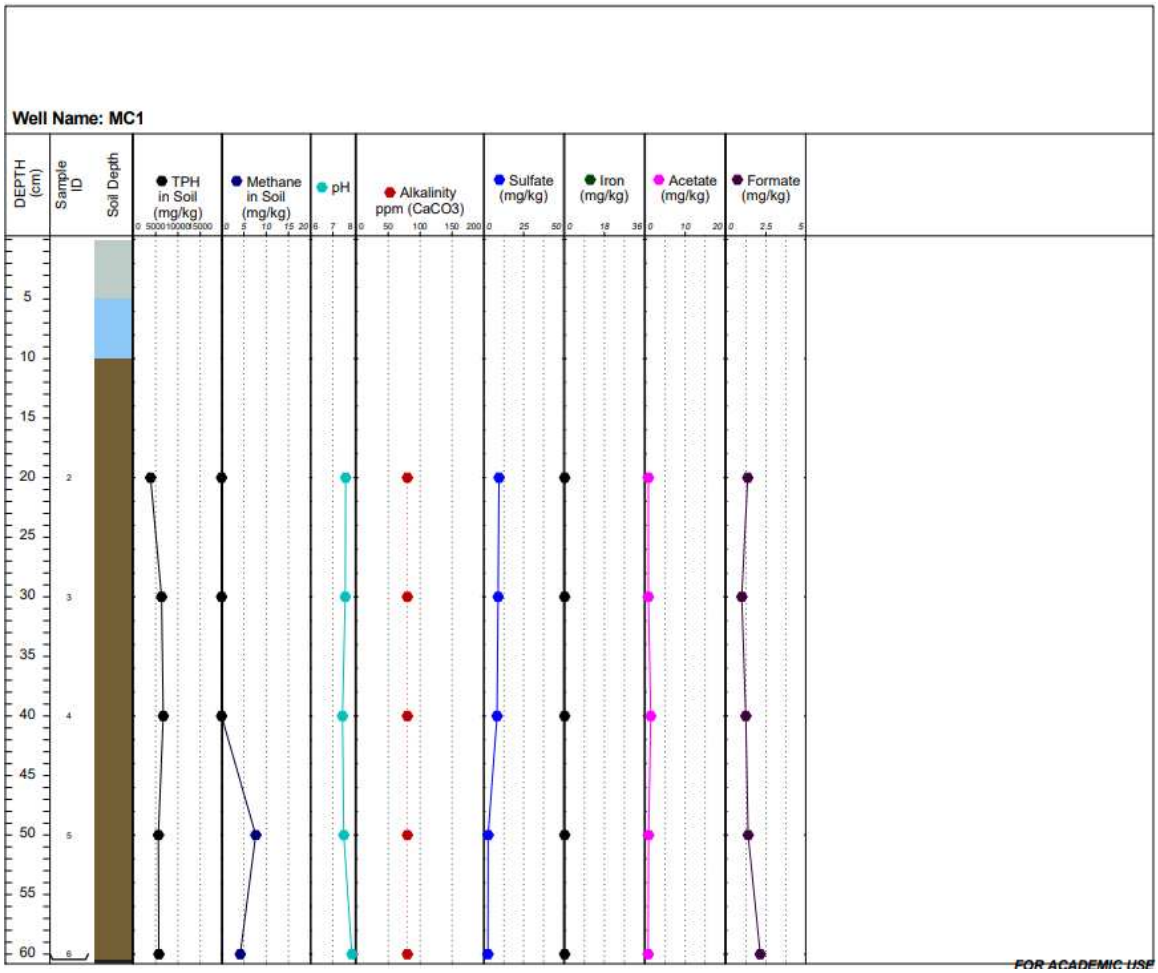

Figure SA.12. Pulsed Air Sparging (Column 1) All Parameters.

Table SA.7. Pulsed Air Sparging (AH) All Parameters

Depth (cm)	Sample ID	TPH (mg/kg)	Methane (mg/kg)	pH	Alkalinity (ppm CaCO3)	Sulfate (mg/kg)	Iron (mg/kg)	Acetate (mg/kg)	Formate (mg/kg)
20	8	2940.87	0.00	7.62	40.00	8.73	1.94	0.97	1.32
30	9	5964.84	0.00	7.79	40.00	3.80	2.75	1.16	2.27
40	10	8635.50	0.00	7.14	40.00	2.06	4.60	0.56	1.05
50	11	12786.82	14.37	7.49	40.00	1.37	5.57	0.66	0.97
60	12	14800.78	16.52	7.16	80.00	2.68	2.75	1.08	1.32

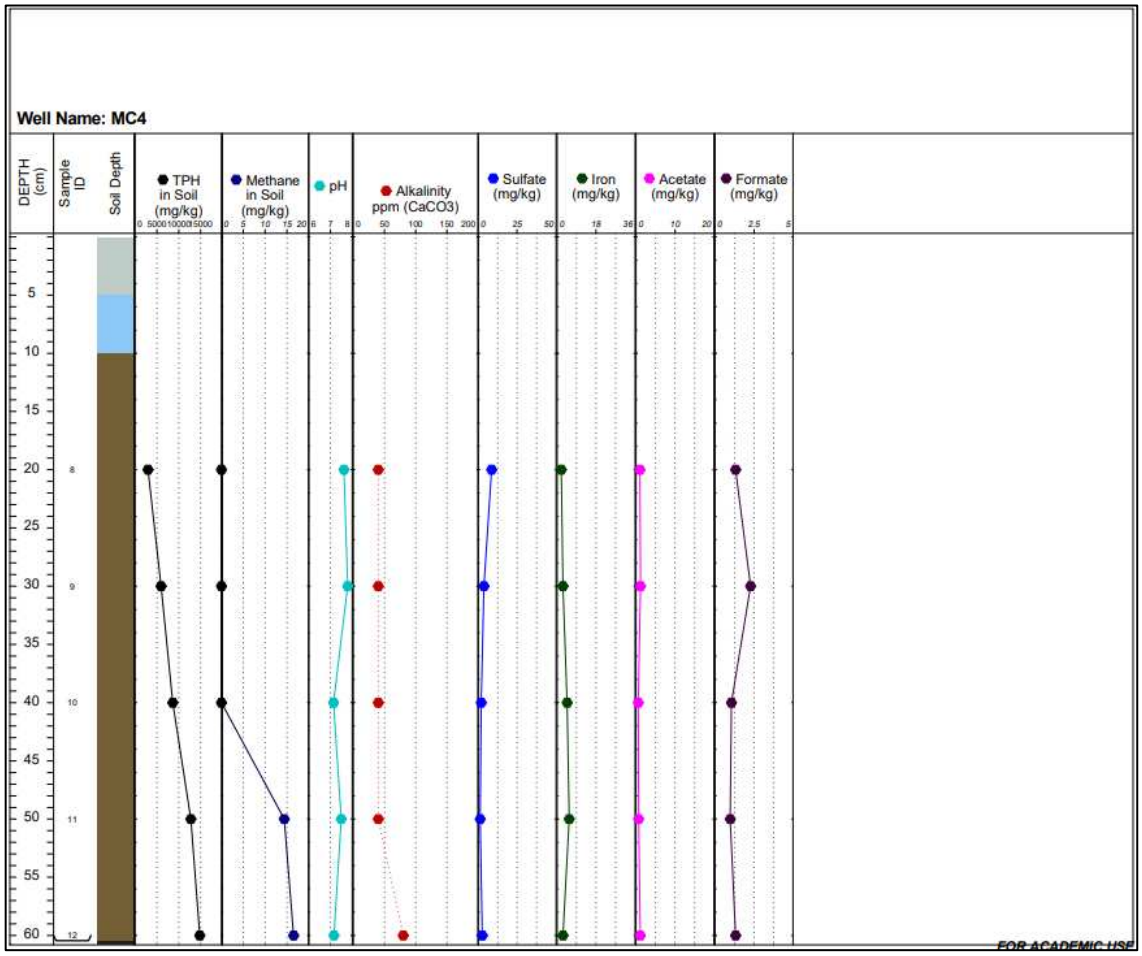

Figure SA.13. Pulsed Air Sparging (Column 4) All Parameters

Table SA.8. Methanogenic (Column ML) Microbiology

Depth (cm)	Sample ID	Bacteria 16S rRNA (gene copies/g of soil)	Bacteria 16S rRNA (transcripts/g of soil)	Archaea 16S rRNA (gene copies/g of soil)	Archaea 16S rRNA (transcripts/g of soil)	*mcrA* 16S rRNA (gene copies/g of soil)	*mcrA* 16S rRNA (transcripts/g of soil)
30	33	ND	2.60E+07	2.39E+05	2.91E+08	ND	2.65E+05
40	34	ND	8.34E+05	7.64E+05	3.94E+08	ND	ND
50	35	5.61E+04	1.23E+08	6.44E+07	4.23E+08	ND	ND

ND = non detect. for 16S rRNA bacterial gene copies and transcripts the detection limit was 477 copies/reaction; for 16S rRNA and *mcrA* gene copies and transcripts the detection limit was 262 copies/reaction

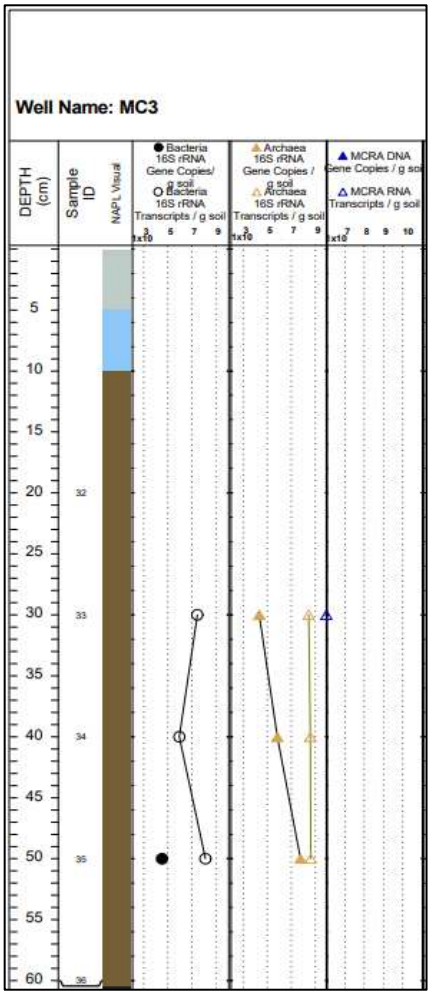

Figure SA.14. Methanogenic (Column ML) Microbiology

Table SA.9. Methanogenic (Column MH) Microbiology

Depth (cm)	Sample ID	Bacteria 16S rRNA (gene copies/g of soil)	Bacteria 16S rRNA (transcripts/g of soil)	Archaea 16S rRNA (gene copies/g of soil)	Archaea 16S rRNA (transcripts/g of soil)	*mcrA* 16S rRNA (gene copies/g of soil)	*mcrA* 16S rRNA (transcripts/g of soil)
30	27	3.47E+03	2.63E+06	3.60E+07	3.51E+08	ND	6.62E+07
40	28	1.05E+06	1.71E+09	3.71E+07	5.16E+08	ND	5.95E+06
50	29	1.23E+05	4.08E+07	2.49E+07	5.09E+08	ND	4.02E+05

ND = non detect. for 16S rRNA bacterial gene copies and transcripts the detection limit was 477 copies/reaction; for 16S rRNA and *mcrA* gene copies and transcripts the detection limit was 262 copies/reaction.

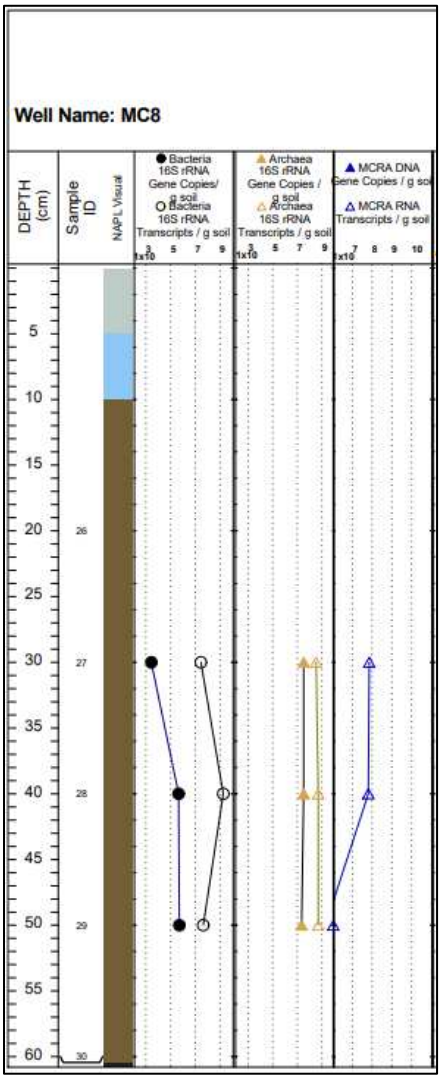

Figure SA.15. Methanogenic (Column MH) Microbiology

Table SA.10. Periodic Sulfate Addition (SL) Microbiology

Depth (cm)	Sample ID	Bacteria 16S rRNA (gene copies/g of soil)	Bacteria 16S rRNA (transcripts/g of soil)	Archaea 16S rRNA (gene copies/g of soil)	Archaea 16S rRNA (transcripts/g of soil)	*mcrA* 16S rRNA (gene copies/g of soil)	*mcrA* 16S rRNA (transcripts/g of soil)
30	15	3.27E+09	2.63E+06	7.41E+06	2.74E+08	ND	ND
40	16	3.05E+04	1.71E+09	3.14E+07	5.41E+07	ND	ND
50	17	3.00E+05	4.08E+07	2.09E+08	7.13E+07	ND	ND

ND = non detect. for 16S rRNA bacterial gene copies and transcripts the detection limit was 477 copies/reaction; for 16S rRNA and *mcrA* gene copies and transcripts the detection limit was 262 copies/reaction.

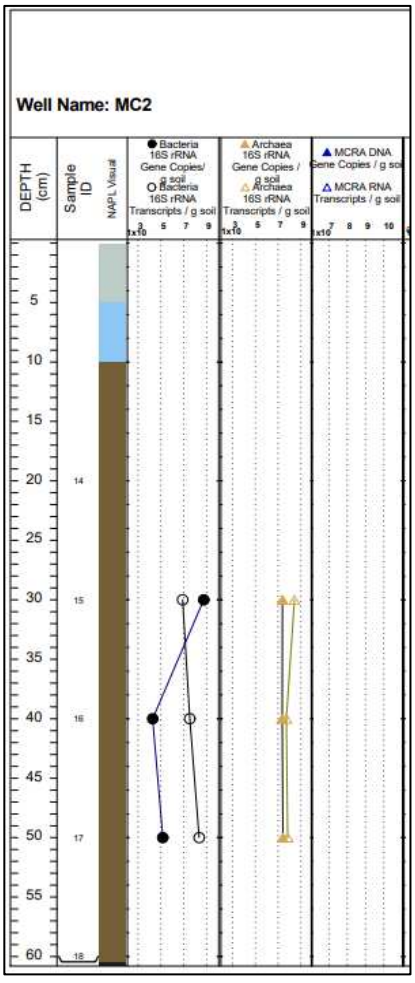

Figure SA.16. Periodic Sulfate (SL) Microbiology

Table SA.11. Periodic Sulfate addition (SH) Microbiology

Depth (cm)	Sample ID	Bacteria 16S rRNA (gene copies/g of soil)	Bacteria 16S rRNA (transcripts/g of soil)	Archaea 16S rRNA (gene copies/g of soil)	Archaea 16S rRNA (transcripts/g of soil)	*mcrA* 16S rRNA (gene copies/g of soil)	*mcrA* 16S rRNA (transcripts/g of soil)
30	21	1.15E+06	1.57E+09	2.42E+07	4.66E+07	ND	6.16E+06
40	22	ND	8.51E+06	5.82E+07	1.53E+07	ND	1.01E+06
50	23	ND	6.61E+10	1.19E+07	1.67E+08	ND	2.63E+06

ND = non detect. for 16S rRNA bacterial gene copies and transcripts the detection limit was 477 copies/reaction; for 16S rRNA and *mcrA* gene copies and transcripts the detection limit was 262 copies/reaction.

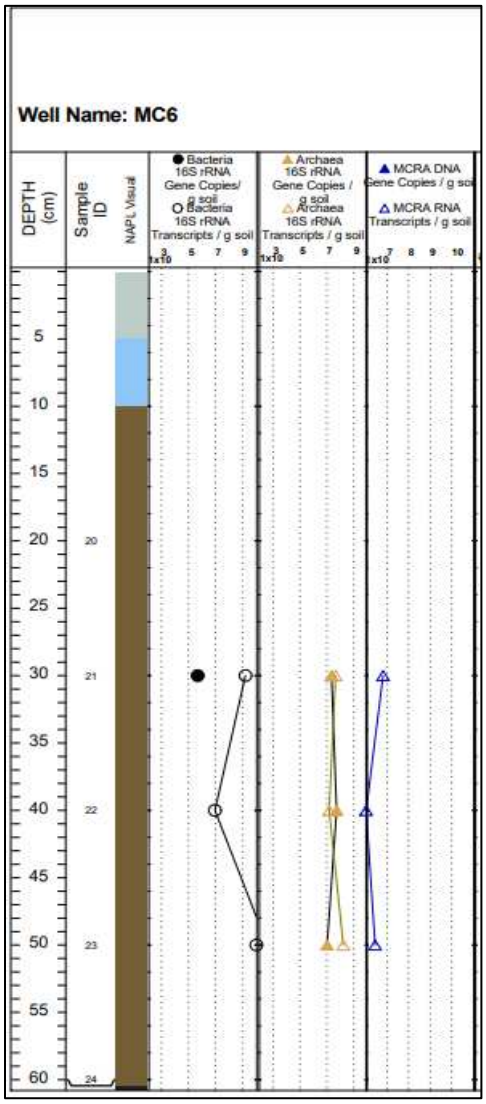

Figure SA.17. Periodic Sulfate (SH). Microbiology

Table SA.12. Pulsed Air Sparging (Column AL) Microbiology

Depth (cm)	Sample ID	Bacteria 16S rRNA (gene copies/g of soil)	Bacteria 16S rRNA (transcripts/g of soil)	Archaea 16S rRNA (gene copies/g of soil)	Archaea 16S rRNA (transcripts/g of soil)	*mcrA* 16S rRNA (gene copies/g of soil)	*mcrA* 16S rRNA (transcripts/g of soil)
30	3	ND	3.17E+10	ND	1.41E+08	ND	ND
40	4	9.89E+05	ND	4.90E+06	1.61E+08	ND	ND
50	5	ND	ND	4.40E+04	1.51E+08	ND	ND

ND = non detect. for 16S rRNA bacterial gene copies and transcripts the detection limit was 477 copies/reaction; for 16S rRNA and *mcrA* gene copies and transcripts the detection limit was 262 copies/reaction.

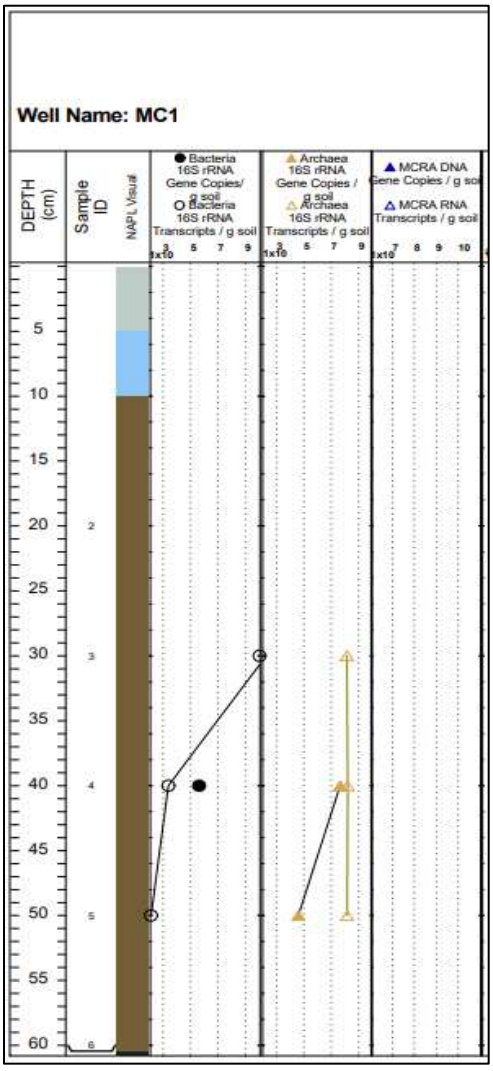

Figure SA.18. Pulsed Air Sparging (Al) Microbiology

Table SA.13. Pulsed Air Sparging (Column AH) Microbiology

Depth (cm)	Sample ID	Bacteria 16S rRNA (gene copies/g of soil)	Bacteria 16S rRNA (transcripts/g of soil)	Archaea 16S rRNA (gene copies/g of soil)	Archaea 16S rRNA (transcripts/g of soil)	*mcrA* 16S rRNA (gene copies/g of soil)	*mcrA* 16S rRNA (transcripts/g of soil)
30	9	4.63E+07	2.10E+07	ND	6.35E+07	ND	ND
40	10	1.31E+05	1.03E+07	4.90E+06	4.35E+05	ND	ND
50	11	2.64E+06	1.18E+07	4.40E+04	3.06E+07	ND	ND

ND = non detect. for 16S rRNA bacterial gene copies and transcripts the detection limit was 477 copies/reaction; for 16S rRNA and mcrA gene copies and transcripts the detection limit was 262 copies/reaction.

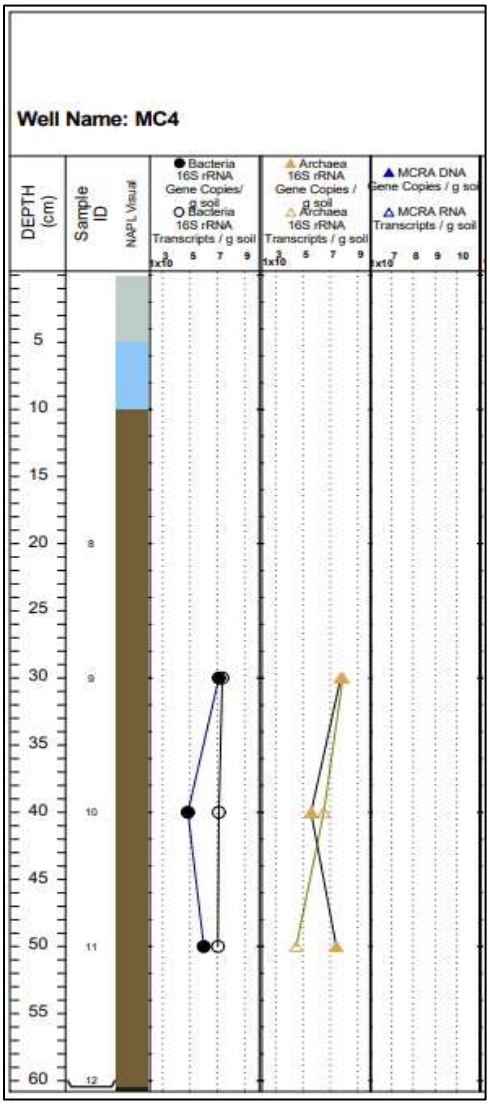

Figure SA.19. Pulsed Air Sparging (AH) Microbiology.

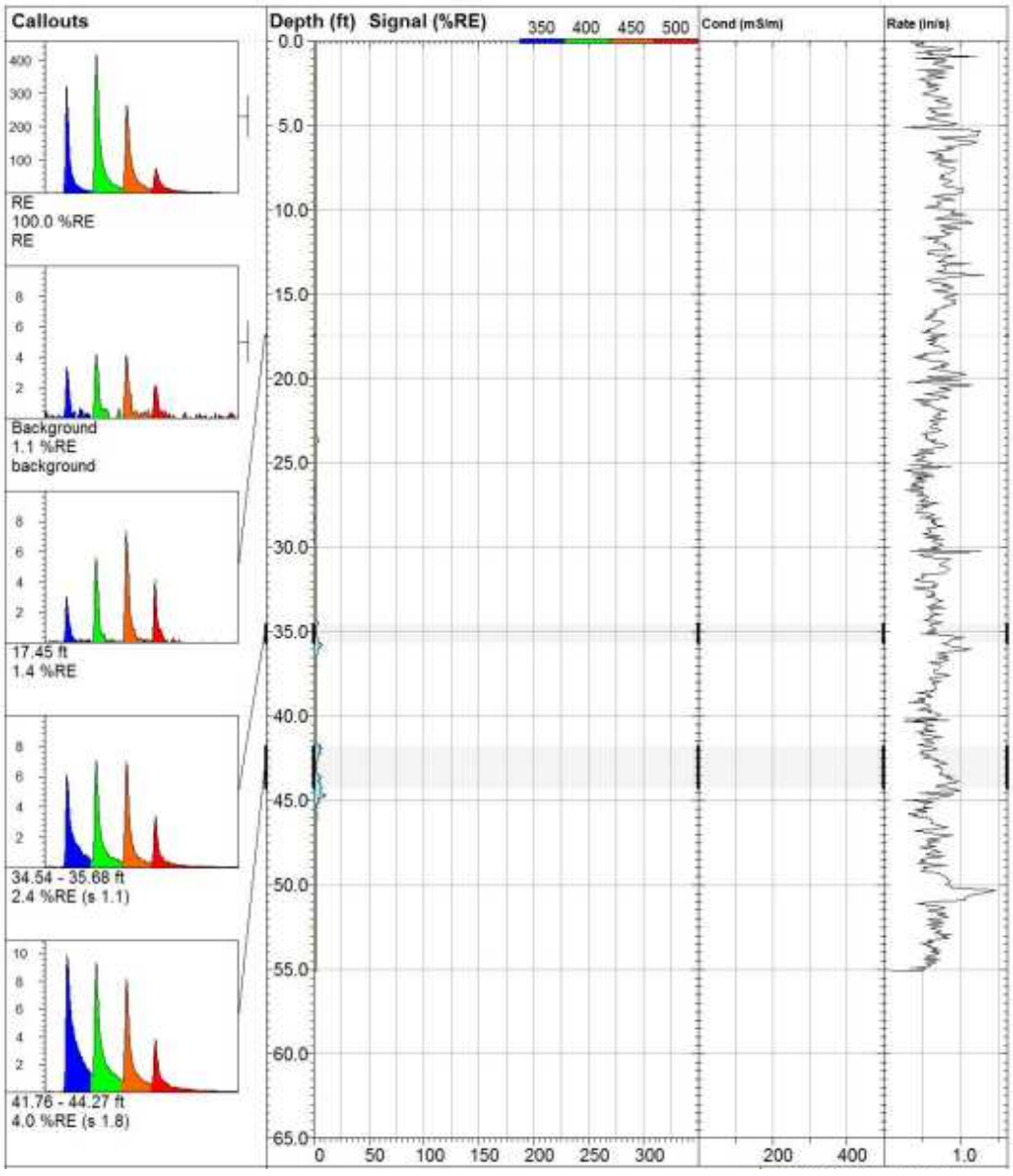

Figure SB.1. LIF-19 located by *no LNAPL* boring.

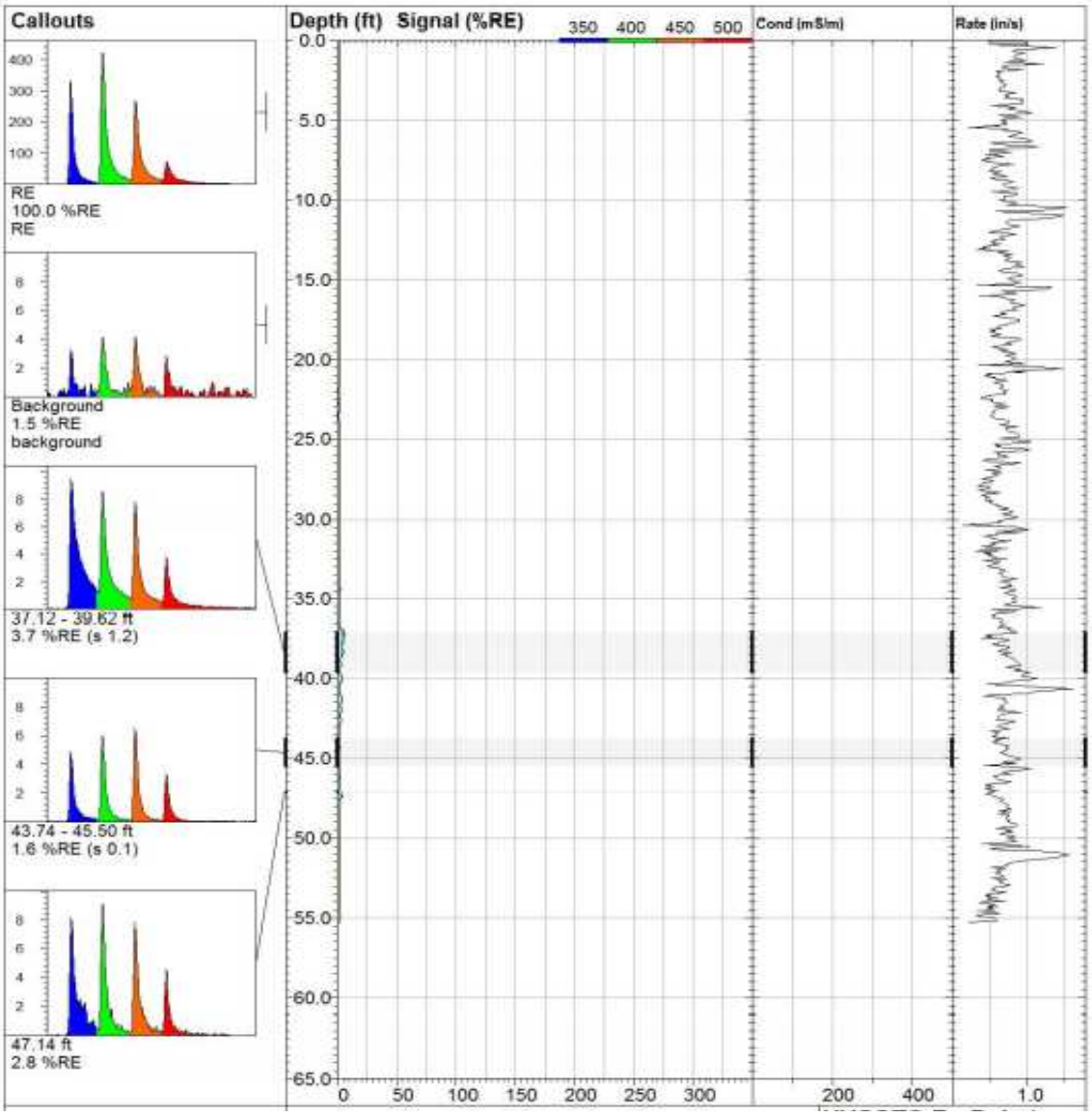

Figure SB.2. LIF-20 located by *no LNAPL* boring.

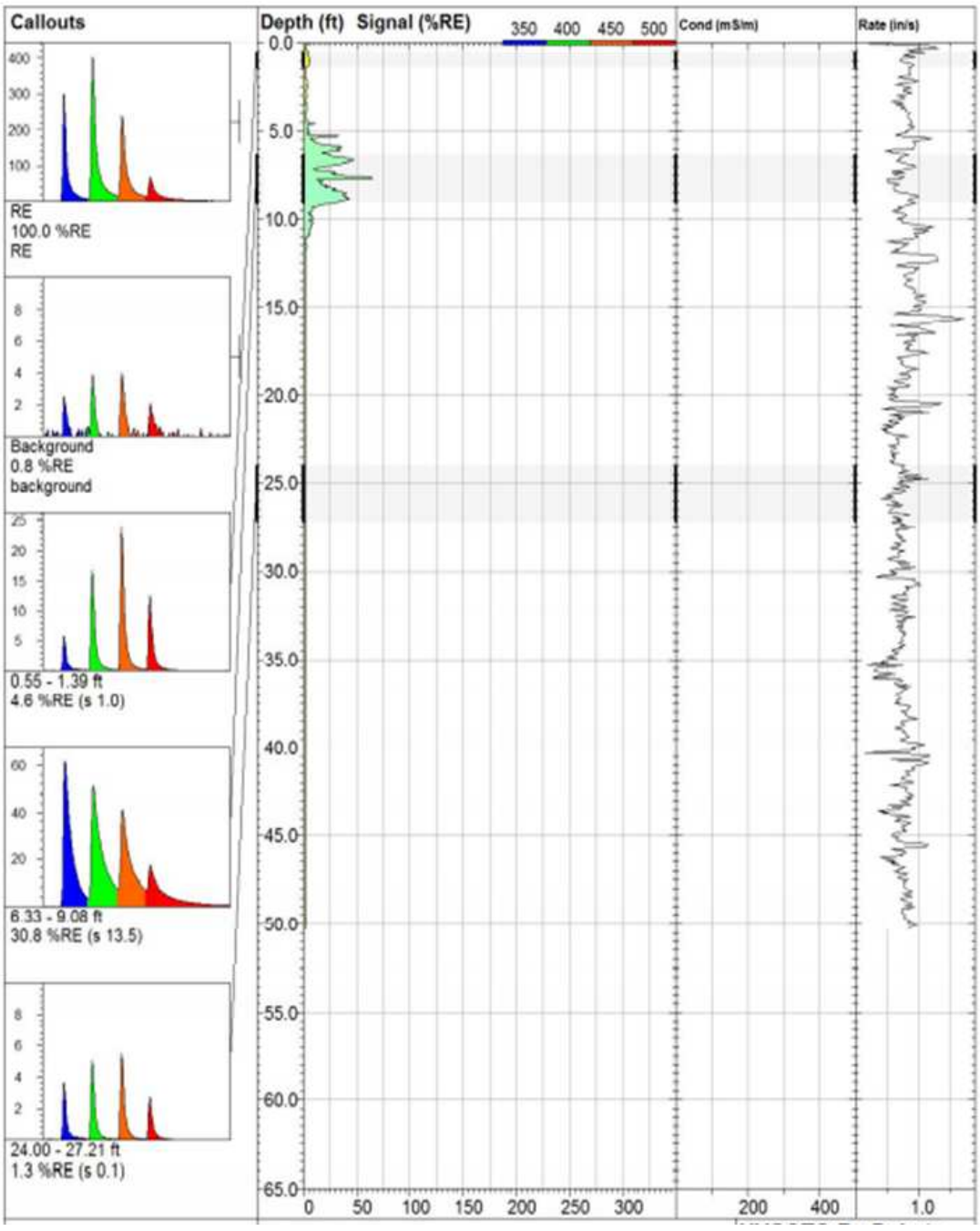

Figure SB.3. LIF-05 located by the *LNAPL-1* boring.

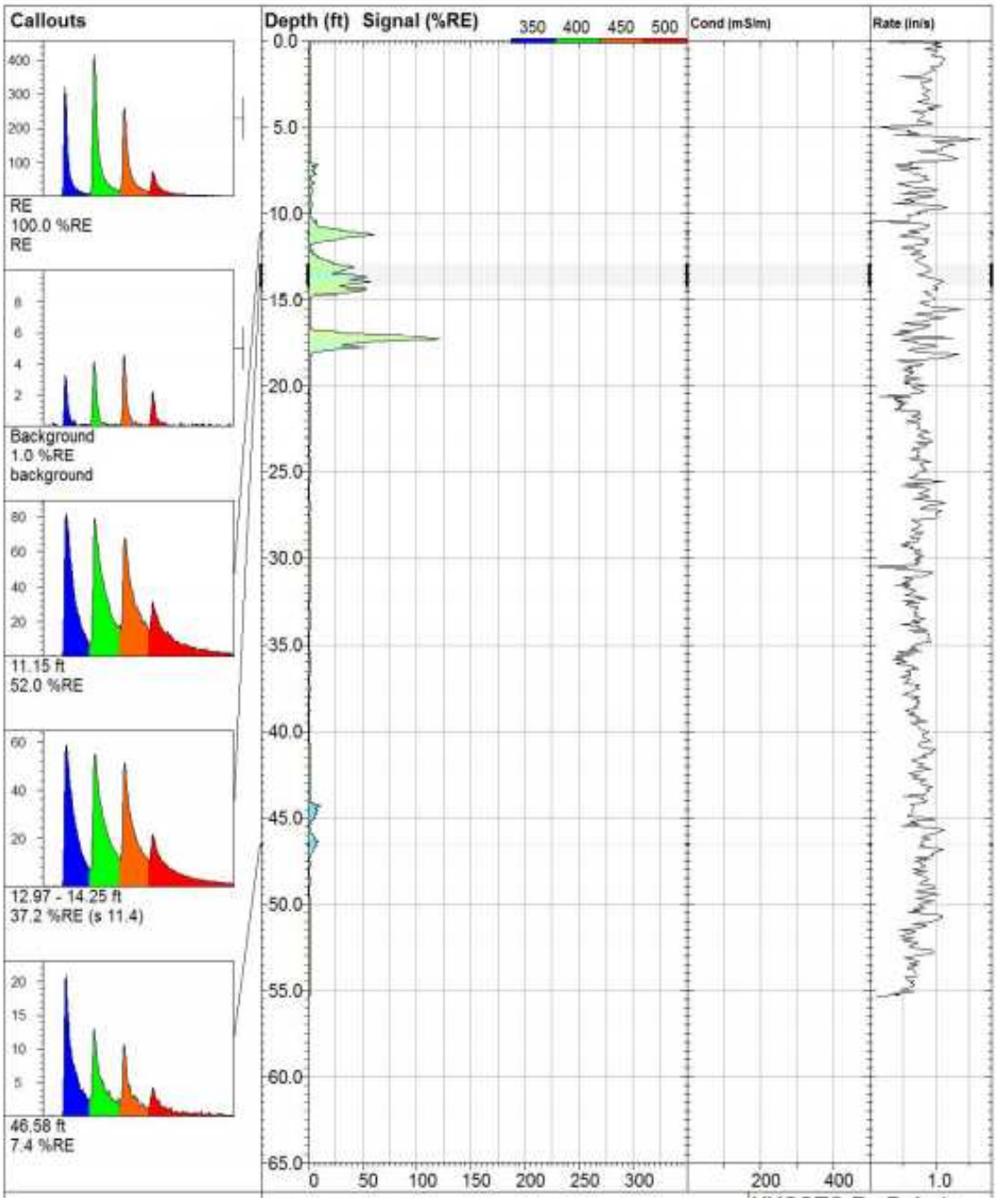

Figure SB.4. LIF-06 located by the *LNAPL-2* boring.

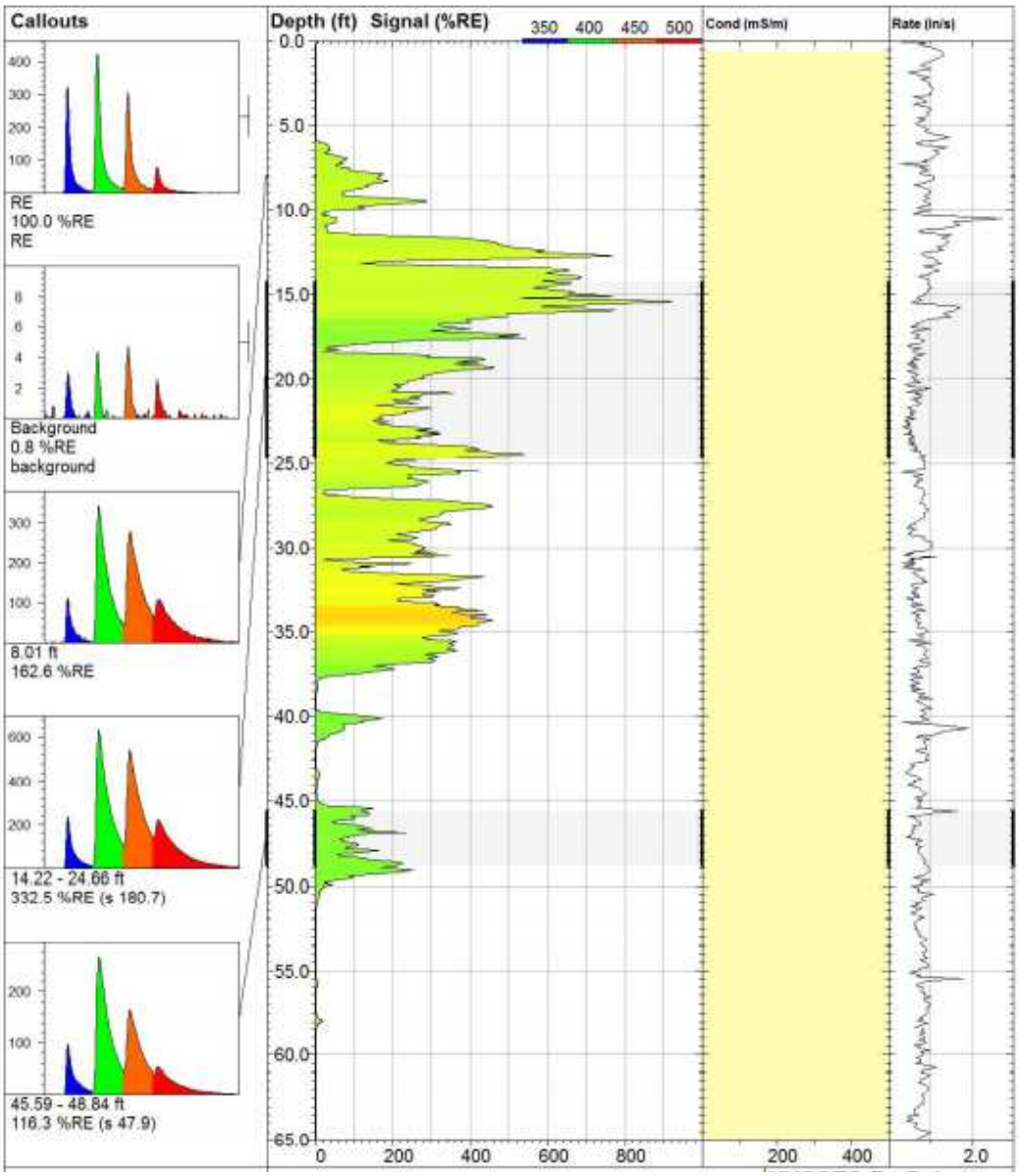

Figure SB.5. LIF-22 located by the LNAPL-2 boring.

Sensor installation and diagrams

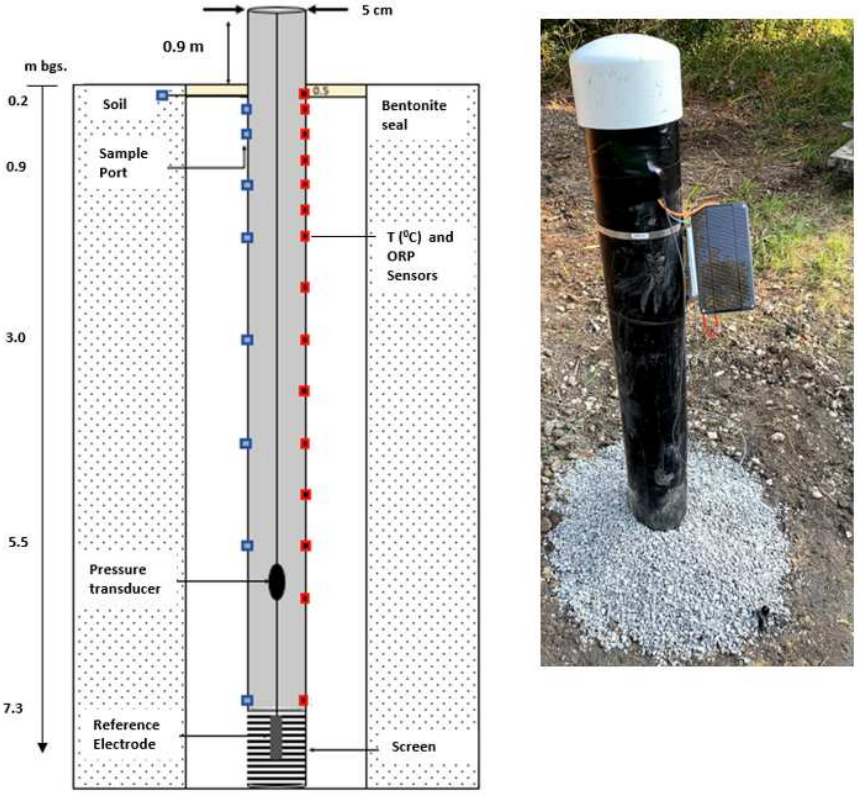

Figure SB.6. Sensor string and MLS installed at the *no LNAPL* Cryocoring location.

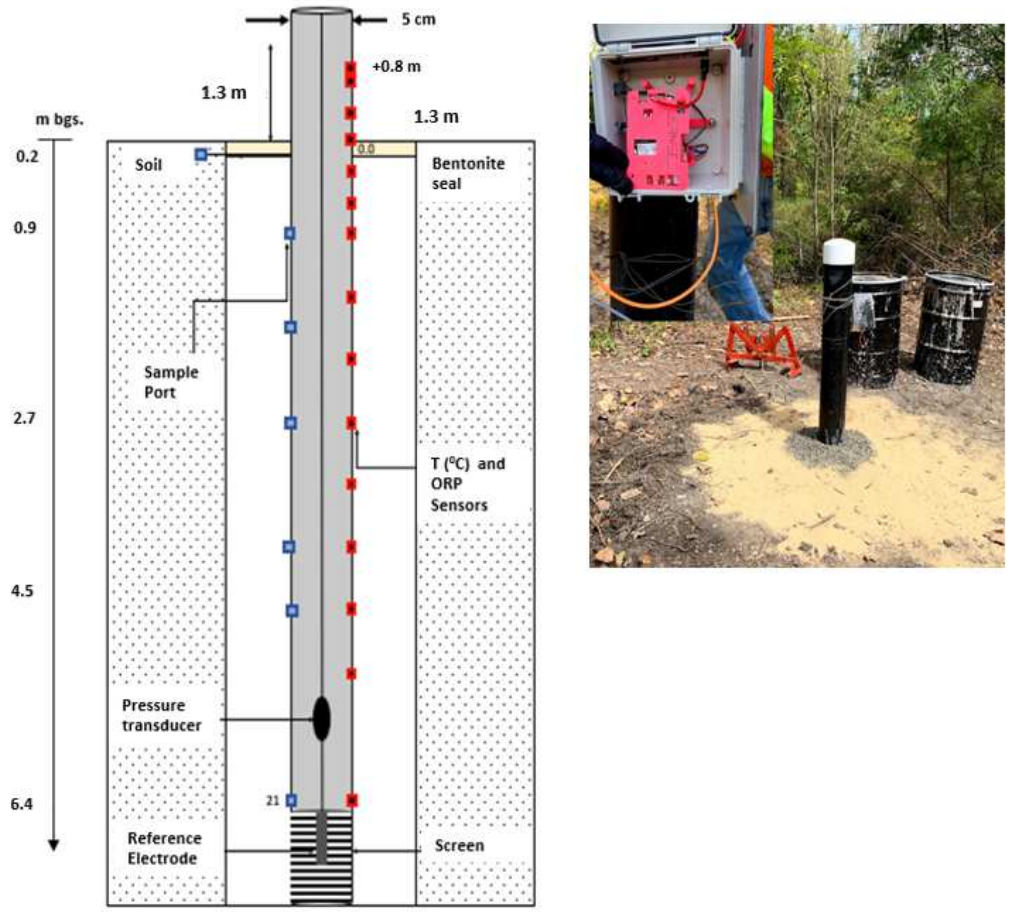

Figure SB.7. Sensor string and MLS installed at the *LNAPL-1* Cryocoring location.

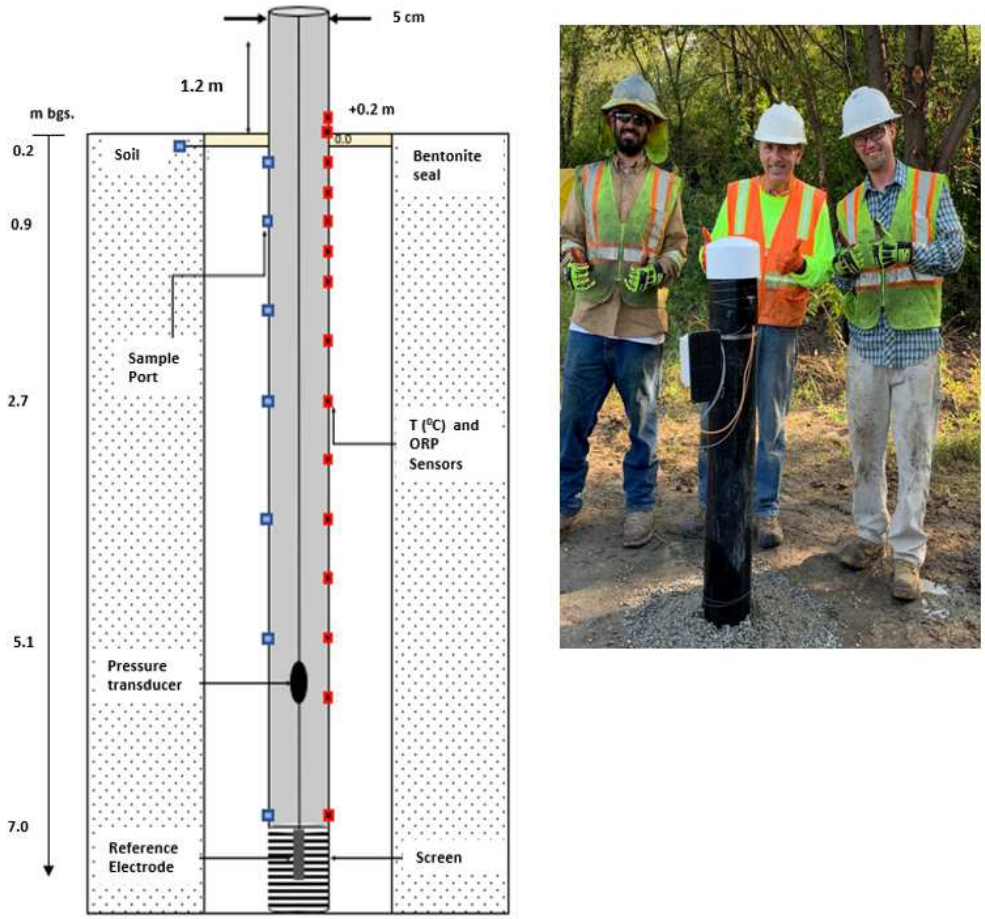

Figure SB.8. Sensor string and MLS installed at the *LNAPL-2* Cryocoring location.

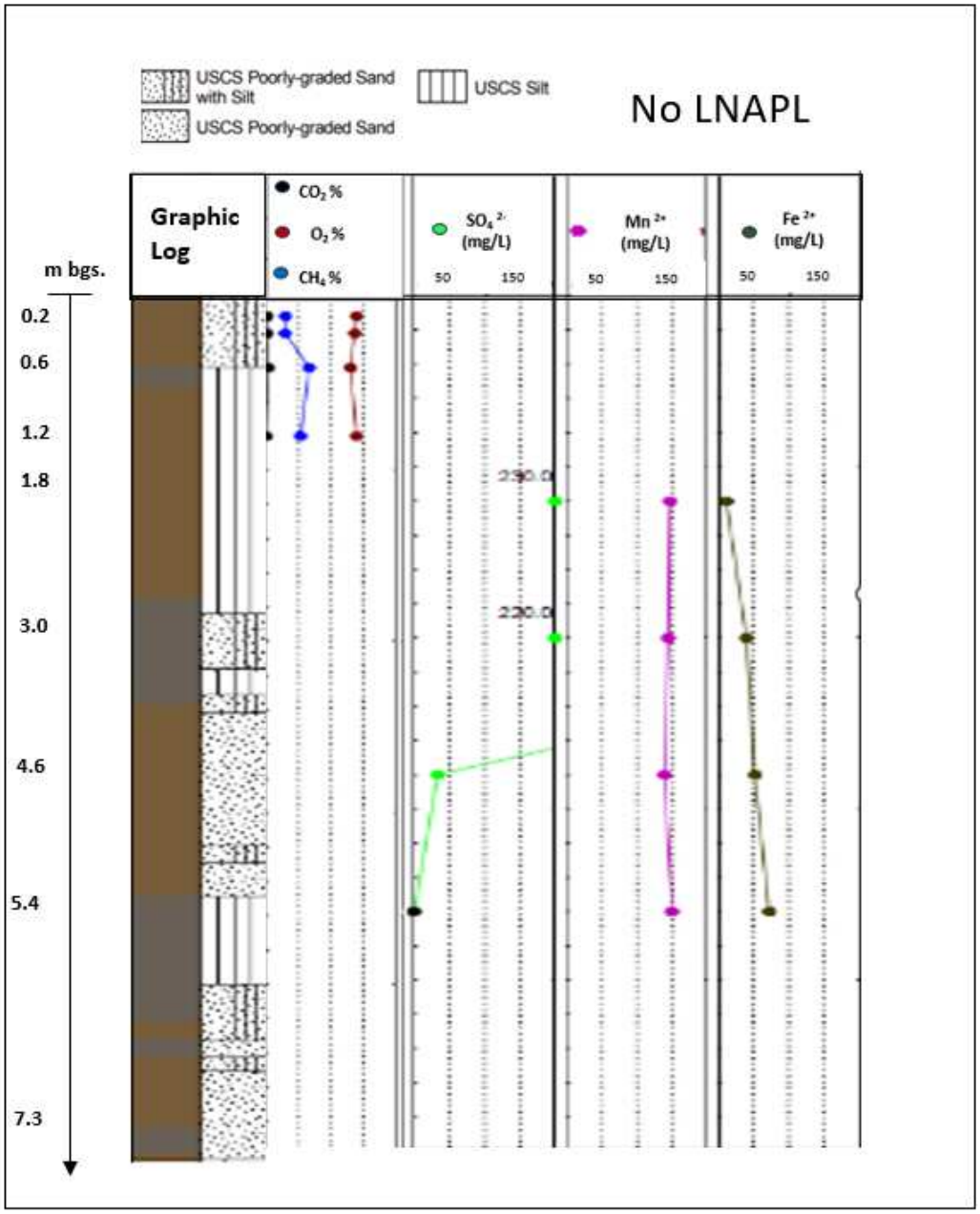

Figure SB.9. Gas and aqueous samples collected from the MLS installed at the *No LNAPL* Cryocoring location.

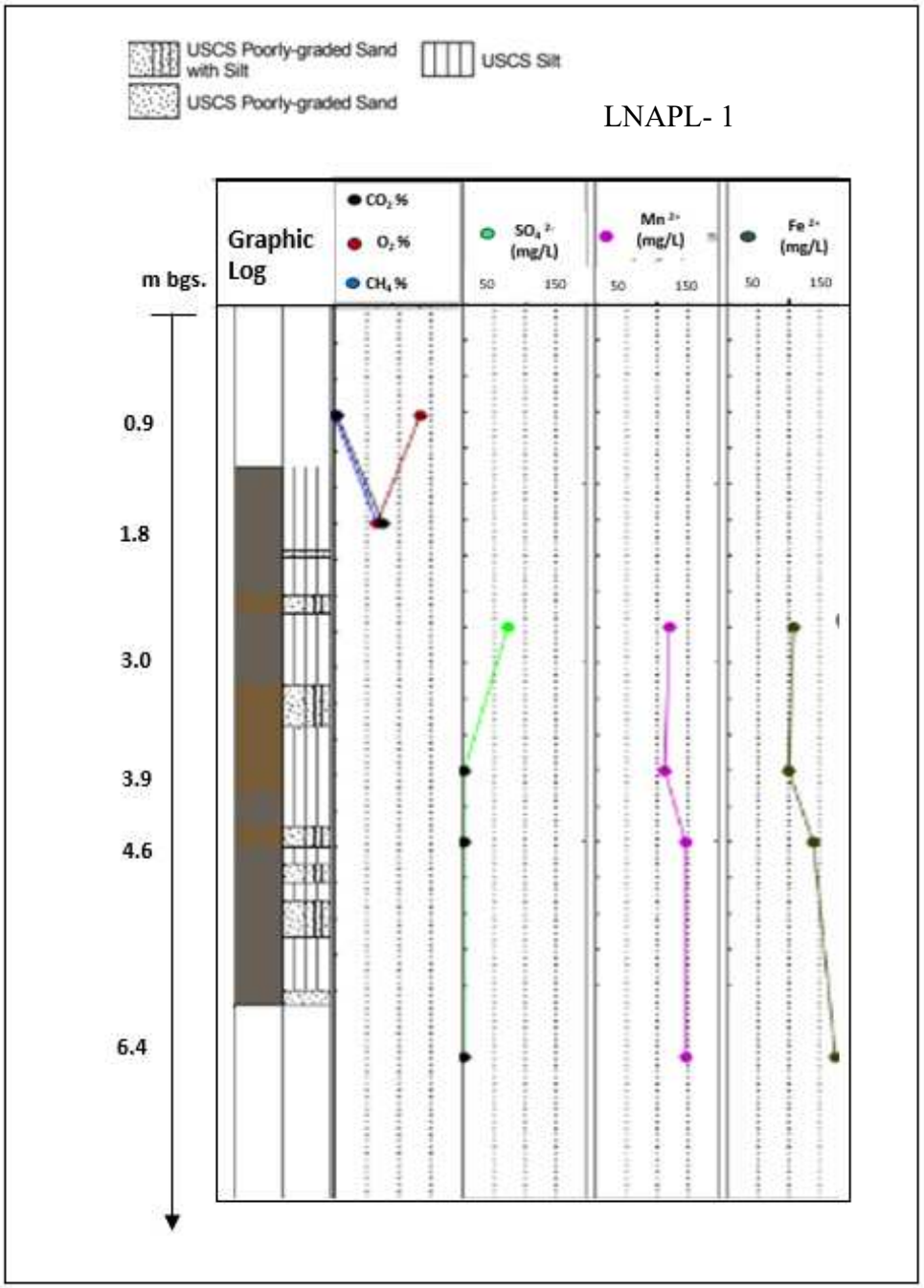

Figure SB.10. Gas and aqueous samples collected from the MLS installed at the *LNAPL-1* Cryocoring location.

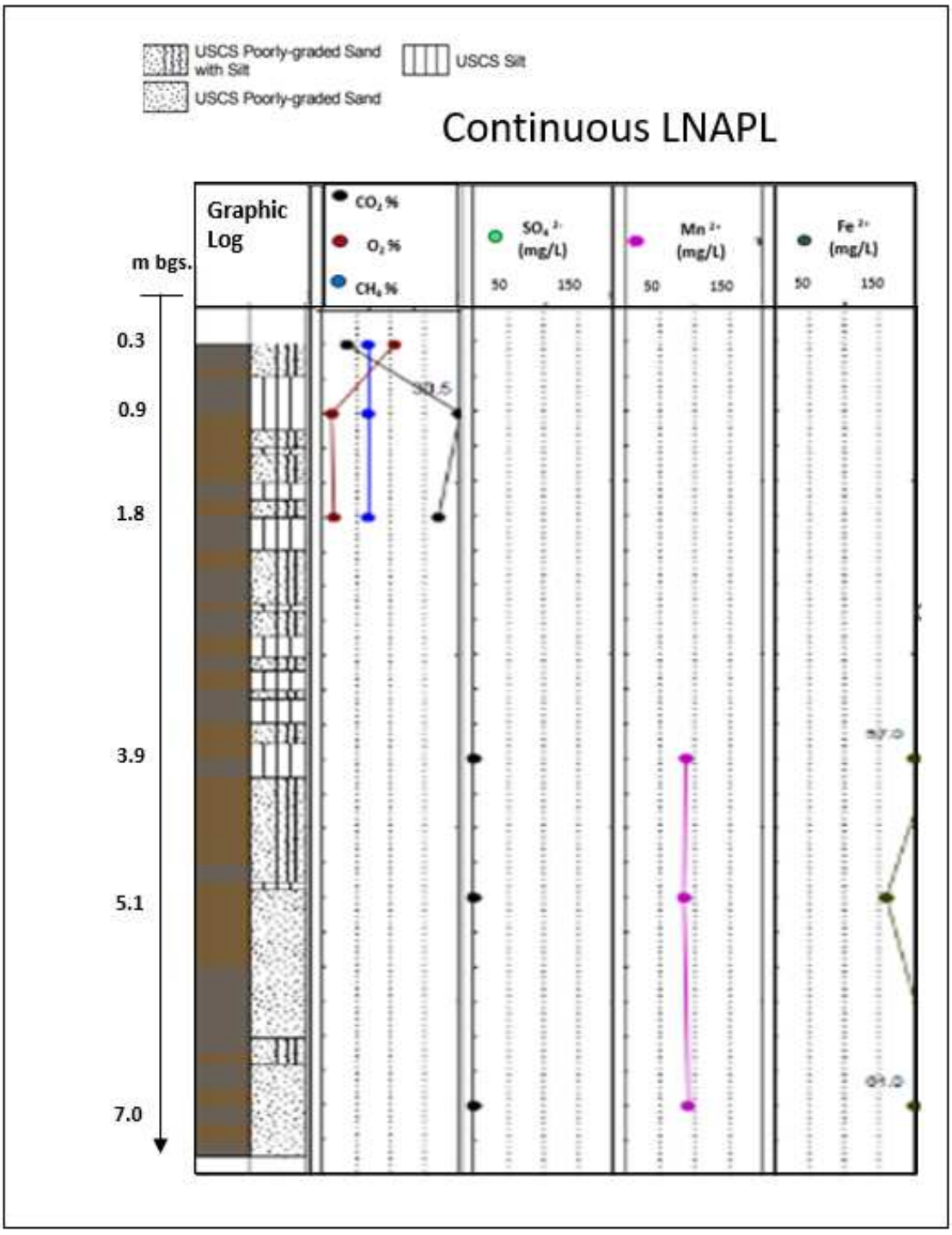

Figure SB.11. Gas and aqueous samples collected from the MLS installed at the *LNAPL-2* Cryocoring location.

Table SB.1. Taxonomic assignment for identified Bacteria and inferred redox process.

Taxonomic assignment	Key	Putative redox process	Citation
Methyloligellaceae_(fam)		Aerobic	(Nan et al, 2020)
Methylobacter_(gen)		Aerobic	(Smith et al, 2018)
Methylocystis_(gen)		Aerobic	(Baani et al, 2008)
Bacillales_(or)		Aerobic/Nitrate reduction	(Sundeberg et al,2013)
Bacillus_(gen)		Aerobic/Nitrate reduction	(Nakano & Zuber, 1998)
Candidatus_Udaeobacter_(gen)		Aerobic/Nitrate reduction	(Liu et al, 2019)
Pseudomonas_(gen)		Nitrate Reduction	(Liang et al, 2014)
Sphingomonas_(gen)		Nitrate Reduction	(Daugulis et al, 2003)
Candidatus_Wosebacteria_(gen)		Nitrate Reduction	(Chen et al, 2020)
Bradyrhizobium_(gen)		Nitrate Reduction	(Gao et al, 2015)
Candidatus_Yanofskybacteria_(gen)		Nitrite reduction	(Liu et al, 2020)
Xanthobacter _(gen)		Nitrate Reduction	(king et al, 2006)
Microtrichales_(or)		Nitrate reduction/Iron reduction	(Chen et al, 2020)
Micromonosporaceae_(fam)		Nitrate reduction/Iron reduction	(Thawai et al, 2006)
Actinobacterium _WWH12 _(sp)		Nitrate reduction/Iron reduction	(Zhang et al, 2021)
Bacteriap25_(gen)		Iron Reduction	(Rubin-Blum et al,2021)
Pseudolabrys (gen)		Iron Reduction	(Antonelli et al, 2020)
Gemmatimonadaceae_(fam)		Iron Reduction	(Tong et al, 2019)
Gaiellales_(or)		Iron Reduction	(Gupta et al, 2021)
Latescibactera_(gen)		Unknown	
RBG-16-55-12_(gen)		Unknown	
Caldisericum (gen)		Iron Reduction	(Gieg et al, 2014)
Vicinamibacterales_(or)		Iron Reduction	(Gong et al, 2021)
Vicinamibacteraceae_(fam)		Iron reduction	(Gong et al, 2021)
Thermodesulfovibriona_(cl)		Sulfate reduction	(Nothaft et al, 2021)
Cryptanaerobacter_(gen)		Sulfate reduction	(Rakoczy et al, 2011)
Rubrobacter_(gen)		Sulfate reduction	(Chen et al, 2004)
OPB41 (gen)		Sulfate reduction	(Ozuolmez et al, 2020)
WCHB1-41_(gen)		Sulfate reduction	(Dojka et al, 1998)
ADurb.Bin180_(gen)		Unknown	
Phyllobacterium_(gen)		Sulfate reduction	(Meziti et al, 2017)
Desulfoprunum (gen)		Sulfate reduction	(Junghare et al.2015)
Desulfovirga (gen)		Sulfate reduction	(Kuever et al,2015)
Desulfosporosinus_(gen)		Sulfate reduction	(Pester et al, 2010)
Desulfatiglans (gen)		Sulfate reduction	(Johcum et al , 2018)
SCADC1-2-3_(gen)		Fermentation	(DePoy et al, 2021)
Anaerolineaceae_(fam)		Sulfate reduction/fermentation	(Peng et al, 2020)

Table SB.1 continued. Taxonomic assignment for identified Bacteria and inferred redox process.

Taxonomic assignment	Key	Putative redox process	Citation
SVA-0485_(gen)		Sulfate reduction/fermentation	(Toth et al, 2021)
Spirochaetaceae_(fam)		Fermentation	(Feng et al, 2019)
Aminicenantales_(gen)		Fermentation	(Hua et al, 2020)
Smithella (gen)		Fermentation	(Liu et al, 1999)
Syntrophus_(gen)		Fermentation	(Irianni-Renno et al, 2016)
Syntrophales_(or)		Fermentation	(Rojas et al, 2021)
Syntrophorhabdus_(gen)		Fermentation	(Qiu et al, 2008)
RB41_(gen)		Fermentation	(Feng et al, 2021)
Pelolinea_(gen)		Fermentation	(Chen et al, 2020)
Leptolinea (gen)		Fermentation	(Wu et al, 2020)
longilinea_(gen)		Fermentation	(Yamada et al, 2015)
Other		NA	

Table SB.2. Taxonomic assignment for identified Archaea and inferred redox process.

Taxonomic assignment	Key	Putative redox process	Citation
Nitrososphaeraceae_(fam)		Nitrate Reduction	(Nan et al, 2020)
Nitrososphaera_(gen)		Nitrate Reduction	(Smith et al, 2018)
Candidatua Altiarchaeum_(gen)		Nitrite Reduction	(Probst et al, 2015)
Bathyarchaea_(gen)		Iron reduction	(Rios del Toro et al, 2018)
Marine group II_(gen)		Unknown	
Candidatus_Pacearchaetoa_(gen)		Anaerobic methane oxidation	(Castelle et al, 2015)
Methanosaeta_(gen)		Acetoclastic methanogenesis	(Irianni-Renno et al, 2016)
Methanobacterium_(gen)		Hydrogenotrphic methanogenesis	(Kim et al, 2014)
Methanoregula_(gen)		Hydrogenotrphic methanogenesis	(Irianni-Renno et al, 2016)
Candidatus_Methanomethylicus_(gen)		Methylotorphic methanogenesis	(Vanwonterghem et al, 2016)
Woesearchaeales_(gen)		Nitrate Red./methane ox.	(Daugulis et al, 2003)
Other		NA	

Table SB.3. Microbial ecology characterization (DNA) for cryogenic samples collected from the *no LNAPL* boring.

Boring	Depth (m bgs)	Taxonomic assignement Bacteria	%	Taxonomic assignement Archaea	%
no LNAPL	**0.63**	Methylobacter (gen)	5.21	Not detected	
		Microtrichales_(or)	12.56		
		Gemmatimonadaceae_(fam)	4.27		
		Micromonosporaceae_(fam)	6.16		
		Vicinamibacterales_(or)	8.29		
		Vicinamibacteraceae_(gen)	4.50		
		RB41_(gen)	4.03		
		Other	54.98		
no LNAPL	**2.62**	Vicinamibacteraceae_(gen)	0.07	Candidatus Methanomethylicus_(gen)	16.67
		Desulfosporosinus_(gen)	1.44	Methanobacterium_(gen)	80.70
		Gaiellales_(or)	0.20	Other	2.63
		Anaerolineaceae_(fam)	1.55		
		Caldisericum_(gen)	1.66		
		Smithella_(gen)	5.46		
		OPB41_(gen)	1.09		
		Desulfoprunum_(gen)	2.18		
		Desulfatiglans_(gen)	1.15		
		Thermodesulfovibrionia_(cl)	1.90		
		Syntrophus (gen)	3.85		
		Pelolinea spp.	0.29		
		bacterium_enrichment_(sp)	53.20		
		Other	25.96		
no LNAPL	2.74	Desulfosporosinus_(gen)	3.43	Candidatus Methanomethylicus_(gen)	100
		Gaiellales_(or)	0.38		
		Anaerolineaceae_(fam)	3.14		
		Caldisericum_(gen)	2.07		
		Smithella_(gen)	7.06		
		OPB41_(gen)	2.92		
		RBG-16-55-12_(gen)	5.24		
		Desulfoprunum spp.	3.18		
		Desulfatiglans_(gen)	2.86		
		Thermodesulfovibrionia_(cl)	2.22		
		Syntrophus (gen)	3.97		
		bacterium_enrichment_(sp)	20.04		
		Other	43.48		
no LNAPL	4.75	Gaiellales_(or)	3.15	Methanosaeta_(gen)	25.09
		Anaerolineaceae_(fam)	0.94	Candidatus Methanomethylicus_(gen)	4.59
		Smithella_(gen)	12.55	Methanobacterium_(gen)	25.09
		SCADC1-2-3_(gen)	3.80	Other	45.23
		Cryptanaerobacter_(gen)	3.78		
		Desulfoprunum_(gen)	0.17		
		Pelolinea_(gen)	3.71		
		bacterium_enrichment_(sp)	0.08		
		Other	71.83		
no LNAPL	**5.66**	not detected		not detected	

Table SB.4. Microbial ecology characterization (RNA) for cryogenic samples collected from the *no LNAPL* boring.

Boring	Depth (m bgs)	Taxonomic assignement Bacteria	%	Taxonomic assignement Archaea	%
no LNAPL	**0.63**	Methyloligellaceae_(fam)	1.41	Nitrososphaeraceae_(fam)	43.64
		Methylobacter_(gen)	9.33	Nitrososphaeraceae_(gen)	44.36
		Methylocystis_(gen)	1.45	Methanobacterium_(gen)	1.82
		Bacillales_(or)	2.18	Other	10.18
		Pseudomonas_(gen)	5.07		
		Bacteriap25_(gen)	1.84		
		Phyllobacterium_(gen)	1.43		
		Bradyrhizobium_(gen)	1.42		
		Xanthobactereae_(gen)	1.26		
		Sphingomonas_(gen)	3.20		
		Desulfoprunum_(gen)	0.08		
		Other	71.33		
no LNAPL	**2.62**	not detected		not detected	
no LNAPL	**2.74**	Gaiellales_(or)	0.28	Candidatus Methanomethylicus_(gen)	100
		Caldisericum spp.	2.57		
		Smithella spp.	0.67		
		SCADC1-2-3 spp.	0.14		
		Spirochaetaceae_(fam)	0.39		
		Leptolinea_(gen)	2.24		
		Anaerolineaceae (fam)	0.37		
		Desulfoprunum_(gen)	4.67		
		Desulfatiglans_(gen)	7.59		
		Desulfovirga_(gen)	3.66		
		Syntrophus_(gen)	36.81		
		Syntrophorhabdus_(gen)	0.99		
		Syntrophales_(or)	0.44		
		Other	39.18		
no LNAPL	**4.75**	Caldisericum spp.	4.32	Methanosaeta_(gen)	19.74
		Smithella spp.	19.77	Candidatus Methanomethylicus_(gen)	64.47
		SCADC1-2-3 spp.	9.52	Methanobacterium_(gen)	5.26
		Gaiellales_(or)	5.47	Bathyarchaeia_(gen)	10.53
		JS1_(gen)	0.36	Other	0.00
		RBG-16-55-12 (gen)	0.87		
		Cryptanaerobacter	2.11		
		Spirochaetaceae_(fam)	4.86		
		Anaerolineaceae (fam)	0.34		
		Syntrophales (or)	3.15		
		Desulfoprunum (gen)	1.10		
		Desulfatiglans (gen)	0.17		
		Leptolinea (gen)	0.82		
		Syntrophus_(gen)	1.36		
		Pelolinea spp.	1.10		
		Syntrophorhabdus spp.	1.63		
		Other	43.07		
no LNAPL	**5.66**	Desulfatiglans_(gen)	0.35	Bathyarchaeia_(gen)	52.42
		JS1_(gen)	9.60	Other	47.58
		Sva0485_(gen)	6.33		
		Syntrophus_(gen)	1.30		
		Other	82.42		

Table SB.5. Microbial ecology characterization (DNA) for cryogenic samples collected from the *LNAPL-1* boring.

Boring	Depth (m bgs)	Taxonomic assignement Bacteria	%	Taxonomic assignement Archae	%
Shallow LNAPL	**1.55**	Bacillus (gen)	0.47	Methanosaeta_(gen)	38.36
		Anaerolineaceae_(fam)	6.63	Candidatus Methanomethylicus_(gen)	6.19
		D8A-2_(gen)	0.21	Candidatus Altiarchaeum_(gen)	0.50
		Smithella_(gen)	18.32	Methanobacterium_ (gen)	49.65
		Leptolinea_ (gen)	3.22	Other	5.29
		SCADC1-2-3_ (gen)	5.23		
		Cryptanaerobacter_(gen)	0.28		
		Spirochaetaceae_(fam)	0.85		
		Aminicenantales_(gen)	2.65		
		Desulfoprunum_(gen)	7.34		
		Syntrophales_(or)	2.60		
		Syntrophorhabdus_(gen)	1.72		
		Pelolinea_ (gen)	2.82		
		Other	47.66		
Shallow LNAPL	**3.07**	Bacillus_ (gen)	0.70	Methanosaeta_(gen)	31.41
		Candidatus Yanofskybacteria (gen)	2.62	Candidatus Methanomethylicus_(gen)	28.88
		Candidatus Woesebacteria (gen)	1.21	Candidatus Altiarchaeum_(gen)	25.63
		ADurb.Bin180 (gen)	1.90	Candidatus Pacearchaeota_(gen)	6.50
		Anaerolineaceae_(fam)	8.82	Woesearchaeales_(gen)	7.58
		D8A-2 (gen)	2.12	Other	0.00
		Smithella spp.	30.12		
		Leptolinea (gen)	3.42		
		SCADC1-2-3 (gen)	1.23		
		OPB41 spp.	4.65		
		Cryptanaerobacter_(gen)	3.84		
		Spirochaetaceae_(fam)	9.50		
		Syntrophales(or)	0.19		
		Syntrophorhabdus_(gen)	1.41		
		Syntrophus (gen)	1.41		
		Pelolinea_(gen)	0.58		
		Other	26.28		
Shallow LNAPL	3.23	Bacillus_ (gen)	1.80	Methanosaeta_(gen)	52.80
		Candidatus Yanofskybacteria (gen)	2.73	Candidatus Methanomethylicus_(gen)	22.36
		Candidatus Woesebacteria (gen)	0.90	Candidatus Altiarchaeum_(gen)	14.91
		ADurb.Bin180 (gen)	1.15	Candidatus Pacearchaeota_(gen)	2.80
		Anaerolineaceae_(fam)	23.11	Methanobacterium_(gen)	7.14
		D8A-2 (gen)	2.64	Other	0.00
		Smithella spp.	28.85		
		Leptolinea (gen)	0.39		
		SCADC1-2-3 (gen)	2.03		
		OPB41_(gen)	1.22		
		Cryptanaerobacter (gen)	2.93		
		Spirochaetaceae_(fam)	2.93		
		Desulfoprunum (gen)	0.06		
		Syntrophales_(or)	0.39		
		Syntrophorhabdus_(gen)	0.49		
		Pelolinea_(gen)	0.24		
		Other	28.15		
Shallow LNAPL	4.37	Bacillus_ (gen)	2.45	Methanosaeta_(gen)	14.11
		Candidatus Yanofskybacteria (gen)	3.99	Candidatus Methanomethylicus_(gen)	42.57
		Candidatus Woesebacteria (gen)	1.40	Methanobacterium_(gen)	19.06
		ADurb.Bin180 (gen)	0.14	Candidatus Altiarchaeum_(gen)	5.45
		Anaerolineaceae_(fam)	16.28	Marine_Group_II_(gen)	7.18
		Smithella_(gen)	17.33	Bathyarchaeia_(gen)	6.44
		Leptolinea (gen)	3.82	Other	5.20
		OPB41_(gen)	9.24		
		Cryptanaerobacter_(gen)	4.21		
		Spirochaetaceae_(fam)	4.93		
		Syntrophales_(or)	0.33		
		Syntrophorhabdus_(gen)	0.24		
		Pelolinea_(gen)	0.30		
		Other	35.34		

Table SB.6. Microbial ecology characterization (RNA) for cryogenic samples collected from the *shallow LNAPL-1* boring.

Boring	Depth (m bgs)	Taxonomic assignement Ba	%	Taxonomic assignement Archae	%
Shallow	**1.55**	Methylocystis_(gen)	3.52	Methanosaeta_(gen)	69.50
LNAPL		Gaiellales_(or)	1.24	Methanoregula_(gen)	5.94
		Caldisericum_(gen)	1.04	Candidatus Methanomethylicus_(gen)	3.34
		Smithella_(gen)	16.57	Methanobacterium_ (gen)	19.98
		SCADC1-2-3_(gen)	19.94	Other	1.25
		Spirochaetaceae_(fam)	0.58		
		Cryptanaerobacter_(gen)	0.10		
		Leptolinea_(gen)	1.02		
		Anaerolineaceae_(fam)	0.45		
		Desulfoprunum_(gen)	20.74		
		Desulfatiglans_(gen)	0.04		
		Syntrophales_(or)	2.99		
		Syntrophorhabdus_(gen)	1.31		
		Pelolinea_(gen)	0.96		
		Other	29.50		
Shallow	**3.07**	Gaiellales_(or)	0.97	Methanosaeta_(gen)	64.43
LNAPL		Smithella_(gen)	56.28	Methanoregula_(gen)	21.53
		SCADC1-2-3_(gen)	3.22	Candidatus Methanomethylicus_(gen)	12.37
		Spirochaetaceae_(fam)	9.20	Candidatus Altiarchaeum_(gen)	0.46
		Cryptanaerobacter_(gen)	1.85	Bathyarchaeia_(gen)	1.22
		Leptolinea_(gen)	2.65	Other	0.00
		Longilinea_(gen)	2.92		
		Anaerolineaceae_(fam)	2.06		
		Desulfoprunum_(gen)	0.05		
		Desulfosporosinus_(gen)	0.27		
		OPB41_(gen)	4.22		
		Clostridia D8A-2_(gen)	1.43		
		Syntrophorhabdus_(gen)	1.48		
		Syntrophales_(or)	0.61		
		Other	12.77		
Shallow	3.23	Gaiellales_(or)	1.04	Methanosaeta_(gen)	85.67
LNAPL		Caldisericum_(gen)	0.53	Candidatus Methanomethylicus_(gen)	8.29
		Smithella_(gen)	33.99	Candidatus Altiarchaeum_(gen)	0.44
		SCADC1-2-3_(gen)	5.66	Candidatus Pacearchaeota_(gen)	0.58
		Spirochaetaceae_(fam)	4.17	Methanobacterium_(gen)	4.22
		Cryptanaerobacter_(gen)	1.74	Bathyarchaeia_(gen)	0.80
		Leptolinea_(gen)	3.25	Other	0.00
		Longilinea_(gen)	1.31		
		Anaerolineaceae_(fam)	10.11		
		Desulfosporosinus_(gen)	4.01		
		OPB41_(gen)	3.04		
		Clostridia D8A-2_(gen)	1.36		
		Syntrophorhabdus_(gen)	1.15		
		Syntrophales_(or)	0.78		
		Other	27.88		
Shallow	4.37	Gaiellales_(or)	0.7202	Methanosaeta_(gen)	47.826
LNAPL		Caldisericum_(gen)	0.1014	Methanoregula_(gen)	9.8398
		Smithella_(gen)	42.656	Candidatus Methanomethylicus_(gen)	17.849
		SCADC1-2-3_(gen)	2.0491	Methanobacterium_(gen)	23.57
		Spirochaetaceae_(fam)	3.4388	Bathyarchaeia_(gen)	0.9153
		Cryptanaerobacter_(gen)	1.7752	Other	0
		Leptolinea_(gen)	3.3881		
		Anaerolineaceae_(fam)	5.7212		
		RBG-16-55-12_(gen)	1.6332		
		Syntrophorhabdus_(gen)	0.3956		
		Syntrophales_(or)	0.4971		
		Other	37.624		

Table SB.7. Microbial ecology characterization (DNA) for cryogenic samples collected from the *continuous LNAPL-2* boring.

Boring	Depth (m bgs)	Taxonomic assignement Bacteria	%	Taxonomic assignement Archaea	%
Continuous	0.56	Methyloligellaceae_(fam)	4.77	Nitrososphaeraceae_(fam)	20.13
LNAPL		Methylobacter_ (gen)	4.88	Nitrososphaera_(gen)	79.13
		Bacillales_(or)	1.22	Other	0.75
		Candidatus_Udaeobacter_ (sp)	4.45		
		Bacteriap25_(sp)	0.86		
		Xanthobactereae_(sp)	1.23		
		Pseudolabrys_ (gen)	0.91		
		Actinobacterium_WWH12_(sp)	0.88		
		Smithella_ (sp)	0.22		
		Cryptanaerobacter_ (sp)	0.04		
		Sphingomonas_(sp)	1.16		
		Other	79.39		
Continuous	3.38	Methylobacter_ (gen)	0.02	Methanosaeta_(gen)	33.29
LNAPL		WCHB1-41_(sp)	1.66	Methanobacterium_(gen)	51.34
		ADurb.Bin180_(sp)	3.95	Candidatus Methanomethylicus_(gen)	14.30
		Gaiellales_(or)	16.53	Bathyarchaeia_(gen)	1.07
		Caldisericum_(sp)	0.99	Other	0.00
		Smithella_ (sp)	17.84		
		SCADC1-2-3_(sp)	9.61		
		OPB41_(gen)	4.82		
		RBG-16-55-12_(gen)	1.63		
		Cryptanaerobacter_(gen)	6.72		
		Spirochaetaceae_(fam)	1.56		
		Syntrophales(or)	1.77		
		Syntrophorhabdus_(gen)	1.43		
		Syntrophus _(gen)	1.33		
		Pelolinea_(sp)	4.69		
		Other	25.44		
Continuous	3.45	Not Detected		Not Detected	
LNAPL					

Table SB.8. Microbial ecology characterization (RNA) for cryogenic samples collected from the *continuous LNAPL* boring.

Boring	Depth (m bgs)	Taxonomic assignement Bacteria	%	Taxonomic assignement Archaea	%
Continuous	0.56	Not Detected		Not Detected	
LNAPL					
Continuous	3.38	Gaiellales_(or)	9.51	Methanosaeta_(gen)	74.42
LNAPL		Caldisericum spp.	3.61	Methanoregula_(gen)	2.01
		Smithella spp.	24.65	Candidatus Methanomethylicus_(gen)	0.96
		SCADC1-2-3 spp.	29.90	Methanobacterium_(gen)	20.80
		Spirochaetaceae_(fam)	1.27	Bathyarchaeia_(gen)	1.81
		Cryptanaerobacter_(gen)	1.66	Other	0.00
		Leptolinea_(gen)	0.61		
		Desulfoprunum_(gen)	0.94		
		Syntrophus _(gen)	2.90		
		Pelolinea_(sp)	1.36		
		Syntrophorhabdus_(gen)	1.38		
		Other	22.21		
Continuous	3.45	Methylobacter_ (gen)	0.36	Methanosaeta_(gen)	63.33
LNAPL		Methylocystis_(gen)	0.15	Nitrososphaeraceae_(gen)	0.52
		Pseudomonas_(gen)	0.17	Methanobacterium_(gen)	17.01
		Bacteriap25_(sp)	0.13	Other	19.14
		Xanthobactereae_(gen)	0.14		
		Gaiellales_(or)	7.78		
		Caldisericum_(gen)	5.51		
		Smithella_(gen)	24.69		
		SCADC1-2-3_(gen)	14.80		
		Cryptanaerobacter_(gen)	2.12		
		Spirochaetaceae_(fam)	2.60		
		Sphingomonas_(gen)	0.14		
		Aminicenantales_(gen)	1.54		
		Desulfoprunum_(gen)	1.59		
		Syntrophus_(gen)	1.33		
		Pelolinea_(gen)	1.85		
		Syntrophorhabdus_(gen)	1.81		
		Other	33.27		